

EUROPEAN ORGANISATION FOR NUCLEAR RESEARCH (CERN)



JHEP 01 (2018) 126
DOI: [10.1007/JHEP01\(2018\)126](https://doi.org/10.1007/JHEP01(2018)126)



CERN-PH-2017-230
5th February 2018

Search for dark matter and other new phenomena in events with an energetic jet and large missing transverse momentum using the ATLAS detector

The ATLAS Collaboration

Results of a search for new phenomena in final states with an energetic jet and large missing transverse momentum are reported. The search uses proton–proton collision data corresponding to an integrated luminosity of 36.1 fb^{-1} at a centre-of-mass energy of 13 TeV collected in 2015 and 2016 with the ATLAS detector at the Large Hadron Collider. Events are required to have at least one jet with a transverse momentum above 250 GeV and no leptons (e or μ). Several signal regions are considered with increasing requirements on the missing transverse momentum above 250 GeV. Good agreement is observed between the number of events in data and Standard Model predictions. The results are translated into exclusion limits in models with pair-produced weakly interacting dark-matter candidates, large extra spatial dimensions, and supersymmetric particles in several compressed scenarios.

1 Introduction

This paper presents the results of a search for events containing an energetic jet and large missing transverse momentum \vec{p}_T^{miss} (with magnitude E_T^{miss}) in a data sample corresponding to a total integrated luminosity of 36.1 fb^{-1} . The data were collected by the ATLAS Collaboration at the Large Hadron Collider (LHC) from proton–proton collisions at a centre-of-mass energy (\sqrt{s}) of 13 TeV. The final-state monojet signature of at least one energetic jet, $E_T^{miss} > 250 \text{ GeV}$, and no leptons (e or μ) constitutes a distinctive signature for new physics beyond the Standard Model (SM) at colliders. The monojet signature has been extensively studied at the LHC in the context of searches for large extra spatial dimensions (LED), supersymmetry (SUSY), and weakly interacting massive particles (WIMPs) as candidates for dark matter (DM) [1–3]. The results of the analysis are therefore interpreted in terms of each of these models, which are described in the following paragraphs.

A range of astrophysical measurements, such as the rotational speed of stars in galaxies and gravitational lensing, point to the existence of a non-baryonic form of matter [4–6]. The existence of a new, weakly interacting massive particle is often hypothesized [7], as it leads to the correct relic density for non-relativistic matter in the early universe [8] as measured from data from the Planck [9] and WMAP [10] Collaborations, if the mass is between a few GeV and one TeV and if it has electroweak-scale interaction cross sections. WIMPs may be pair-produced at the LHC and when accompanied by a jet of particles, for example from initial-state radiation (ISR), these events produce the signature of a jet and missing transverse momentum.

As with the initial results obtained in this search channel at $\sqrt{s} = 13 \text{ TeV}$ [1], simplified models are used to interpret the results, providing a framework to characterize the new particles acting as mediators of the interaction between the SM and the dark sector [11–13]. The results from simplified models involving s -channel Feynman diagrams such as the one shown in Figure 1(a) are comparable to those previously obtained [14] by using an effective-field-theory approach [15] when the mediator mass considered is above 10 TeV [16].

Results are presented for DM models where Dirac fermion WIMPs (χ) are pair-produced from quarks via s -channel exchange of a spin-1 mediator particle (Z_A) with axial-vector couplings, a spin-1 mediator particle (Z_V) with vector couplings, or a spin-0 pseudoscalar (Z_P). These models are defined by four free parameters: the WIMP mass (m_χ); the mediator mass (m_{Z_A} , m_{Z_V} or m_{Z_P} , depending on the model); the flavour-universal coupling to quarks (g_q), where all three quark generations are included; and the coupling of the mediator to WIMPs (g_χ). Couplings to other SM particles are not considered. In each case, a minimal mediator width is defined, as detailed in Refs. [12, 13], which in the case of the axial-vector mediator takes the form:

$$\Gamma(m_{Z_A})_{\min} = \frac{g_\chi^2 m_{Z_A}}{12\pi} \beta_\chi^3 \theta(m_{Z_A} - 2m_\chi) + \sum_q \frac{3g_q^2 m_{Z_A}}{12\pi} \beta_q^3 \theta(m_{Z_A} - 2m_q) ,$$

where $\theta(x)$ denotes the Heaviside step function and $\beta_f = \sqrt{1 - 4m_f^2/m_{Z_A}^2}$ is the velocity in the mediator rest frame of fermion f (either χ or q) with mass m_f . The quark sum runs over all flavours. The monojet signature in this model emerges from initial-state radiation of a gluon as shown in Figure 1(a).

Results are also presented for a DM model in which WIMPs are produced via the exchange of a coloured scalar mediator, which is assumed to couple as a colour-triplet, SU(2) doublet to the left-handed quarks [17–19]. The model contains a variety of new production mechanisms such as the production

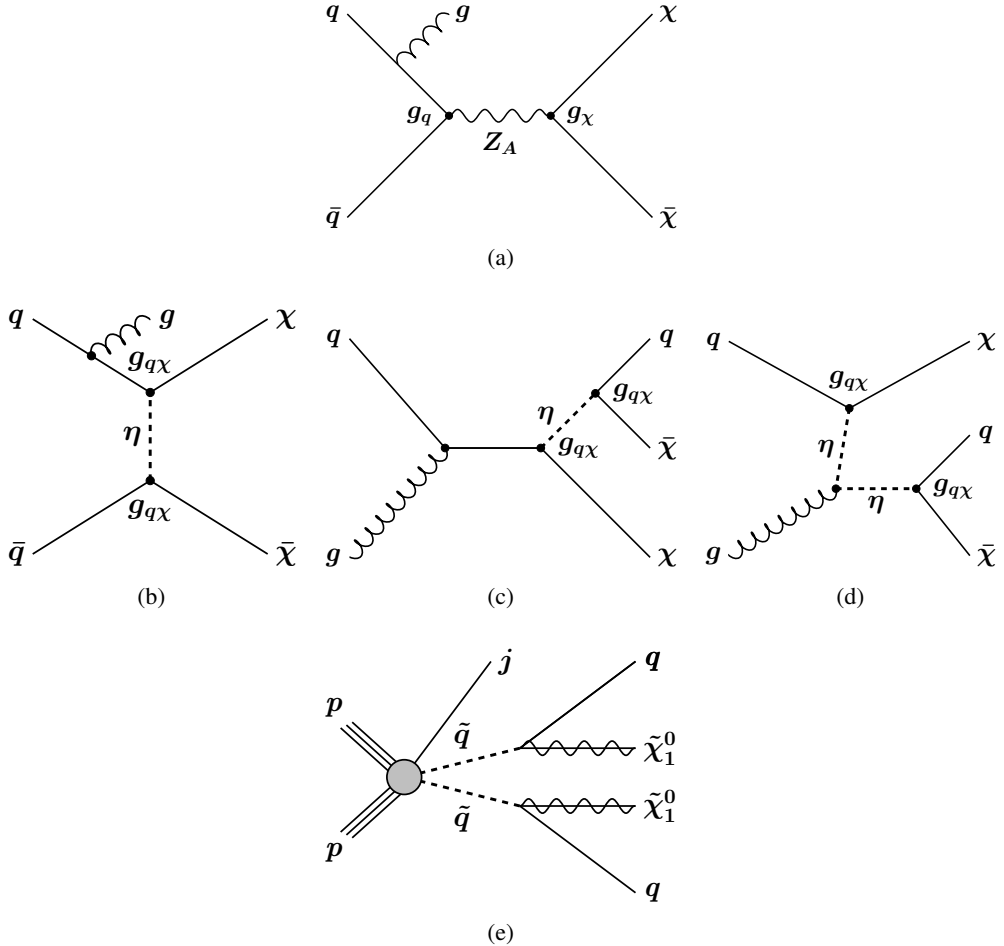


Figure 1: (a) Diagram for the pair-production of weakly interacting massive particles χ , with a mediator Z_A with axial-vector couplings exchanged in the s -channel. (b)(c)(d) Example of diagrams for the pair-production of weakly interacting massive particles χ via a coloured scalar mediator η . (e) A generic diagram for the pair-production of squarks with the decay mode $\tilde{q} \rightarrow q + \tilde{\chi}_1^0$. The presence of a gluon from initial-state radiation resulting in a jet is indicated for illustration purposes.

of WIMP pairs via u - and t -channel diagrams with direct couplings of dark matter and SM particles or even s -channel exchange of two mediators, leading to a different phenomenology. A set of representative diagrams relevant for a monojet final state are collected in Figures 1(b)–1(d). A model with simplified assumptions is defined by the following three parameters: m_χ , a single mediator mass (m_η), and a flavour-universal coupling to quarks and WIMPs ($g_{q\chi} \equiv g$). The mediator is also assumed to couple only to the first two generations of quarks, with minimal decay widths of the form:

$$\Gamma(\eta)_{\min} = \frac{g^2}{16\pi m_\eta^3} \left(m_\eta^2 - m_q^2 - m_\chi^2 \right) \sqrt{\left(m_\eta^2 - (m_q + m_\chi)^2 \right) \left(m_\eta^2 - (m_q - m_\chi)^2 \right)},$$

where, to ensure that the DM particle is stable and the mediator width is always defined, $m_\chi^2 + m_q^2 < m_\eta^2$ and $4m_\chi^2/m_\eta^2 < (1 - m_q^2/m_\eta^2 + m_\chi^2/m_\eta^2)^2$ are required.

Supersymmetry is a theory of physics beyond the SM which naturally solves the hierarchy problem and provides candidates for dark matter [20–28]. SUSY introduces a new supersymmetric partner (sparticle) for each particle in the SM. Specifically, a new scalar field is associated with each left- or right-handed quark state. Two squark mass eigenstates \tilde{q}_1 and \tilde{q}_2 result from the mixing of the scalar fields for a particular flavour. Naturalness arguments suggest that the third-generation squarks should be light, with masses below about 1 TeV [29]. In addition, many SUSY scenarios have a significant mass difference between the two eigenstates in the bottom-squark (sbottom) and top-squark (stop) sectors, which leads to light sbottom \tilde{b}_1 and stop \tilde{t}_1 masses. In supersymmetric extensions of the SM that assume R-parity conservation [30–34], sparticles are produced in pairs and the lightest supersymmetric particle (LSP) is stable. The LSP is assumed to be the lightest neutralino $\tilde{\chi}_1^0$.

The results are interpreted in terms of searches for squark production using simplified models in scenarios for which the mass difference $\Delta m \equiv m_{\tilde{q}} - m_{\tilde{\chi}_1^0}$ is small (compressed-mass scenario). Four such scenarios with compressed mass spectra are considered: stop-pair production, where the stop decays into a charm quark and the LSP ($\tilde{t}_1 \rightarrow c + \tilde{\chi}_1^0$), stop-pair production in the four-body decay mode $\tilde{t}_1 \rightarrow b + f\bar{f}' + \tilde{\chi}_1^0$, sbottom-pair production with $\tilde{b}_1 \rightarrow b + \tilde{\chi}_1^0$, and squark-pair production with $\tilde{q} \rightarrow q + \tilde{\chi}_1^0$ ($q = u, d, c, s$). For relatively small Δm ($\lesssim 25$ GeV), both the transverse momenta of the quark jets and the E_T^{miss} in the final state are small, making it difficult to fully reconstruct the signal given the kinematic thresholds for reconstruction. The presence of jets from ISR is thus used to identify signal events (see Figure 1(e)). In this case, the squark-pair system is boosted, leading to larger E_T^{miss} .

The final model considered is that of extra spatial dimensions, the existence of which has been postulated to explain the large difference between the electroweak unification scale at $O(10^2)$ GeV and the Planck scale M_{Pl} at $O(10^{19})$ GeV. In the Arkani-Hamed, Dimopoulos, and Dvali (ADD) model of LED [35], the presence of n extra spatial dimensions of size R leads to a fundamental Planck scale in $4+n$ dimensions given by $M_{\text{Pl}}^2 \sim M_D^{2+n} R^n$, where M_D is the fundamental scale of the $4+n$ -dimensional theory. Motivation for the theory comes from the possibility that M_D is of order 1 TeV, a scale accessible at the LHC. In this model, SM particles and gauge interactions are confined to the usual 3+1 space-time dimensions, whereas gravity is free to propagate through the entire multidimensional space, which effectively dilutes its perceived strength. The extra spatial dimensions are compactified, resulting in a Kaluza–Klein tower of massive graviton modes (KK graviton). If produced in high-energy proton–proton collisions, a KK graviton escaping into the extra dimensions can be inferred from E_T^{miss} , and can lead to a monojet event signature.

The paper is organized as follows. The ATLAS detector is described in the next Section. Section 3 provides details of the Monte Carlo simulations used in the analysis for background and signal processes. Section 4 discusses the reconstruction and identification of jets, leptons, and missing transverse momentum, while Section 5 describes the event selection. The estimation of background contributions and the study of systematic uncertainties are discussed in Sections 6 and 7. The results are presented in Section 8 and are interpreted in terms of limits in models of WIMP-pair production, ADD, and SUSY in compressed scenarios. Finally, Section 9 is devoted to the conclusions.

2 ATLAS detector

The ATLAS detector [36] covers almost the whole solid angle¹ around the collision point with layers of tracking detectors, calorimeters and muon chambers. The ATLAS inner detector covers the pseudorapidity range $|\eta| < 2.5$. It consists of a silicon pixel detector, a silicon microstrip detector, and a straw-tube tracker that also measures transition radiation for particle identification, all immersed in a 2 T axial magnetic field produced by a solenoid. During the first LHC long shutdown, a new tracking layer, known as the insertable B-Layer [37], was added just outside a narrower beam pipe at a radius of 33 mm.

High-granularity lead/liquid-argon (LAr) electromagnetic sampling calorimeters cover the pseudorapidity range $|\eta| < 3.2$. Hadronic calorimetry in the range $|\eta| < 1.7$ is provided by a steel/scintillator-tile calorimeter, consisting of a large barrel and two smaller extended barrel cylinders, one on either side of the central barrel. In the endcaps ($|\eta| > 1.5$), copper/LAr and tungsten/LAr hadronic calorimeters match the outer $|\eta|$ limits of the endcap electromagnetic calorimeters. The LAr forward calorimeters provide both the electromagnetic and hadronic energy measurements, and extend the coverage to $|\eta| < 4.9$.

The muon spectrometer measures the deflection of muons in the magnetic field provided by large superconducting air-core toroidal magnets in the pseudorapidity range $|\eta| < 2.7$, instrumented with separate trigger and high-precision tracking chambers. Over most of the η range, a measurement of the track coordinates in the bending direction of the magnetic field is provided by monitored drift tubes. Cathode strip chambers with higher granularity are used in the innermost plane over $2.0 < |\eta| < 2.7$. The muon fast trigger detectors cover the pseudorapidity range $|\eta| < 2.4$ and provide a measurement of the coordinate in the non-bending plane.

The data were collected using an online two-level trigger system [38] that selects events of interest and reduces the event rate from an average of 33 MHz to about 1 kHz for recording and offline processing.

3 Monte Carlo simulation

Monte Carlo (MC) simulated event samples are used to compute detector acceptance and reconstruction efficiencies, determine signal and background contributions, and estimate systematic uncertainties in the final results. Samples are processed with the full ATLAS detector simulation [39] based on GEANT4 [40]. Simulated events are then reconstructed and analysed with the same analysis chain as for the data, using the same trigger and event selection criteria. The effects of multiple proton–proton interactions in the same or neighbouring bunch-crossings (pile-up) are taken into account by overlaying simulated minimum-bias events from PYTHIA 8.205 [41] onto the hard-scattering process, distributed according to the frequency in data.

¹ ATLAS uses a right-handed coordinate system with its origin at the nominal interaction point (IP) in the centre of the detector and the z -axis along the beam pipe. The x -axis points from the IP to the centre of the LHC ring, and the y -axis points upward. Cylindrical coordinates (r, ϕ) are used in the transverse plane, ϕ being the azimuthal angle around the z -axis. The pseudorapidity is defined in terms of the polar angle θ as $\eta = -\ln \tan(\theta/2)$.

3.1 Signal simulation

WIMP s -channel signal samples are simulated in PowHEG-Box v2 [42–44] (revision 3049) using two implementations of simplified models, introduced in Ref. [45]. The DMV model of WIMP-pair production is used for s -channel spin-1 axial-vector or vector mediator exchange at next-to-leading order (NLO) in the strong coupling, and the DMS_tloop model is used for WIMP-pair production with the s -channel spin-0 pseudoscalar mediator exchange with the full quark-loop calculation at leading order (LO) [46]. Renormalization and factorization scales are set to $H_T/2$ on an event-by-event basis, where $H_T = \sqrt{m_{\chi\chi}^2 + p_{T,j1}^2}$ is defined by the invariant mass of the WIMP pair ($m_{\chi\chi}$) and the transverse momentum of the highest- p_T parton-level jet ($p_{T,j1}$). The mediator propagator is described by a Breit–Wigner distribution. Events are generated using the NNPDF30 [47] parton distribution functions (PDFs) and interfaced to PYTHIA 8.205 with the A14 set of tuned parameters (tune) [48] for parton showering, hadronization and the underlying event. Couplings of the mediator to WIMP particles and those of the SM quarks are set to $g_\chi = 1$ and $g_q = 1/4$ for the DMV model whereas both couplings are set to one in the case of the DMS_tloop model. A grid of samples is produced for WIMP masses ranging from 1 GeV to 1 TeV and mediator masses between 10 GeV and 10 TeV.

Samples for DM production in the coloured scalar mediator model are generated with MG5_aMC@NLO v2.3.3 [49] at LO using NNPDF23LO [50] PDFs and interfaced to PYTHIA 8.186 with the A14 tune for modelling of parton showering, hadronization and the underlying event. The generation of the different subprocesses is performed following a procedure outlined in Ref. [18]. Specifically, the generation is split between DM production with an off-shell mediator and on-shell mediator production followed by decay, and the associated production of up to two partons in the final state is included. As already mentioned, only diagrams involving the first two quark generations are considered and processes with electroweak bosons are suppressed. The matching between MADGRAPH and PYTHIA is performed following the CKKW-L prescription [51]. The parton matching scale is set to $m_\eta/8$, where m_η denotes the mass of the mediator, in the case of mediator-pair production, and to 30 GeV otherwise. This particular choice of matching scales optimizes the generation of the samples in the full phase space, and minimizes the impact from scale variations on the shape of the predicted kinematic distributions. The coupling is set to $g = 1$, and a grid of samples is produced for WIMP masses ranging from 1 GeV to 1 TeV and mediator masses between 100 GeV and 2.5 TeV.

SUSY signals for stop-pair production are generated with MG5_aMC@NLO v2.2.3 and interfaced to PYTHIA 8.186 with the A14 tune for modelling of the squark decay, parton showering, hadronization, and the underlying event. The PDF set used for the generation is NNPDF23LO, and the renormalization and factorization scales are set to $\mu = \sum_i \sqrt{m_i^2 + p_{T,i}^2}$, where the sum runs over all final-state particles from the hard-scatter process. The matrix-element calculation is performed at tree level, and includes the emission of up to two additional partons. Matching to parton-shower calculations is accomplished by the CKKW-L prescription, with a matching scale set to one quarter of the pair-produced superpartner mass. Signal cross sections are calculated at NLO in the strong coupling constant, adding the resummation of soft-gluon emission at next-to-leading-logarithm (NLO+NLL) accuracy [52–54]. The nominal cross section and its uncertainty are taken from an envelope of cross-section predictions using different PDF sets and factorization and renormalization scales, as described in Ref. [55]. Simulated samples are produced with squark masses in the range between 250 GeV and 700 GeV, and squark–neutralino mass differences Δm varying between 5 GeV and 25 GeV.

Simulated samples for the ADD LED model with different numbers of extra dimensions in the range

$n = 2\text{--}6$ and a fundamental scale M_D in the range 3.0–5.3 TeV are generated using PYTHIA 8.205 with NNPDF23LO PDFs. The renormalization scale is set to the geometric mean of the squared transverse masses of the two produced particles, $\sqrt{(p_{T,G}^2 + m_G^2)(p_{T,p}^2 + m_p^2)}$, where $p_{T,G}$ and m_G ($p_{T,p}$ and m_p) denote, respectively, the mass and the transverse momentum of the KK graviton (parton) in the final state. The factorization scale is set to the minimum transverse mass, $\sqrt{p_T^2 + m^2}$, of the KK graviton and the parton.

3.2 Background simulation

After applying the selection described in Section 5, the primary SM background contributing to monojet event signatures is $Z(\rightarrow \nu\bar{\nu})+\text{jets}$. There are also significant contributions from $W+\text{jets}$ events, primarily from $W(\rightarrow \tau\nu)+\text{jets}$. Small contributions are expected from $Z/\gamma^*(\rightarrow \ell^+\ell^-)+\text{jets}$ ($\ell = e, \mu, \tau$), multijet, $t\bar{t}$, single-top, and diboson (WW , WZ , ZZ) processes. Contributions from top-quark production associated with additional vector bosons ($t\bar{t}+W$, $t\bar{t}+Z$, or $t+Z+q/b$ processes) are negligible and not considered in this analysis.

Events containing W or Z bosons with associated jets are simulated using the SHERPA 2.2.1 [56] event generator. Matrix elements (ME) are calculated for up to two partons at NLO and four partons at LO using OpenLoops [57] and Comix [58], and merged with the SHERPA parton shower (PS) [59] using the ME+PS@NLO prescription [60]. The NNPDF3.0NNLO [47] PDF set is used in conjunction with a dedicated parton-shower tuning developed by the authors of SHERPA. The MC predictions are initially normalized to next-to-next-to-leading-order (NNLO) perturbative QCD (pQCD) predictions according to DYNNLO [61, 62] using the MSTW2008 90% CL NNLO PDF set [63].

The $W+\text{jets}$ and $Z+\text{jets}$ MC predictions are reweighted to account for higher-order QCD and electroweak corrections as described in Ref. [64], where parton-level predictions for $W/Z+\text{jets}$ production, including NLO QCD corrections and NLO electroweak corrections supplemented by Sudakov logarithms at two loops, are provided as a function of the vector-boson p_T , improving the description of the measured Z -boson p_T distribution [65]. The predictions are provided separately for the different $W+\text{jets}$ and $Z+\text{jets}$ processes together with the means for a proper estimation of theoretical uncertainties and their correlations (see Section 7). The reweighting procedure takes into account the difference between the QCD NLO predictions as included already in SHERPA and as provided by the parton-level calculations.

For the generation of $t\bar{t}$ and single top quarks in the Wt -channel and s -channel, the PowHEG-Box v2 [66] event generator is used with CT10 [67] PDFs. Electroweak t -channel single-top-quark events are generated using the PowHEG-Box v1 event generator. This event generator uses the four-flavour scheme to calculate NLO matrix elements, with the CT10 four-flavour PDF set. The parton shower, hadronization, and underlying event are simulated using PYTHIA 8.205 with the A14 tune. The top-quark mass is set to 172.5 GeV. The EvtGen v1.2.0 program [68] is used to model the decays of the bottom and charm hadrons. Alternative samples are generated using MADGRAPH5_aMC@NLO (v2.2.1) [49] interfaced to Herwig++ (v2.7.1) [69] in order to estimate the effects of the choice of matrix-element event generator and parton-shower algorithm.

Diboson samples (WW , WZ , and ZZ production) are generated using either SHERPA 2.2.1 or SHERPA 2.1.1 with NNPDF3.0NNLO or CT10nlo PDFs, respectively, and are normalized to NLO pQCD predictions [70]. Diboson samples are also generated using PowHEG-Box [43] interfaced to PYTHIA 8.186 and using CT10 PDFs for studies of systematic uncertainties.

4 Event reconstruction

Jets are reconstructed from energy deposits in the calorimeters using the anti- k_t jet algorithm [71, 72] with the radius parameter (in $y-\phi$ space) set to 0.4. The measured jet transverse momentum is corrected for detector effects by weighting energy deposits arising from electromagnetic and hadronic showers differently. In addition, jets are corrected for contributions from pile-up, as described in Ref. [73]. Jets with $p_T > 20$ GeV and $|\eta| < 2.8$ are considered in the analysis. Track-based variables to suppress pile-up jets have been developed, and a combination of two such variables, called the jet-vertex tagger [74], is constructed. In order to remove jets originating from pile-up collisions, for central jets ($|\eta| < 2.4$) with $p_T < 50$ GeV a significant fraction of the tracks associated with each jet must have an origin compatible with the primary vertex, as defined by the jet-vertex tagger.

Jets with $p_T > 30$ GeV and $|\eta| < 2.5$ are identified as b -jets if tagged by a multivariate algorithm which uses information about the impact parameters of inner-detector tracks matched to the jet, the presence of displaced secondary vertices, and the reconstructed flight paths of b - and c -hadrons inside the jet [75, 76]. A 60% efficient b -tagging working point, as determined in a simulated sample of $t\bar{t}$ events, is chosen. This corresponds to a rejection factor of approximately 1500, 35 and 180 for light-quark and gluon jets, c -jets, and τ -leptons decaying hadronically, respectively.

The presence of electrons or muons in the final state is used in the analysis to define control samples and to reject background contributions in the signal regions (see Sections 5 and 6).

Electrons are found by combining energy deposits in the calorimeter with tracks found in the inner detector, and are initially required to have $p_T > 20$ GeV and $|\eta| < 2.47$, to satisfy the ‘Loose’ electron shower shape and track selection criteria described in Refs. [77], and must also be isolated. The latter uses track-based isolation requirements with an efficiency of about 99%, as determined using $Z/\gamma^*(\rightarrow e^+e^-)$ data. Overlaps between identified electrons and jets with $p_T > 30$ GeV in the final state are resolved. Jets are discarded if they are not b -tagged and their separation $\Delta R = \sqrt{(\Delta\eta)^2 + (\Delta\phi)^2}$ from an identified electron is less than 0.2. Otherwise, the electron is removed as it most likely originates from a semileptonic b -hadron decay. The electrons separated by ΔR between 0.2 and 0.4 from any remaining jet are removed.

Muon candidates are formed by combining information from the muon spectrometer and inner tracking detectors. They are required to pass ‘Medium’ identification requirements, as described in Ref. [78], and to have $p_T > 10$ GeV and $|\eta| < 2.5$. Jets with $p_T > 30$ GeV and fewer than three tracks with $p_T > 0.5$ GeV associated with them are discarded if their separation ΔR from an identified muon is less than 0.4. The muon is discarded if it is matched to a jet with $p_T > 30$ GeV that has at least three tracks associated with it.

The E_T^{miss} value is reconstructed using all energy deposits in the calorimeter up to pseudorapidity $|\eta| = 4.9$. Clusters associated with either electrons, photons or jets with $p_T > 20$ GeV make use of the corresponding calibrations. Softer jets and clusters not associated with electrons, photons or jets are calibrated using tracking information [79]. As discussed below, in this analysis the missing transverse momentum is not corrected for the presence of muons in the final state.

5 Event selection

The data sample considered corresponds to a total integrated luminosity of 36.1 fb^{-1} , and was collected in 2015 and 2016. The uncertainty in the combined 2015+2016 integrated luminosity is 3.2%. It is derived, following a methodology similar to that detailed in Ref. [80], from a calibration of the luminosity scale using x - y beam-separation scans performed in August 2015 and May 2016. The data were collected using a trigger that selects events with E_T^{miss} above 90 GeV, as computed from calorimetry information at the final stage of the two-level trigger system. After analysis selections, the trigger was measured to be fully efficient for events with $E_T^{\text{miss}} > 250 \text{ GeV}$, as determined using a data sample with muons in the final state. Events are required to have at least one reconstructed primary vertex consistent with the beamspot envelope and that contains at least two associated tracks of $p_T > 0.4 \text{ GeV}$. When more than one such vertex is found, the vertex with the largest summed p_T^2 of the associated tracks is chosen. Events having identified muons with $p_T > 10 \text{ GeV}$ or electrons with $p_T > 20 \text{ GeV}$ in the final state are vetoed.

Events are selected with $E_T^{\text{miss}} > 250 \text{ GeV}$, a leading jet with $p_{T,j1} > 250 \text{ GeV}$ and $|\eta| < 2.4$, and a maximum of four jets with $p_T > 30 \text{ GeV}$ and $|\eta| < 2.8$. Separation in the azimuthal angle of $\Delta\phi(\text{jet}, \vec{p}_T^{\text{miss}}) > 0.4$ between the missing transverse momentum direction and each selected jet is required to reduce the multijet background contribution, where a large E_T^{miss} can originate from jet energy mismeasurement.

Jet quality criteria [81] are imposed, which involve selections based on quantities such as the pulse shape of the energy depositions in the cells of the calorimeters, electromagnetic fraction in the calorimeter, calorimeter sampling fraction, and the charged-particle fraction.² Loose selection criteria are applied to all jets with $p_T > 30 \text{ GeV}$ and $|\eta| < 2.8$, which remove anomalous energy depositions due to coherent noise and electronic noise bursts in the calorimeter [82]. Events with any jet not satisfying the loose criteria, as described in Ref. [81], are discarded.

Non-collision backgrounds, for example energy depositions in the calorimeters due to muons of beam-induced or cosmic-ray origin, are suppressed by imposing tight selection criteria on the leading jet and the ratio of the jet charged-particle fraction to the calorimeter sampling fraction,³ $f_{\text{ch}}/f_{\text{max}}$, is required to be larger than 0.1. These requirements have a negligible effect on the signal efficiency.

The analysis uses two sets of signal regions, with inclusive and exclusive E_T^{miss} selections, where the regions are defined with increasing E_T^{miss} thresholds from 250 GeV to 1000 GeV (Table 1). The inclusive selections are used for a model-independent search for new physics, and the exclusive selections are used for the interpretation of the results within different models of new physics.

6 Background estimation

The W +jets, Z +jets, and top-quark-related backgrounds are constrained using MC event samples normalized with data in selected control regions. By construction, there is no overlap between events in the signal and the different control regions. The control regions are defined using the same requirements for E_T^{miss} , leading-jet p_T , event topologies, and jet vetoes as in the signal regions, such that no extrapolation in E_T^{miss}

² The charged-particle fraction is defined as $f_{\text{ch}} = \sum p_T^{\text{track,jet}} / p_T^{\text{jet}}$, where $\sum p_T^{\text{track,jet}}$ is the scalar sum of the transverse momenta of tracks associated with the primary vertex within a cone of radius $\Delta R = 0.4$ around the jet axis, and p_T^{jet} is the transverse momentum of the jet as determined from calorimetric measurements.

³ The variable f_{max} denotes the maximum fraction of the jet energy collected by a single calorimeter layer.

Table 1: Inclusive (IM1–IM10) and exclusive (EM1–EM10) signal regions with increasing E_T^{miss} thresholds from 250 GeV to 1000 GeV. In the case of IM10 and EM10, both signal regions contain the same selected events in data. In the case of the IM10 signal region, the background predictions are computed considering only data and simulated events with $E_T^{\text{miss}} > 1$ TeV, whereas the EM10 background prediction is obtained from fitting the full E_T^{miss} shape in data and simulation, as described in Section 6.

Inclusive (IM)	IM1	IM2	IM3	IM4	IM5	IM6	IM7	IM8	IM9	IM10
E_T^{miss} [GeV]	>250	>300	>350	>400	>500	>600	>700	>800	>900	>1000
Exclusive (EM)	EM1	EM2	EM3	EM4	EM5	EM6	EM7	EM8	EM9	EM10
E_T^{miss} [GeV]	250–300	300–350	350–400	400–500	500–600	600–700	700–800	800–900	900–1000	>1000

or jet p_T is needed from control to signal regions. The normalization factors are extracted simultaneously using a global fit that includes systematic uncertainties, to properly take into account correlations.

Different control samples are used to help constrain the yields of the $W+\text{jets}$ and $Z+\text{jets}$ background processes in the signal regions. This includes $W(\rightarrow \mu\nu)+\text{jets}$, $W(\rightarrow e\nu)+\text{jets}$, and $Z/\gamma^*(\rightarrow \mu^+\mu^-)+\text{jets}$ control samples, enriched in $W(\rightarrow \mu\nu)+\text{jets}$, $W(\rightarrow e\nu)+\text{jets}$, and $Z/\gamma^*(\rightarrow \mu^+\mu^-)+\text{jets}$ background processes, respectively. The dominant $Z(\rightarrow \nu\bar{\nu})+\text{jets}$ and $W(\rightarrow \tau\nu)+\text{jets}$ background contributions are constrained in the fit by using both $W+\text{jets}$ control regions and the $Z/\gamma^*(\rightarrow \mu^+\mu^-)+\text{jets}$ control region. As discussed in Section 6.4, this translates into a reduced uncertainty in the estimation of the main irreducible background contribution, due to a partial cancelling out of systematic uncertainties and the superior statistical power of the $W+\text{jets}$ control sample in data, compared to that of the $Z/\gamma^*(\rightarrow \mu^+\mu^-)+\text{jets}$ control sample. A small $Z/\gamma^*(\rightarrow e^+e^-)+\text{jets}$ and $Z/\gamma^*(\rightarrow \tau^+\tau^-)+\text{jets}$ background contribution is also constrained via the $W+\text{jets}$ and $Z/\gamma^*(\rightarrow \mu^+\mu^-)+\text{jets}$ control samples.⁴

Finally, a top control sample constrains top-quark-related background processes. The remaining SM backgrounds from diboson processes are determined using MC simulated samples, while the multijet background contribution is extracted from data. The contributions from non-collision backgrounds are estimated in data using the beam-induced background identification techniques described in Ref. [82].

In the following subsections, details of the definition of the $W/Z+\text{jets}$ and top control regions, and of the data-driven determination of the multijet and beam-induced backgrounds are given. This is followed by a description of the background fits.

6.1 Control samples

A $W(\rightarrow \mu\nu)+\text{jets}$ control sample is selected by requiring a muon consistent with originating from the primary vertex with $p_T > 10$ GeV, and transverse mass in the range $30 < m_T < 100$ GeV. The transverse mass $m_T = \sqrt{2p_T^\ell p_T^\nu [1 - \cos(\phi^\ell - \phi^\nu)]}$ is defined by the lepton and neutrino transverse momenta, where the (x, y) components of the neutrino momentum are taken to be the same as the corresponding \vec{p}_T^{miss} components. Events with identified electrons in the final state are vetoed. In addition, events with an identified b -jet in the final state are vetoed in order to reduce the contamination from top-quark-related processes. Similarly, a $Z/\gamma^*(\rightarrow \mu^+\mu^-)+\text{jets}$ control sample is selected by requiring the presence of two muons with $p_T > 10$ GeV and invariant mass in the range $66 < m_{\mu\mu} < 116$ GeV. In the $W(\rightarrow \mu\nu)+\text{jets}$

⁴ The use of an additional $Z/\gamma^*(\rightarrow e^+e^-)+\text{jets}$ control sample to help constrain the $Z/\gamma^*(\rightarrow e^+e^-)+\text{jets}$ and $Z(\rightarrow \nu\bar{\nu})+\text{jets}$ background contributions leads to an insignificant improvement in the background determination [1].

and $Z/\gamma^*(\rightarrow \mu^+\mu^-)$ +jets control regions, the E_T^{miss} value is not corrected for the presence of the muons in the final state, motivated by the fact that these control regions are used to estimate the $Z(\rightarrow \nu\bar{\nu})$ +jets, $W(\rightarrow \mu\nu)$ +jets and $Z/\gamma^*(\rightarrow \mu^+\mu^-)$ +jets backgrounds in the signal regions with no identified muons. The E_T^{miss} -based online trigger used in the analysis does not include muon information in the E_T^{miss} calculation. This allows the collection of $W(\rightarrow \mu\nu)$ +jets and $Z/\gamma^*(\rightarrow \mu^+\mu^-)$ +jets control samples with the same trigger as for the signal regions.

A $W(\rightarrow e\nu)$ +jets-dominated control sample was collected using online triggers that select events with an electron in the final state. The control sample is defined with an isolated electron candidate with $p_T > 30$ GeV, $30 < m_T < 100$ GeV, and no additional identified leptons in the final state. Electron candidates in the transition region between the barrel and endcaps of the electromagnetic calorimeter, $1.37 < |\eta| < 1.52$, are excluded. The E_T^{miss} value is corrected by subtracting the contribution from the electron cluster in the calorimeter. In this way, the measured E_T^{miss} in the event better reflects the magnitude of the W -boson p_T in the final state, which is necessary for a proper implementation of the W -boson p_T reweighting procedure, as explained in Section 3, that accounts for higher-order QCD and electroweak corrections. In order to suppress backgrounds from multijet processes with jets faking high- p_T electrons, the events are required to have $E_T^{\text{miss}} / \sqrt{H_T} > 5$ GeV $^{1/2}$, where in this case E_T^{miss} still includes the contribution from the electron energy deposits in the calorimeter and H_T denotes the scalar sum of the p_T of the identified jets in the final state.

Finally, a control sample enriched in $t\bar{t}$ events is constructed using the same selection criteria as in the case of the $W(\rightarrow \mu\nu)$ +jets but requiring that at least one of the jets is b -tagged.

6.2 Multijet background

The multijet background with large E_T^{miss} mainly originates from the misreconstruction of the energy of a jet in the calorimeter and to a lesser extent is due to the presence of neutrinos in the final state from heavy-flavour hadron decays. In this analysis, the multijet background is determined from data, using the jet smearing method as described in Ref. [83], which relies on the assumption that the E_T^{miss} value of multijet events is dominated by fluctuations in the jet response in the detector, which can be measured in the data. For the IM1 and EM1 selections, the multijet background constitutes about 0.3% and 0.4% of the total background, respectively, and it is negligible for the other signal regions.

6.3 Non-collision background

Remaining non-collision background contributions in the signal regions, mostly from muons originating in the particle cascades due to beam-halo protons intercepting the LHC collimators, are estimated following closely the methods set out in Ref. [82]. In particular, the jet timing, t_j , calculated from the energy-weighted average of the time of the jet energy deposits, defined with respect to the event time in nominal collisions, is used. A dedicated region enhanced in beam-induced background, defined by inverting the tight jet-quality selection imposed on the leading jet, is used to estimate the amount of non-collision background from the fraction of events with a leading-jet timing $|t_j| > 5$ ns. The results indicate an almost negligible contribution from non-collision backgrounds in the signal regions.

6.4 Background fit

The use of control regions to constrain the normalization of the dominant background contributions reduces the relatively large theoretical and experimental systematic uncertainties, of the order of 20%–40%, associated with purely simulation-based background predictions in the signal regions. A complete study of systematic uncertainties is carried out, as detailed in Section 7. To determine the final uncertainty in the total background, all systematic uncertainties are treated as Gaussian-distributed nuisance parameters in a fit based on the profile likelihood method [84], which takes into account correlations among systematic variations. The likelihood also takes into account cross-contamination between different background sources in the control regions.

The E_T^{miss} distribution is the observable used. A simultaneous background-only likelihood fit to the E_T^{miss} distributions in the $W(\rightarrow \mu\nu)+\text{jets}$, $W(\rightarrow e\nu)+\text{jets}$, $Z/\gamma^*(\rightarrow \mu^+\mu^-)+\text{jets}$, and top control regions is performed to normalize and constrain the background estimates in the signal regions. In the analysis, two different fitting strategies are considered, potentially giving slightly different results. A binned likelihood fit is performed using simultaneously all the exclusive E_T^{miss} regions EM1–EM10, as described in Section 5. The fit includes a single floating normalization factor common to all $W+\text{jets}$ and $Z+\text{jets}$ processes, and a single floating normalization factor for top-quark-related processes. The nuisance parameters, implementing the impact of systematic uncertainties, are defined bin-by-bin and correlations across E_T^{miss} bins are taken into account. As a result, the fit exploits the information of the shape of the E_T^{miss} distribution in constraining the normalization of $W/Z+\text{jets}$ and top-quark-related background. In addition, one-bin likelihood fits are performed separately for each of the inclusive regions IM1–IM10. In this case, the two normalization factors for $W/Z+\text{jets}$ and top-quark-related processes, respectively, and the nuisance parameters related to systematic uncertainties refer to the given E_T^{miss} inclusive region.

The results of the background-only fit in the control regions are presented in Table 2 for the $E_T^{\text{miss}} > 250 \text{ GeV}$ inclusive selection. The $W/Z+\text{jets}$ background predictions receive a multiplicative normalization factor of 1.27. Similarly, top-quark-related processes receive a normalization factor of 1.06. When the binned likelihood fit is performed simultaneously over the different exclusive E_T^{miss} regions, thus including information from the shape of the measured E_T^{miss} distribution, the normalization factor of the $W/Z+\text{jets}$ background predictions remains essentially unchanged, dominated by the low- E_T^{miss} region, and that of the top-quark-related processes becomes 1.31, correlated with a less than 1σ pull of the top-quark-related uncertainties within the fit.

Figures 2 and 3 show the distributions of the E_T^{miss} and the leading-jet p_T in data and MC simulation in the different control regions. In this case, the MC predictions include the data-driven normalization factors as extracted from the binned likelihood fit to the different exclusive E_T^{miss} bins. Altogether, the MC simulation provides a good description, within uncertainties, of the shape of the measured distributions in the different control regions.

Table 2: Data and background predictions in the control regions before and after the fit is performed for the $E_T^{\text{miss}} > 250$ GeV inclusive selection. The background predictions include both the statistical and systematic uncertainties. The individual uncertainties are correlated, and do not necessarily add in quadrature to the total background uncertainty. The dash “–” denotes negligible background contributions.

$E_T^{\text{miss}} > 250$ GeV Control Regions	$W(\rightarrow \mu\nu)$	$W(\rightarrow e\nu)$	$Z/\gamma^*(\rightarrow \mu^+\mu^-)$	Top
Observed events (36.1 fb^{-1})	110938	68973	17372	9729
SM prediction (post-fit)	110810 ± 350	69030 ± 260	17440 ± 130	9720 ± 130
$W(\rightarrow e\nu)$	7 ± 2	54500 ± 1000	–	$0.2_{-0.2}^{+0.4}$
$W(\rightarrow \mu\nu)$	94940 ± 900	7 ± 7	32 ± 3	2160 ± 650
$W(\rightarrow \tau\nu)$	5860 ± 160	4110 ± 140	3 ± 1	164 ± 40
$Z/\gamma^*(\rightarrow e^+e^-)$	–	5 ± 4	–	–
$Z/\gamma^*(\rightarrow \mu^+\mu^-)$	1774 ± 75	0.4 ± 0.2	16360 ± 160	59 ± 12
$Z/\gamma^*(\rightarrow \tau^+\tau^-)$	277 ± 21	212 ± 15	16 ± 3	12 ± 2
$Z(\rightarrow \nu\bar{\nu})$	37 ± 3	1.8 ± 0.3	–	6 ± 1
$t\bar{t}$, single top	4700 ± 790	8200 ± 1000	486 ± 64	7220 ± 820
Diboson	3220 ± 230	2020 ± 160	540 ± 39	108 ± 38
SM prediction from simulation (pre-fit)	87500 ± 8700	56600 ± 5600	14100 ± 1400	9200 ± 2000
$W(\rightarrow e\nu)$	5 ± 1	43300 ± 4700	–	$0.15_{-0.15}^{+0.41}$
$W(\rightarrow \mu\nu)$	73700 ± 7900	5 ± 5	24 ± 3	1960 ± 580
$W(\rightarrow \tau\nu)$	4600 ± 480	3260 ± 350	2.2 ± 0.5	148 ± 37
$Z/\gamma^*(\rightarrow e^+e^-)$	–	6 ± 5	–	–
$Z/\gamma^*(\rightarrow \mu^+\mu^-)$	1420 ± 160	0.5 ± 0.2	13100 ± 1400	53 ± 11
$Z/\gamma^*(\rightarrow \tau^+\tau^-)$	226 ± 29	175 ± 20	13 ± 3	10 ± 2
$Z(\rightarrow \nu\bar{\nu})$	30 ± 4	1.5 ± 0.3	–	5 ± 1
$t\bar{t}$, single top	4300 ± 1200	7800 ± 2100	460 ± 120	6900 ± 1800
Diboson	3180 ± 230	2050 ± 170	541 ± 40	128 ± 44

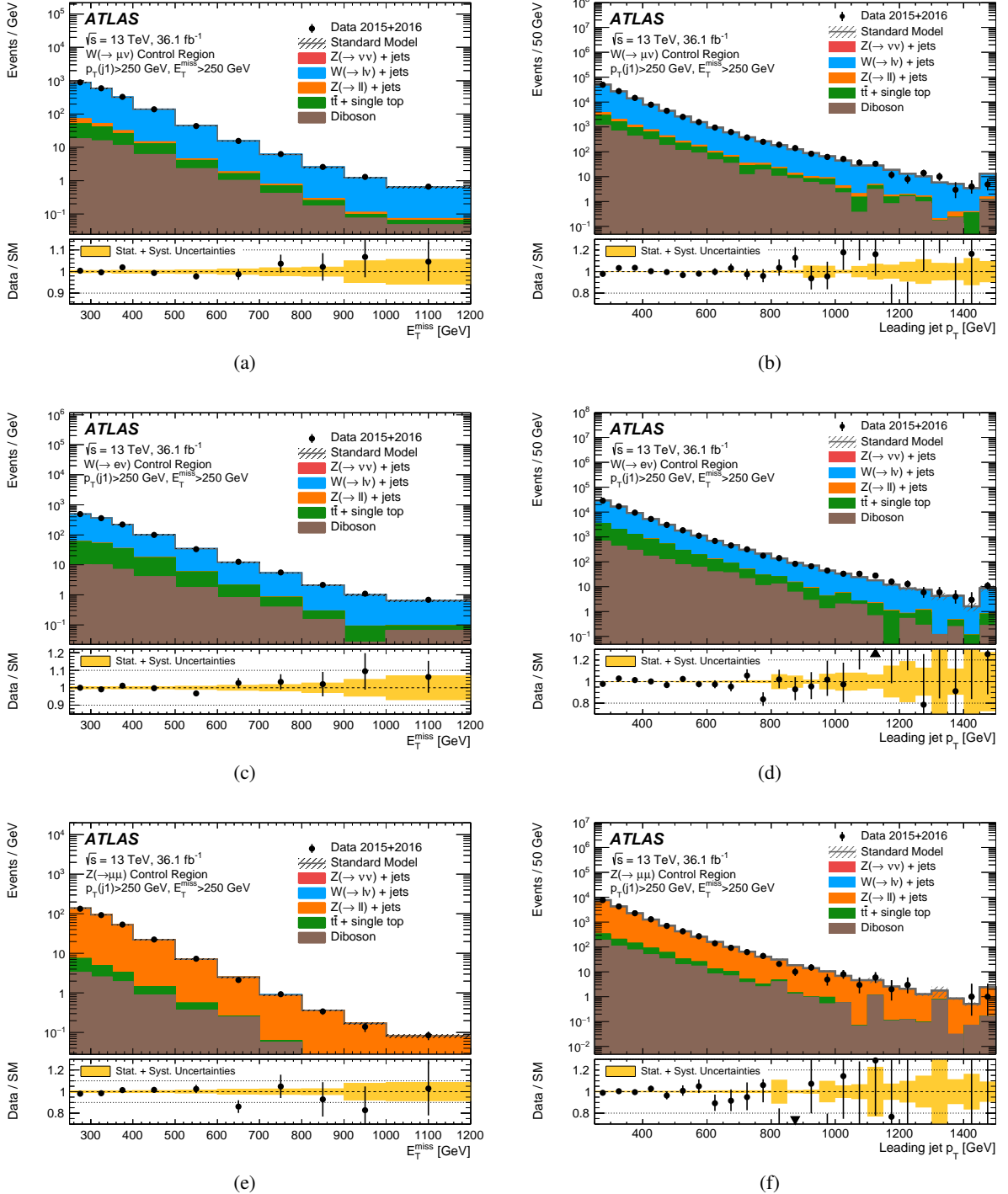


Figure 2: The measured (a),(c),(e) E_T^{miss} and (b),(d),(f) leading-jet p_T distributions in the $W(\rightarrow \mu\nu)+\text{jets}$, $W(\rightarrow e\nu)+\text{jets}$, and $Z/\gamma^*(\rightarrow \mu^+\mu^-)+\text{jets}$ control regions, for the $E_T^{\text{miss}} > 250$ GeV inclusive selection, compared to the background predictions. The latter include the global normalization factors extracted from the fit. The error bands in the ratios include the statistical and systematic uncertainties in the background predictions as determined by the binned-likelihood fit to the data in the control regions. The last bin of the E_T^{miss} and leading-jet p_T distributions contains overflows. The contributions from multijet and non-collision backgrounds are negligible and are not shown in the Figures.

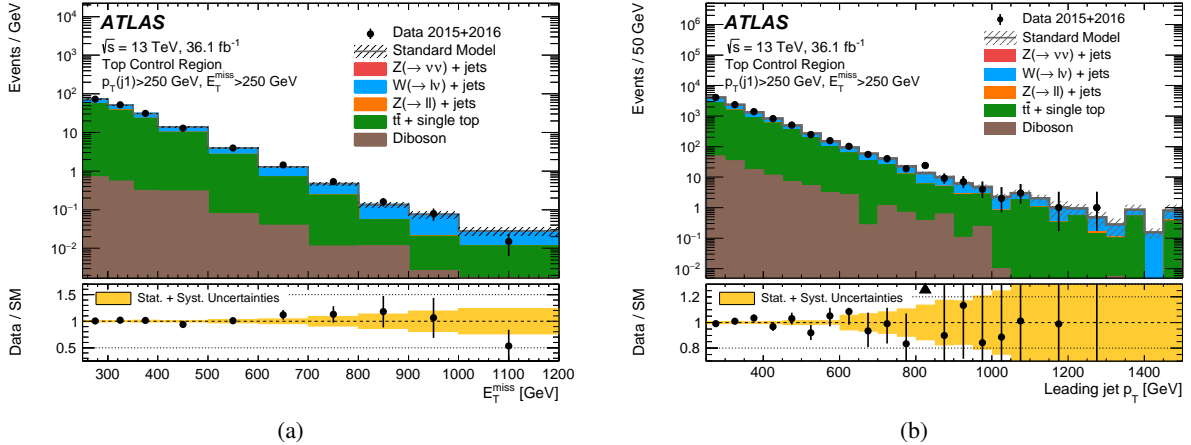


Figure 3: The measured (a) E_T^{miss} and (b) leading-jet p_T distributions in the top control region, for the $E_T^{\text{miss}} > 250$ GeV inclusive selection, compared to the background predictions. The latter include the global normalization factors extracted from the fit. The error bands in the ratios include the statistical and systematic uncertainties in the background predictions as determined by the binned-likelihood fit to the data in the control regions. The last bin of the E_T^{miss} and leading-jet p_T distributions contains overflows. The contributions from multijet and non-collision backgrounds are negligible and are not shown in the Figures.

7 Systematic uncertainties

In this Section, the systematic uncertainties for both the background and signal models are presented. The impacts of the various sources of systematic uncertainty on the total background predictions are determined by the likelihood fits described in Section 6.4. Inclusive and exclusive E_T^{miss} selections are considered separately. For the latter, correlations of systematic uncertainties across E_T^{miss} bins are taken into account. The impact of the different sources of uncertainty in representative inclusive E_T^{miss} bins, as determined using one-bin likelihood fits, is presented below. Experimental and theoretical uncertainties in the signal model predictions are also presented.

7.1 Background systematic uncertainties

Uncertainties in the absolute jet and E_T^{miss} energy scales and resolutions [73] translate into uncertainties in the total background which vary between 0.5% for IM1 and 5.3% for IM10. Uncertainties related to jet quality requirements, pile-up description and corrections to the jet p_T and E_T^{miss} introduce a 0.9% to 1.8% uncertainty in the background predictions. Uncertainties in the b -tagging efficiency, relevant for the definition of the $W(->\mu\nu)$ +jets and $t\bar{t}$ control regions, translate into an uncertainty in the total background that varies between 0.9% for IM1 and 0.5% for IM10. Uncertainties in soft contributions to E_T^{miss} translate into an uncertainty in the total background yields that varies between 0.4% for IM1 and 1.7% for IM10.

Uncertainties in the simulated lepton identification and reconstruction efficiencies, energy/momentum scale and resolution [78, 85, 86] translate into an uncertainty in the total background which varies between 0.2% and 1.7% for IM1 and between 0.3% and 2.3% for IM10 selection.

Uncertainties in W/Z +jets predictions [65, 87] related to the modelling of parton showers in **SHERPA** and the choice of PDFs translate into an uncertainty in the total background that varies between 0.8% for IM1 and 0.7% for IM10. Uncertainties on the implementation of higher-order QCD and electroweak parton-level calculations in the MC predictions, as described in Ref. [64], include: uncertainties in the QCD renormalization/factorization scales, affecting both the normalization and the shape of the predicted boson- p_T distribution; uncertainties associated with the non-universality of QCD corrections across W +jets and Z +jets processes; uncertainties in electroweak corrections beyond NNLO, unknown electroweak NLO correction terms at very high boson- p_T , and limitations of the Sudakov approximation adopted in the calculation; uncertainties in the QCD and electroweak interference terms; and uncertainties on the implementation of the higher-order QCD corrections in **SHERPA**, affected by a limited MC statistics at large boson- p_T . Altogether, this translates into an uncertainty in the total background that varies between 0.4% for IM1 and 2% for IM10.

Theoretical uncertainties in the predicted background yields for top-quark-related processes include variations in parton-shower parameters and the amount of initial- and final-state soft gluon radiation, and the difference between predictions from different MC event generators [88]. This introduces an uncertainty in the total background of about 0.3% for IM1, becoming negligible at very high E_T^{miss} .

Uncertainties in the diboson contribution are estimated as the difference between the yields of the **SHERPA** and PowHEG event generators [89], after taking into account the difference between the cross sections, which is then summed in quadrature with a 6% theory uncertainty in the NLO cross section. This translates into an uncertainty on the total background of about 0.2% for IM1 and about 0.8% for IM10.

Uncertainties in the estimation of multijet and non-collision backgrounds translate into a 0.5% uncertainty of the total background for IM1 and have a negligible impact on the total background predictions at larger E_T^{miss} . Similarly, the 3.2% uncertainty in the integrated luminosity is included in the fit. It nearly cancels out in the data-driven determination of the SM background and translates into an uncertainty in the total background yield of about 0.1% for IM1.

7.2 Signal systematic uncertainties

Sources of systematic uncertainty in the predicted signal yields are considered separately for each model of new physics using a common set of procedures. The procedures are described here, while the numerical uncertainties are given with the associated results for each model in Section 8. Experimental uncertainties include those related to the jet and E_T^{miss} reconstruction, energy scales and resolutions, and the integrated luminosity. Other uncertainties related to the jet quality requirements are negligible.

Uncertainties affecting the signal acceptance in the generation of signal samples include: uncertainties in the modelling of the initial- and final-state gluon radiation, determined using simulated samples with modified parton-shower parameters (by factors of two or one half); uncertainties due to PDFs and variations of the $\alpha_s(m_Z)$ value employed, as computed from the envelope of CT10, MMHT2014 [90] and NNPDF30 error sets; and uncertainties due to the choice of renormalization and factorization scales. In addition, theoretical uncertainties in the predicted cross sections, including PDF and renormalization- and factorization-scale uncertainties, are assessed separately for the different models.

Table 3: Data and SM background predictions in the signal region for several inclusive E_T^{miss} selections, as determined using separate one-bin likelihood fits in the control regions. For the SM prediction, both the statistical and systematic uncertainties are included. In each signal region, the individual uncertainties for the different background processes can be correlated, and do not necessarily add in quadrature to the total background uncertainty. The dash “–” denotes negligible background contributions.

Inclusive Signal Region	IM1	IM3	IM5	IM7	IM10
Observed events (36.1 fb^{-1})	255486	76808	13680	2122	245
SM prediction	245900 ± 5800	73000 ± 1900	12720 ± 340	2017 ± 90	238 ± 23
$W(\rightarrow e\nu)$	20600 ± 620	4930 ± 220	682 ± 33	63 ± 8	7 ± 2
$W(\rightarrow \mu\nu)$	20860 ± 840	5380 ± 280	750 ± 44	115 ± 13	17 ± 2
$W(\rightarrow \tau\nu)$	50300 ± 1500	12280 ± 520	1880 ± 63	261 ± 13	24 ± 3
$Z/\gamma^*(\rightarrow e^+e^-)$	0.11 ± 0.03	0.03 ± 0.01	–	–	–
$Z/\gamma^*(\rightarrow \mu^+\mu^-)$	564 ± 32	107 ± 9	10 ± 1	1.8 ± 0.5	0.2 ± 0.2
$Z/\gamma^*(\rightarrow \tau^+\tau^-)$	812 ± 32	178 ± 8	24 ± 1	3.5 ± 0.5	0.4 ± 0.1
$Z(\rightarrow \nu\bar{\nu})$	137800 ± 3900	45700 ± 1300	8580 ± 260	1458 ± 76	176 ± 18
$t\bar{t}$, single top	8600 ± 1100	2110 ± 280	269 ± 42	26 ± 10	0 ± 1
Diboson	5230 ± 400	2220 ± 170	507 ± 64	88 ± 19	13 ± 4
Multijet background	700 ± 700	51 ± 50	8 ± 8	1 ± 1	0.1 ± 0.1
Non-collision background	360 ± 360	51 ± 51	4 ± 4	–	–

8 Results and interpretation

The number of events in the data and the individual background predictions in several inclusive and exclusive signal regions, as determined using the background estimation procedure discussed in Section 6.4, are presented in Tables 3 and 4. The results for all the signal regions are summarized in Table 5. Good agreement is observed between the data and the SM predictions in each case. The SM predictions for the inclusive selections are determined with a total uncertainty of 2.4%, 2.7%, and 9.7% for the IM1, IM5, and IM10 signal regions, respectively, which include correlations between uncertainties in the individual background contributions.

Figure 4 shows several measured distributions compared to the SM predictions in the region $E_T^{\text{miss}} > 250 \text{ GeV}$, for which the normalization factors applied to the MC predictions, and the related uncertainties, are determined from the global fit carried out in exclusive E_T^{miss} bins. For illustration purposes, the distributions include the impact of example ADD, SUSY, and WIMP scenarios. In general, the SM predictions provide a good description of the measured distributions. The differences observed in the jet multiplicity distribution do not have an impact in the results. Statistical tests using the binned profile likelihood fit described above, and considering different scenarios for new physics, give p -values for a background-only hypothesis in the range 0.01–0.04, corresponding to agreement with the SM predictions within approximately 2.1σ to 1.7σ .

The levels of agreement between the data and the SM predictions for the total number of events in inclusive and exclusive signal regions are translated into upper limits for the presence of new phenomena, using a simultaneous likelihood fit in both the control and signal regions, and the CL_s modified frequentist approach [91]. The inclusive regions are used to set model-independent exclusion limits, and the exclusive regions are used for the interpretation of the results within different models of new physics. In general, the observed exclusion limits are worse than the expected sensitivity due to the slight excess of events in

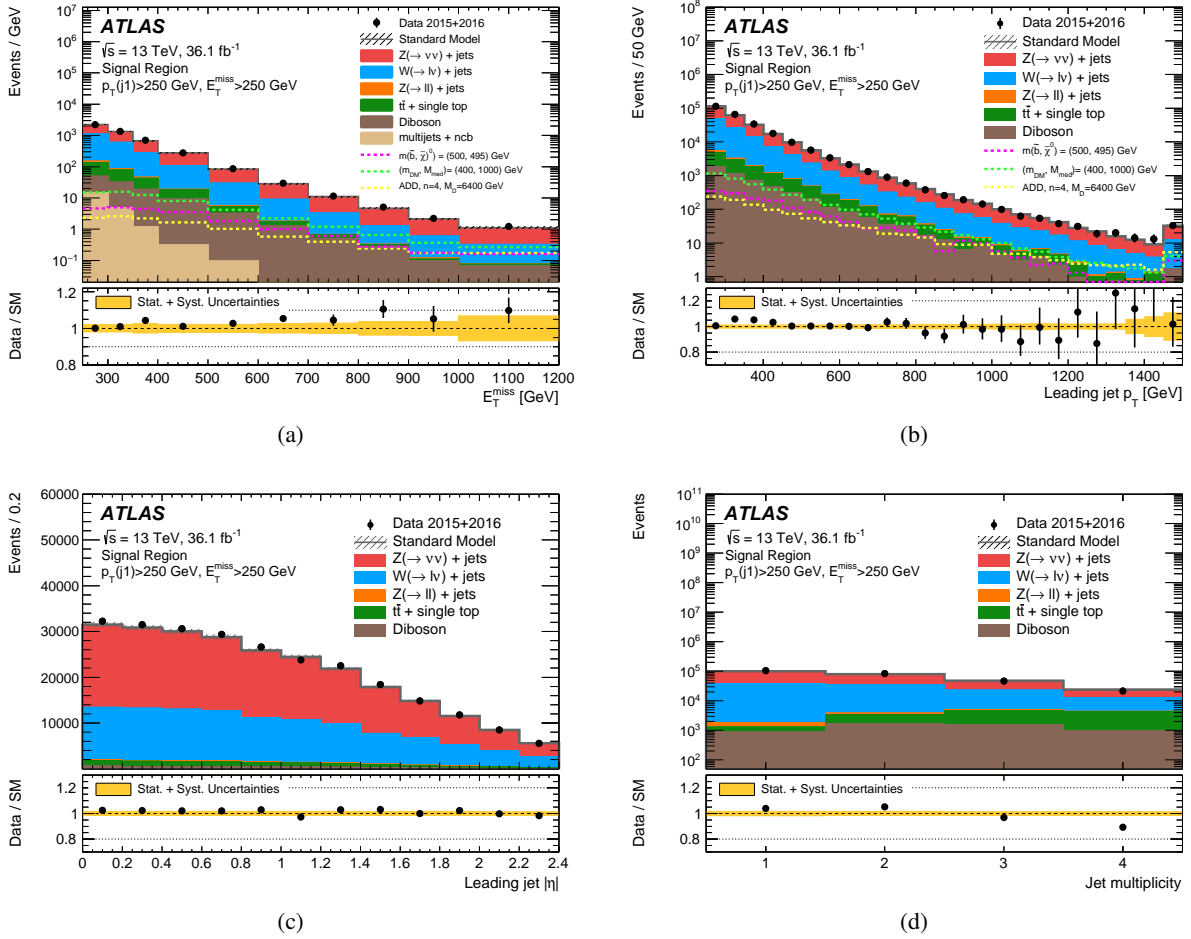


Figure 4: Measured distributions of the (a) E_T^{miss} , (b) leading-jet p_T , (c) leading-jet $|\eta|$, and (d) jet multiplicity for the $E_T^{\text{miss}} > 250$ GeV selection compared to the SM predictions. The latter are normalized with normalization factors as determined by the global fit that considers exclusive E_T^{miss} regions. For illustration purposes, the distributions of example ADD, SUSY, and WIMP scenarios are included. The error bands in the ratios shown in the lower panels include both the statistical and systematic uncertainties in the background predictions. The last bin of the E_T^{miss} and leading-jet p_T distributions contains overflows. The contributions from multijet and non-collision backgrounds are negligible and are only shown in the case of the E_T^{miss} distribution.

the data compared to the SM predictions, as shown in Table 5.

8.1 Model-independent exclusion limits

A likelihood fit is performed separately for each of the inclusive regions IM1–IM10. As a result, model-independent observed and expected 95% confidence level (CL) upper limits on the visible cross section, defined as the product of production cross section, acceptance and efficiency $\sigma \times A \times \epsilon$, are extracted from the ratio between the 95% CL upper limit on the number of signal events and the integrated luminosity, taking into consideration the systematic uncertainties in the SM backgrounds and the uncertainty in the integrated luminosity. The results are presented in Table 6. Values of $\sigma \times A \times \epsilon$ above 531 fb (for IM1)

Table 4: Data and SM background predictions in the signal region for several exclusive E_T^{miss} selections, as determined using a binned likelihood fit in the control regions. For the SM prediction, both the statistical and systematic uncertainties are included. In each signal region, the individual uncertainties for the different background processes can be correlated, and do not necessarily add in quadrature to the total background uncertainty. The dash “–” denotes negligible background contributions.

Exclusive Signal Region	EM2	EM4	EM6	EM8	EM9
Observed events (36.1 fb^{-1})	67475	27843	2975	512	223
SM prediction	67100 ± 1400	27640 ± 610	2825 ± 78	463 ± 19	213 ± 9
$W(\rightarrow e\nu)$	5510 ± 140	1789 ± 59	147 ± 9	18 ± 1	8 ± 1
$W(\rightarrow \mu\nu)$	6120 ± 200	2021 ± 82	173 ± 9	21 ± 5	11 ± 1
$W(\rightarrow \tau\nu)$	13680 ± 310	4900 ± 110	397 ± 11	55 ± 5	29 ± 2
$Z/\gamma^*(\rightarrow e^+e^-)$	0.03 ± 0	0.02 ± 0.02	–	–	–
$Z/\gamma^*(\rightarrow \mu^+\mu^-)$	167 ± 8	36 ± 2	2.0 ± 0.2	0.4 ± 0.1	0.5 ± 0.1
$Z/\gamma^*(\rightarrow \tau^+\tau^-)$	185 ± 6	68 ± 4	5.1 ± 0.3	0.3 ± 0.1	0.31 ± 0.04
$Z(\rightarrow \nu\bar{\nu})$	37600 ± 970	17070 ± 460	1933 ± 57	337 ± 12	153 ± 7
$t\bar{t}$, single top	2230 ± 200	848 ± 86	43 ± 6	4 ± 1	1.3 ± 0.4
Diboson	1327 ± 90	874 ± 64	124 ± 16	26 ± 5	10 ± 2
Multijet background	170 ± 160	13 ± 13	1 ± 1	1 ± 1	0.1 ± 0.1
Non-collision background	71 ± 71	18 ± 18	–	–	–

Table 5: Data and SM background predictions in the signal region for the different selections. For the SM predictions both the statistical and systematic uncertainties are included.

Region	Inclusive Signal Region		Exclusive Signal Region		
	Predicted	Observed	Region	Predicted	Observed
IM1	245900 ± 5800	255486	EM1	111100 ± 2300	111203
IM2	138000 ± 3400	144283	EM2	67100 ± 1400	67475
IM3	73000 ± 1900	76808	EM3	33820 ± 940	35285
IM4	39900 ± 1000	41523	EM4	27640 ± 610	27843
IM5	12720 ± 340	13680	EM5	8360 ± 190	8583
IM6	4680 ± 160	5097	EM6	2825 ± 78	2975
IM7	2017 ± 90	2122	EM7	1094 ± 33	1142
IM8	908 ± 55	980	EM8	463 ± 19	512
IM9	464 ± 34	468	EM9	213 ± 9	223
IM10	238 ± 23	245	EM10	226 ± 16	245

and above 1.6 fb (for IM10) are excluded at 95% CL.

8.2 Weakly interacting massive particles

The results are translated into exclusion limits on WIMP-pair production. Different simplified models are considered with the exchange of an axial-vector, vector or a pseudoscalar mediator in the s -channel. In addition, a model with the exchange of a coloured scalar mediator is considered, as described in Section 1.

In the case of the exchange of an axial-vector mediator, and for WIMP-pair production with $m_{Z_A} > 2m_\chi$, typical $A \times \epsilon$ values for the signal models with a 1 TeV mediator range from 25% to 0.4% for IM1 and

Table 6: Observed and expected 95% CL upper limits on the number of signal events, S_{obs}^{95} and S_{exp}^{95} , and on the visible cross section, defined as the product of cross section, acceptance and efficiency, $\langle\sigma\rangle_{\text{obs}}^{95}$, for the IM1–IM10 selections.

Selection	$\langle\sigma\rangle_{\text{obs}}^{95}$ [fb]	S_{obs}^{95}	S_{exp}^{95}
IM1	531	19135	11700^{+4400}_{-3300}
IM2	330	11903	7000^{+2600}_{-2600}
IM3	188	6771	4000^{+1400}_{-1100}
IM4	93	3344	2100^{+770}_{-590}
IM5	43	1546	770^{+280}_{-220}
IM6	19	696	360^{+130}_{-100}
IM7	7.7	276	204^{+74}_{-57}
IM8	4.9	178	126^{+47}_{-35}
IM9	2.2	79	76^{+29}_{-21}
IM10	1.6	59	56^{+21}_{-16}

IM10 selections, respectively. Very similar values are obtained in the case of the vector mediator, whereas $A \times \epsilon$ values in the range between 32% and 1% are computed for the pseudoscalar mediator model with $m_{Z_P} = 1$ TeV and $m_\chi = 10$ GeV. Finally, in the case of the coloured scalar mediator, $A \times \epsilon$ values in the range from 35% to 0.7% are obtained for IM1 and IM10 selections, respectively, for a mediator mass of 1 TeV and $m_\eta \gg m_\chi$.

The experimental uncertainties related to the jet and E_T^{miss} scales and resolutions introduce similar uncertainties in the signal yields for axial-vector, vector and pseudoscalar models. They vary between 2% and 7% for the IM1 selection and between 3% and 9% for the IM10 selection, depending on the parameters of the model. In the case of the coloured scalar mediator model, these uncertainties vary between 2% and 6% for IM1 and between 4% and about 10% for IM10. The uncertainty related to the modelling of the initial- and final-state radiation translates into a 20% uncertainty in the signal acceptance, common to all the s -channel models. In the case of the coloured scalar mediator model, this uncertainty varies between 10% and 30%, depending on the kinematic selection. The choice of different PDF sets results in up to a 20% uncertainty in the acceptance and up to a 10% uncertainty in the cross section, depending on the model considered. Varying the renormalization and factorization scales introduces up to 25% variations of the cross section and up to 10% change in the acceptance, depending on the model considered. In addition, the uncertainty in the integrated luminosity is included.

A simultaneous fit to the signal and control regions in the exclusive E_T^{miss} bins is performed, and used to set observed and expected 95% CL exclusion limits on the parameters of the model. Uncertainties in the signal acceptance times efficiency, the background predictions, and the luminosity are considered, and correlations between systematic uncertainties in signal and background predictions are taken into account. The fit accounts for the contamination of the control regions by signal events which a priori is estimated to be very small.

Figure 5(a) shows the observed and expected 95% CL exclusion contours in the m_{Z_A} – m_χ parameter plane for a simplified model with an axial-vector mediator, Dirac WIMPs, and couplings $g_q = 1/4$ and $g_\chi = 1$. In addition, observed limits are shown using $\pm 1\sigma$ theoretical uncertainties in the signal cross sections.

In the on-shell regime, the models with mediator masses up to 1.55 TeV are excluded for $m_\chi = 1$ GeV. For $m_\chi < 1$ GeV, the monojet analysis maintains its sensitivity for excluding DM models. This analysis loses sensitivity to the models in the off-shell regime, where cross sections are suppressed due to the virtual production of the mediator. Perturbative unitarity is violated in the parameter region defined by $m_\chi > \sqrt{\pi/2} m_{Z_A}$ [92]. The masses corresponding to the relic density [93] as determined by the Planck and WMAP satellites [9, 10], within the WIMP dark-matter model and in the absence of any interaction other than the one considered, are indicated in the Figure as a line that crosses the excluded region at $m_{Z_A} \sim 1200$ GeV and $m_\chi \sim 440$ GeV. The region towards lower WIMP masses or higher mediator masses corresponds to dark-matter overproduction.

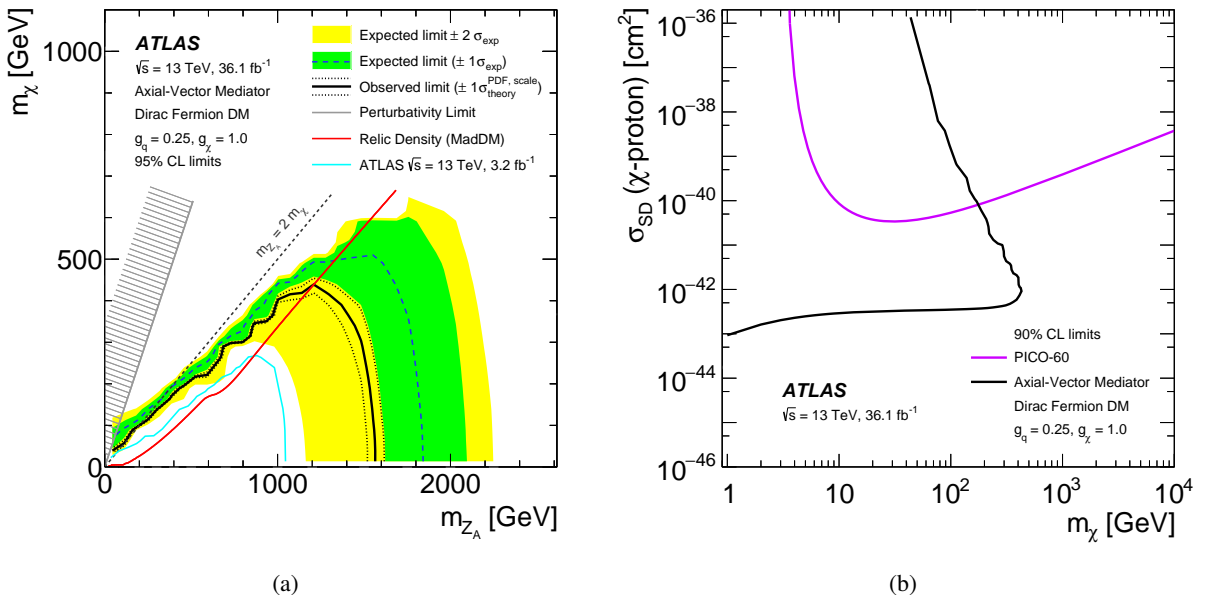


Figure 5: (a) Axial-vector 95% CL exclusion contours in the m_{Z_A} – m_χ parameter plane. The solid (dashed) curve shows the observed (expected) limit, while the bands indicate the $\pm 1\sigma$ theory uncertainties in the observed limit and $\pm 1\sigma$ and $\pm 2\sigma$ ranges of the expected limit in the absence of a signal. The red curve corresponds to the set of points for which the expected relic density is consistent with the WMAP measurements (i.e. $\Omega h^2 = 0.12$), as computed with MADDM [94]. The region on the right of the curve corresponds to higher predicted relic abundance than these measurements. The region excluded due to perturbativity, defined by $m_\chi > \sqrt{\pi/2} m_{Z_A}$, is indicated by the hatched area. The dotted line indicates the kinematic limit for on-shell production $m_{Z_A} = 2 \times m_\chi$. The cyan line indicates previous results at 13 TeV [1] using 3.2 fb^{-1} . (b) A comparison of the inferred limits (black line) to the constraints from direct detection experiments (purple line) on the spin-dependent WIMP–proton scattering cross section in the context of the simplified model with axial-vector couplings. Unlike in the m_{Z_A} – m_χ parameter plane, the limits are shown at 90% CL. The results from this analysis, excluding the region to the left of the contour, are compared with limits from the PICO [95] experiment. The comparison is model-dependent and solely valid in the context of this model, assuming minimal mediator width and the coupling values $g_q = 1/4$ and $g_\chi = 1$.

The results are translated into 90% CL exclusion limits on the spin-dependent WIMP–proton scattering cross section σ_{SD} as a function of the WIMP mass, following the prescriptions from Refs. [13, 93]. Among results from different direct-detection experiments, in Figure 5(b) the exclusion limits obtained in this analysis are compared to the most stringent limits from the PICO direct-detection experiment [95]. The limit at the maximum value of the WIMP–proton scattering cross section displayed corresponds to the lowest excluded values $m_{Z_A} = 45$ GeV and $m_\chi = 45$ GeV of the mediator and dark matter masses

displayed in Figure 5(a). This comparison is model-dependent and solely valid in the context of this particular model. In this case, stringent limits on the scattering cross section of the order of $2.9 \times 10^{-43} \text{ cm}^2$ ($3.5 \times 10^{-43} \text{ cm}^2$) for WIMP masses below 10 GeV (100 GeV) are inferred from this analysis, and complement the results from direct-detection experiments for $m_\chi < 10 \text{ GeV}$. The kinematic loss of model sensitivity is expressed by the turn of the WIMP exclusion line, reaching back to low WIMP masses and intercepting the exclusion lines from the direct-detection experiments at around $m_\chi = 200 \text{ GeV}$.

In Figure 6, the results are translated into 95% CL exclusion contours in the m_{Z_V} - m_χ parameter plane for the simplified model with a vector mediator, Dirac WIMPs, and couplings $g_q = 1/4$ and $g_\chi = 1$. The results are obtained from those for the axial-vector model, taking into account the cross-section differences between models, motivated by the fact that the two models present compatible particle-level selection acceptances. For very light WIMPs, mediator masses below about 1.55 TeV are excluded. As in the case of the axial-vector mediator model, in the regime $m_{Z_V} < 2m_\chi$, the sensitivity for exclusion is drastically reduced to low mass differences below 400 GeV in m_χ .

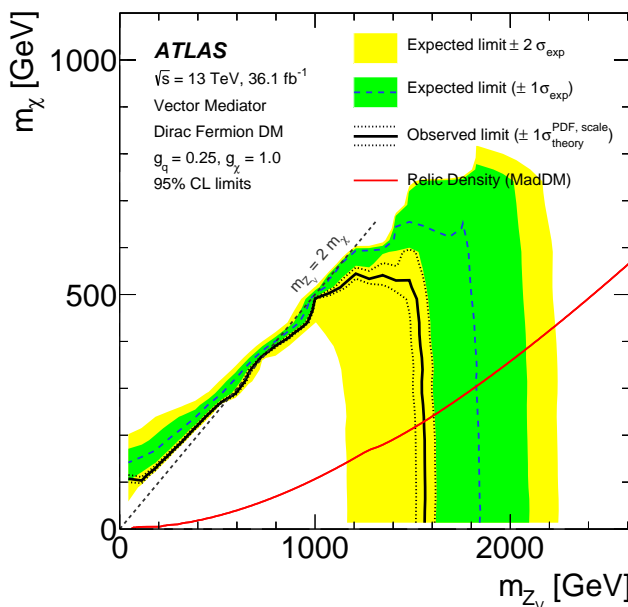


Figure 6: Observed (solid line) and expected (dashed line) exclusions at 95% CL on the vector mediator models with $g_q = 1/4$, $g_\chi = 1.0$ and minimal mediator width, as a function of the assumed mediator and DM masses. The regions within the drawn contours are excluded. The red curve corresponds to the set of points for which the expected relic density is consistent with the WMAP measurements (i.e. $\Omega h^2 = 0.12$), as computed with MADDM [94]. The region on the right of the curve corresponds to higher predicted relic abundance than these measurements. The dotted line indicates the kinematic limit for on-shell production $m_{Z_V} = 2 \times m_\chi$.

The simplified model with a pseudoscalar mediator was considered with couplings to quarks and dark matter equal to unity. For WIMP masses in the range 0–300 GeV and m_{Z_p} in the range 0–700 GeV, the analysis does not yet have enough sensitivity. As an example, Figure 7 presents the analysis sensitivity in terms of 95% CL limits on the signal strength, $\mu \equiv \sigma^{95\% \text{ CL}}/\sigma$, as a function of m_{Z_p} , for very light WIMPs, and as a function of m_χ , for $m_{Z_p} = 10 \text{ GeV}$. For mediator masses below 300 GeV and very light WIMPs, cross sections of the order of 2-to-3 times larger than that of the corresponding signal are excluded. For mediator masses above 300 GeV or larger dark-matter masses, the sensitivity of the analysis

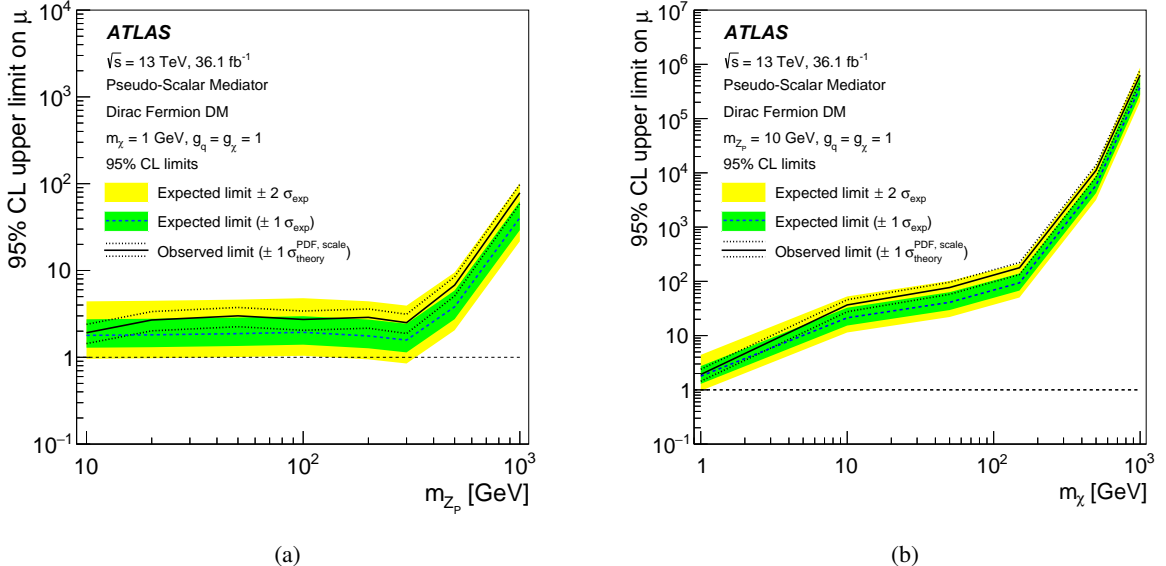


Figure 7: Observed and expected 95 % CL limits on the signal strength $\mu \equiv \sigma^{95\% \text{ CL}}/\sigma$ as a function of (a) the mediator mass for a very light WIMP and (b) the WIMP mass for $m_{Z_p} = 10 \text{ GeV}$, in a model with spin-0 pseudoscalar mediator and $g_q = g_\chi = 1.0$. The bands indicate the $\pm 1\sigma$ theory uncertainties in the observed limit and the $\pm 1\sigma$ and $\pm 2\sigma$ ranges of the expected limit in the absence of a signal.

to this particular model vanishes rapidly.

Finally, Figure 8 presents the observed and expected 95% CL exclusion contours in the m_η – m_χ parameter plane for the dark-matter production model with a coloured scalar mediator, Dirac WIMPs, and couplings set to $g = 1$. Mediator masses up to about 1.67 TeV are excluded at 95% CL for light dark-matter particles. In the case of $m_\chi = m_\eta$, masses up to 620 GeV are excluded.

8.3 Squark-pair production

Different models of squark-pair production are considered: stop-pair production with $\tilde{t}_1 \rightarrow c + \tilde{\chi}_1^0$, stop-pair production with $\tilde{t}_1 \rightarrow b + ff' + \tilde{\chi}_1^0$, sbottom-pair production with $\tilde{b}_1 \rightarrow b + \tilde{\chi}_1^0$, and squark-pair production with $\tilde{q} \rightarrow q + \tilde{\chi}_1^0$ ($q = u, d, c, s$). In each case separately, the results are translated into exclusion limits as a function of the squark mass for different neutralino masses.

The results are translated into exclusion limits on the pair production cross section of top squarks with $\tilde{t}_1 \rightarrow c + \tilde{\chi}_1^0$ (with branching fraction B=100%) as a function of the stop mass for different neutralino masses. The typical value of $A \times \epsilon$ of the selection criteria varies, with increasing stop and neutralino masses, between 0.7% and 1.4% for IM1, and between 0.04% and 1.3% for IM10. Observed and expected 95% CL exclusion limits are set as in the case of the WIMP models. In addition, observed limits are computed using $\pm 1\sigma$ variations of the theoretical predictions for the SUSY cross sections.

The uncertainties related to the jet and E_T^{miss} scales and resolutions introduce uncertainties in the signal yields which vary between 1% and 3% for different selections and squark and neutralino masses. In ad-

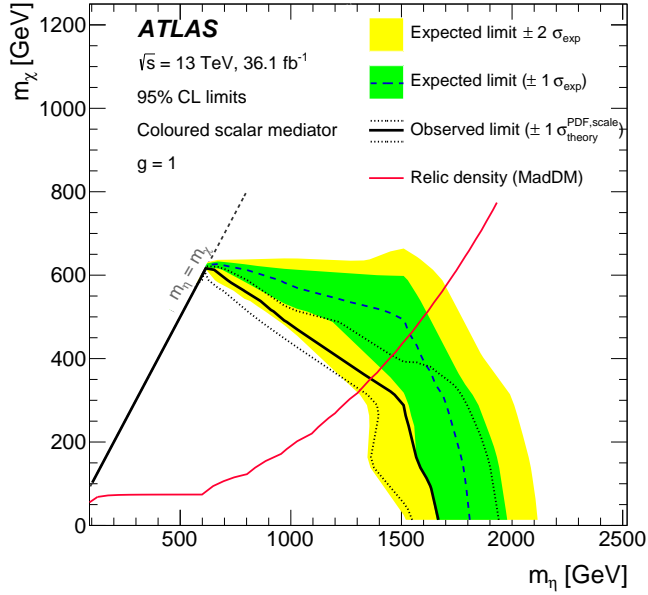


Figure 8: Exclusion contours at 95% CL in the m_η – m_χ parameter plane for the coloured scalar mediator model, with minimal width and coupling set to $g = 1$. The solid (dashed) curve shows the observed (expected) limit, while the bands indicate the $\pm 1\sigma$ theory uncertainties in the observed limit and $\pm 1\sigma$ and $\pm 2\sigma$ ranges of the expected limit in the absence of a signal. The red curve corresponds to the expected relic density, as computed with MADDM [94]. The kinematic limit for the mediator on-shell production $m_\eta = m_\chi$, is indicated by the dotted line.

dition, the uncertainty in the integrated luminosity is included. The uncertainties related to the modelling of initial- and final-state gluon radiation translate into a 7% to 17% uncertainty in the signal yields. The uncertainties due to the PDFs result in a 5% to 17% uncertainty in the signal yields. Finally, the variations of the renormalization and factorization scales introduce a 4% to 13% uncertainty in the signal yields.

Figure 9(a) presents the results in the case of the $\tilde{t}_1 \rightarrow c + \tilde{\chi}_1^0$ decays. The previous limits from the ATLAS Collaboration [1], corresponding to a luminosity of 3.2 fb^{-1} , are also shown. This analysis has significantly higher sensitivity at very low stop–neutralino mass difference. In the compressed scenario with the stop and neutralino nearly degenerate in mass, the exclusion extends up to stop masses of 430 GeV. The region with stop–neutralino mass differences below 5 GeV is not considered in the exclusion since in this regime the stop could become long-lived. Figure 9(b) shows the observed and expected 95% CL exclusion limits as a function of the stop and neutralino masses for the $\tilde{t}_1 \rightarrow b + ff' + \tilde{\chi}_1^0$ ($B=100\%$) decay channel. For $m_{\tilde{t}_1} - m_{\tilde{\chi}_1^0} \sim m_b$, stop masses up to 390 GeV are excluded at 95% CL.

Figure 10(a) presents the observed and expected 95% CL exclusion limits as a function of the sbottom and neutralino masses for the $\tilde{b}_1 \rightarrow b + \tilde{\chi}_1^0$ ($B=100\%$) decay channel. In the scenario with $m_{\tilde{b}_1} - m_{\tilde{\chi}_1^0} \sim m_b$, this analysis extends the 95% CL exclusion limits up to a sbottom mass of 430 GeV. In the case of light neutralinos with $m_{\tilde{\chi}_1^0} \sim 1 \text{ GeV}$, sbottom masses up to 610 GeV are excluded at 95% CL. Finally, Figure 10(b) presents the observed and expected 95% CL exclusion limits as a function of the squark mass and the squark–neutralino mass difference for $\tilde{q} \rightarrow q + \tilde{\chi}_1^0$ ($q = u, d, c, s$). In the compressed scenario with similar squark and neutralino masses, squark masses below 710 GeV are excluded at 95% CL. These results are a significant improvement on previous exclusion limits [1], and complement inclusive SUSY searches [96] in such mass-compressed regime.

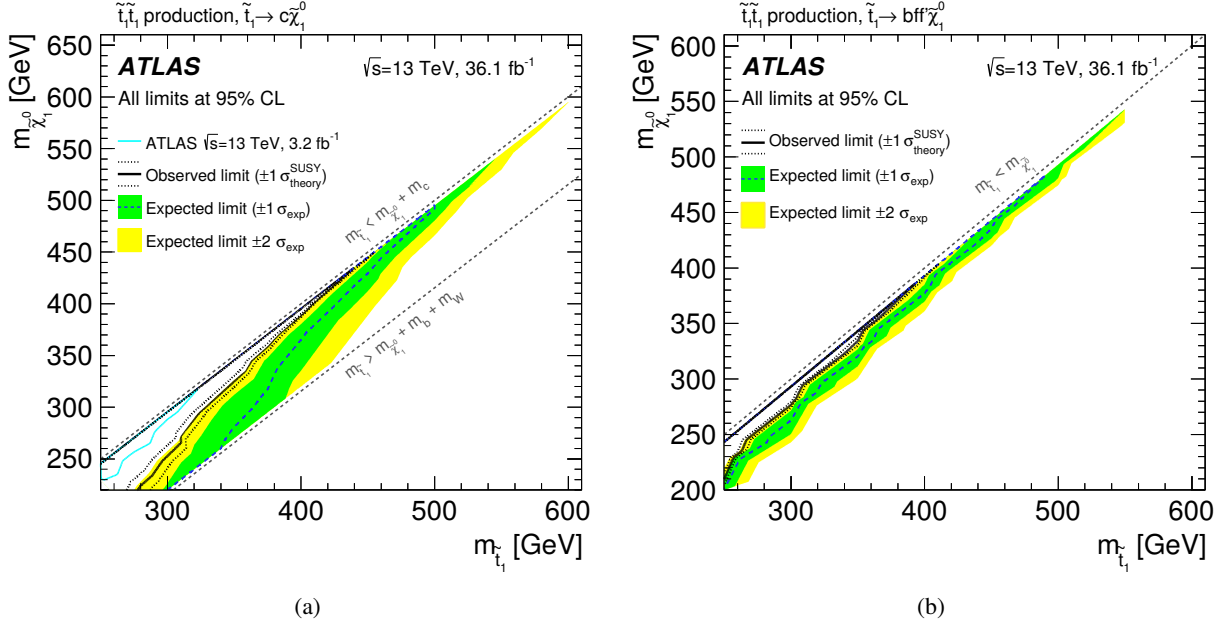


Figure 9: Excluded regions at the 95% CL in the $(\tilde{t}_1, \tilde{\chi}_1^0)$ mass plane for (a) the decay channel $\tilde{t}_1 \rightarrow c + \tilde{\chi}_1^0$ ($B = 100\%$) and (b) the decay channel $\tilde{t}_1 \rightarrow b + f' + \tilde{\chi}_1^0$ ($B=100\%$). The dotted lines around the observed limits indicate the range of observed limits corresponding to $\pm 1\sigma$ variations of the NLO SUSY cross-section predictions. The bands around the expected limits indicate the expected $\pm 1\sigma$ and $\pm 2\sigma$ ranges of limits in the absence of a signal. The results from this analysis are compared to previous results from the ATLAS Collaboration at $\sqrt{s} = 13$ TeV [1] using 3.2 fb^{-1} .

8.4 Large extra spatial dimensions

The level of agreement between the data and the SM predictions is also translated into limits on the parameters of the ADD model, as described in Section 1. Only the signal regions with $E_T^{\text{miss}} > 400 \text{ GeV}$, where the SM background is moderate and the shape difference between signal and the SM background becomes apparent, have sufficient sensitivity to ADD signal. The typical value of $A \times \epsilon$ of the selection criteria varies, as the number of extra dimensions n increases from $n = 2$ to $n = 6$, between 13% and 17% for IM4 and between 0.8% and 1.4% for IM10.

The effect of experimental uncertainties related to jet and E_T^{miss} scales and resolutions is found to be similar to the effect in the WIMP models. The uncertainties related to the modelling of the initial- and final-state gluon radiation translate into uncertainties in the ADD signal acceptance which vary between 11% and 13% with increasing E_T^{miss} and approximately independent of n . The uncertainties due to the PDFs, affecting the predicted signal yields, increase from 11% at $n = 2$ to 43% at $n = 6$. Similarly, the variations of the renormalization and factorization scales introduce a 23% to 36% uncertainty in the signal yields, with increasing n .

Observed and expected 95% CL exclusion limits are set as in the case of the WIMP and SUSY models. The -1σ variations of the ADD theoretical cross sections result in about a 7% to 10% decrease in the nominal observed limits, depending on n . Figure 11 and Table 7 present the results. Values of M_D below

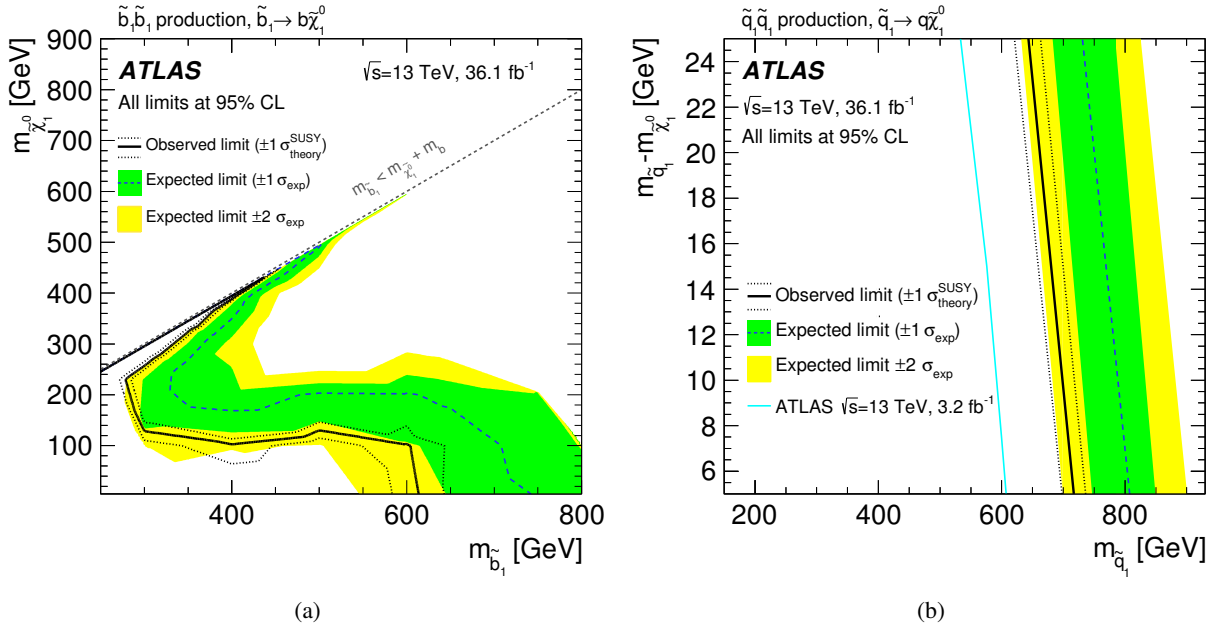


Figure 10: (a) Exclusion plane at 95% CL as a function of sbottom and neutralino masses for the decay channel $\tilde{b}_1 \rightarrow b + \tilde{\chi}_1^0$ (B=100%). (b) Exclusion region at 95% CL as a function of squark mass and the squark–neutralino mass difference for $\tilde{q} \rightarrow q + \tilde{\chi}_1^0$ ($q = u, d, c, s$). The dotted lines around the observed limit indicate the range of observed limits corresponding to $\pm 1\sigma$ variations of the NLO SUSY cross-section predictions. The bands around the expected limit indicates the expected $\pm 1\sigma$ and $\pm 2\sigma$ ranges of limits in the absence of a signal. The results from this analysis are compared to previous results from the ATLAS Collaboration at $\sqrt{s} = 13$ TeV [1] using 3.2 fb^{-1} .

7.7 TeV at $n = 2$ and below 4.8 TeV at $n = 6$ are excluded at 95% CL, which improve on the exclusion limits from previous results using 3.2 fb^{-1} of 13 TeV data [1].

As discussed in Refs. [14, 97], the analysis partially probes the phase-space region with $\hat{s} > M_D^2$, where $\sqrt{\hat{s}}$ is the centre-of-mass energy of the hard interaction. This challenges the validity of the model implementation and the lower bounds on M_D , as they depend on the unknown ultraviolet behaviour of the effective theory. The observed 95% CL limits are recomputed after suppressing, with a weighting factor M_D^4/\hat{s}^2 , the signal events with $\hat{s} > M_D^2$, here referred to as damping. This results in a negligible decrease of the quoted 95% CL lower limits on M_D , as also shown in Table 7.

Table 7: The 95% CL observed and expected lower limits on the fundamental Planck scale in $4 + n$ dimensions, M_D , as a function of the number of extra dimensions n , considering nominal LO signal cross sections. The impact of the $\pm 1\sigma$ theoretical uncertainty on the observed limits and the expected $\pm 1\sigma$ range of limits in the absence of a signal are also given. Finally, the 95% CL observed limits after damping of the signal cross section for $\hat{s} > M_D^2$ (see text) are quoted.

ADD Model Limits on M_D (95% CL)			
	Expected [TeV]	Observed [TeV]	Observed (damped) [TeV]
$n = 2$	$9.2^{+0.8}_{-1.0}$	$7.7^{+0.4}_{-0.5}$	7.7
$n = 3$	$7.1^{+0.5}_{-0.6}$	$6.2^{+0.4}_{-0.5}$	6.2
$n = 4$	$6.1^{+0.3}_{-0.4}$	$5.5^{+0.3}_{-0.5}$	5.5
$n = 5$	$5.5^{+0.3}_{-0.3}$	$5.1^{+0.3}_{-0.5}$	5.1
$n = 6$	$5.2^{+0.2}_{-0.3}$	$4.8^{+0.3}_{-0.5}$	4.8

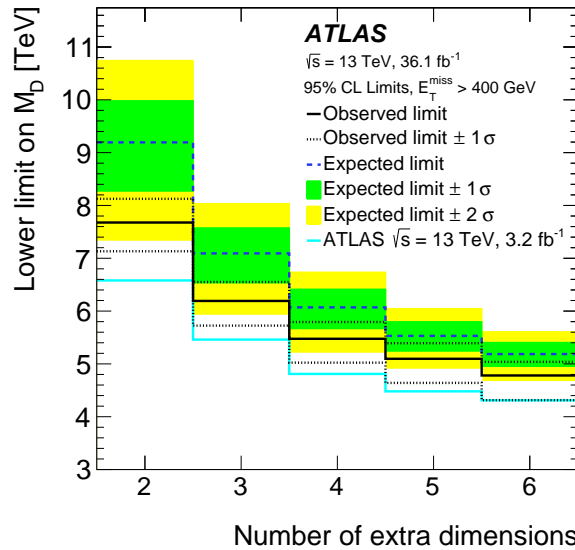


Figure 11: Observed and expected 95% CL lower limits on the fundamental Planck scale in $4 + n$ dimensions, M_D , as a function of the number of extra dimensions. The bands indicate the $\pm 1\sigma$ theory uncertainties in the observed limit and the $\pm 1\sigma$ and $\pm 2\sigma$ ranges of the expected limit in the absence of a signal. The 95% CL limits are computed with no suppression of the events with $\hat{s} > M_D^2$. The results from this analysis are compared to previous results from the ATLAS Collaboration using 3.2fb^{-1} of $\sqrt{s} = 13 \text{ TeV}$ data [1].

9 Conclusions

Results are reported from a search for new phenomena in events with an energetic jet and large missing transverse momentum in proton–proton collisions at $\sqrt{s} = 13$ TeV at the LHC, based on data corresponding to an integrated luminosity of 36.1 fb^{-1} collected by the ATLAS detector in 2015 and 2016. The measurements are in agreement with the SM predictions. The results are translated into model-independent 95% CL upper limits on $\sigma \times A \times \epsilon$ in the range $531\text{--}1.6 \text{ fb}$, decreasing with increasing missing transverse momentum.

The results are translated into exclusion limits on WIMP-pair production. Different simplified models are considered with the exchange of an axial-vector, vector or a pseudoscalar mediator in the s -channel, and with Dirac fermions as dark-matter candidates. In the case of axial-vector or vector mediator models, mediator masses below 1.55 TeV are excluded at 95% CL for very light WIMPs (for coupling values $g_q = 1/4$ and $g_\chi = 1$), whereas the analysis does not have the sensitivity to exclude a pseudoscalar scenario. In the case of the axial-vector mediator model, the results are translated, in a model-dependent manner, into upper limits on spin-dependent contributions to the WIMP–nucleon elastic cross section as a function of the WIMP mass. WIMP–proton cross sections above $2.9 \times 10^{-43} \text{ cm}^2$ ($3.5 \times 10^{-43} \text{ cm}^2$) are excluded at 90% CL for WIMP masses below 10 GeV (100 GeV), complementing results from direct-detection experiments. In addition, a simplified model of dark-matter production including a coloured scalar mediator is considered, for which mediator masses below 1.67 TeV are excluded at 95% CL for very light WIMPs (with coupling set to $g = 1$).

Similarly, the results are interpreted in terms of a search for squark-pair production in a compressed-mass supersymmetric scenario. In the case of stop- and sbottom-pair production with $\tilde{t}_1 \rightarrow c + \tilde{\chi}_1^0$ or $\tilde{t}_1 \rightarrow b + f' + \tilde{\chi}_1^0$ and $\tilde{b}_1 \rightarrow b + \tilde{\chi}_1^0$, respectively, squark masses below about 430 GeV are excluded at 95% CL. In the case of squark-pair production with $\tilde{q} \rightarrow q + \tilde{\chi}_1^0$ ($q = u, d, c, s$), squark masses below 710 GeV are excluded.

Finally, the results are presented in terms of lower limits on the fundamental Planck scale M_D in $4 + n$ dimensions, versus the number of extra spatial dimensions in the ADD LED model. Values of M_D below 7.7 TeV at $n = 2$ and below 4.8 TeV at $n = 6$ are excluded at 95% CL.

Acknowledgements

We thank CERN for the very successful operation of the LHC, as well as the support staff from our institutions without whom ATLAS could not be operated efficiently.

We acknowledge the support of ANPCyT, Argentina; YerPhI, Armenia; ARC, Australia; BMWFW and FWF, Austria; ANAS, Azerbaijan; SSTC, Belarus; CNPq and FAPESP, Brazil; NSERC, NRC and CFI, Canada; CERN; CONICYT, Chile; CAS, MOST and NSFC, China; COLCIENCIAS, Colombia; MSMT CR, MPO CR and VSC CR, Czech Republic; DNRF and DNSRC, Denmark; IN2P3-CNRS, CEA-DRF/IRFU, France; SRNSF, Georgia; BMBF, HGF, and MPG, Germany; GSRT, Greece; RGC, Hong Kong SAR, China; ISF, I-CORE and Benoziyo Center, Israel; INFN, Italy; MEXT and JSPS, Japan; CNRST, Morocco; NWO, Netherlands; RCN, Norway; MNiSW and NCN, Poland; FCT, Portugal; MNE/IFA, Romania; MES of Russia and NRC KI, Russian Federation; JINR; MESTD, Serbia; MSSR, Slovakia; ARRS and MIZŠ, Slovenia; DST/NRF, South Africa; MINECO, Spain; SRC and Wallenberg Foundation, Sweden; SERI, SNSF and Cantons of Bern and Geneva, Switzerland; MOST, Taiwan;

TAEK, Turkey; STFC, United Kingdom; DOE and NSF, United States of America. In addition, individual groups and members have received support from BCKDF, the Canada Council, CANARIE, CRC, Compute Canada, FQRNT, and the Ontario Innovation Trust, Canada; EPLANET, ERC, ERDF, FP7, Horizon 2020 and Marie Skłodowska-Curie Actions, European Union; Investissements d’Avenir Labex and Idex, ANR, Région Auvergne and Fondation Partager le Savoir, France; DFG and AvH Foundation, Germany; Herakleitos, Thales and Aristea programmes co-financed by EU-ESF and the Greek NSRF; BSF, GIF and Minerva, Israel; BRF, Norway; CERCA Programme Generalitat de Catalunya, Generalitat Valenciana, Spain; the Royal Society and Leverhulme Trust, United Kingdom.

The crucial computing support from all WLCG partners is acknowledged gratefully, in particular from CERN, the ATLAS Tier-1 facilities at TRIUMF (Canada), NDGF (Denmark, Norway, Sweden), CC-IN2P3 (France), KIT/GridKA (Germany), INFN-CNAF (Italy), NL-T1 (Netherlands), PIC (Spain), ASGC (Taiwan), RAL (UK) and BNL (USA), the Tier-2 facilities worldwide and large non-WLCG resource providers. Major contributors of computing resources are listed in Ref. [98].

References

- [1] ATLAS Collaboration, *Search for new phenomena in final states with an energetic jet and large missing transverse momentum in pp collisions at $\sqrt{s} = 13$ TeV using the ATLAS detector*, *Phys. Rev. D* **94** (2016) 032005, arXiv: [1604.07773 \[hep-ex\]](#).
- [2] CMS Collaboration, *Search for dark matter produced with an energetic jet or a hadronically decaying W or Z boson at $\sqrt{s} = 13$ TeV*, *JHEP* **07** (2017) 014, arXiv: [1703.01651 \[hep-ex\]](#).
- [3] ATLAS Collaboration, *Measurement of detector-corrected observables sensitive to the anomalous production of events with jets and large missing transverse momentum in pp collisions at $\sqrt{s} = 13$ TeV using the ATLAS detector*, (2017), arXiv: [1707.03263 \[hep-ex\]](#).
- [4] V. Trimble, *Existence and Nature of Dark Matter in the Universe*, *Ann. Rev. Astron. Astrophys.* **25** (1987) 425.
- [5] G. Bertone, D. Hooper and J. Silk, *Particle dark matter: Evidence, candidates and constraints*, *Phys. Rept.* **405** (2005) 279, arXiv: [hep-ph/0404175](#).
- [6] J. L. Feng, *Dark Matter Candidates from Particle Physics and Methods of Detection*, *Ann. Rev. Astron. Astrophys.* **48** (2010) 495, arXiv: [1003.0904 \[astro-ph.CO\]](#).
- [7] G. Steigman and M. S. Turner, *Cosmological Constraints on the Properties of Weakly Interacting Massive Particles*, *Nucl. Phys. B* **253** (1985) 375.
- [8] E. W. Kolb and M. S. Turner, *The Early Universe*, *Front. Phys.* **69** (1990) 1.
- [9] R. Adam, et al., Planck Collaboration, *Planck 2015 results. I. Overview of products and scientific results*, *Astron. Astrophys.* **594** (2016) A1, arXiv: [1502.01582 \[astro-ph.CO\]](#).
- [10] G. Hinshaw et al., *Nine-year Wilkinson Microwave Anisotropy Probe (WMAP) Observations: Cosmological Parameter Results*, *ApJS* **208** (2013) 19, arXiv: [1212.5226 \[astro-ph.CO\]](#).
- [11] J. Abdallah et al., *Simplified Models for Dark Matter Searches at the LHC*, *Phys. Dark Univ.* **9-10** (2015) 8, arXiv: [1506.03116 \[hep-ph\]](#).

- [12] D. Abercrombie et al., *Dark Matter Benchmark Models for Early LHC Run-2 Searches: Report of the ATLAS/CMS Dark Matter Forum*, (2015), arXiv: [1507.00966 \[hep-ex\]](#).
- [13] O. Buchmueller, M. J. Dolan, S. A. Malik and C. McCabe, *Characterising dark matter searches at colliders and direct detection experiments: Vector mediators*, *JHEP* **01** (2015) 037, arXiv: [1407.8257 \[hep-ph\]](#).
- [14] ATLAS Collaboration, *Search for new phenomena in final states with an energetic jet and large missing transverse momentum in pp collisions at $\sqrt{s} = 8$ TeV with the ATLAS detector*, *Eur. Phys. J. C* **75** (2015) 299, arXiv: [1502.01518 \[hep-ex\]](#), Erratum: *Eur. Phys. J. C* **75** (2015) 408.
- [15] J. Goodman et al., *Constraints on dark matter from colliders*, *Phys. Rev. D* **82** (2010) 116010, arXiv: [1008.1783 \[hep-ph\]](#).
- [16] G. Busoni, A. De Simone, E. Morgante and A. Riotto, *On the Validity of the Effective Field Theory for Dark Matter Searches at the LHC*, *Phys. Lett. B* **728** (2014) 412, arXiv: [1307.2253 \[hep-ph\]](#).
- [17] N. F. Bell et al., *Searching for Dark Matter at the LHC with a Mono-Z*, *Phys. Rev. D* **86** (2012) 096011, arXiv: [1209.0231 \[hep-ph\]](#).
- [18] M. Papucci, A. Vichi and K. M. Zurek, *Monojet versus the rest of the world I: t-channel models*, *JHEP* **11** (2014) 024, arXiv: [1402.2285 \[hep-ph\]](#).
- [19] A. J. Brennan, M. F. McDonald, J. Gramling and T. D. Jacques, *Collide and conquer: constraints on simplified dark matter models using mono-X collider searches*, *JHEP* **05** (2016) 112, arXiv: [1603.01366 \[hep-ph\]](#).
- [20] H. Miyazawa, *Baryon Number Changing Currents*, *Prog. Theor. Phys.* **36** (1966) 1266.
- [21] P. Ramond, *Dual Theory for Free Fermions*, *Phys. Rev. D* **3** (1971) 2415.
- [22] Y. A. Golfand and E. P. Likhtman, *Extension of the Algebra of Poincare Group Generators and Violation of p Invariance*, *JETP Lett.* **13** (1971) 323.
- [23] A. Neveu and J. H. Schwarz, *Factorizable dual model of pions*, *Nucl. Phys. B* **31** (1971) 86.
- [24] A. Neveu and J. H. Schwarz, *Quark Model of Dual Pions*, *Phys. Rev. D* **4** (1971) 1109.
- [25] J. Gervais and B. Sakita, *Field theory interpretation of supergauges in dual models*, *Nucl. Phys. B* **34** (1971) 632.
- [26] D. V. Volkov and V. P. Akulov, *Is the Neutrino a Goldstone Particle?*, *Phys. Lett. B* **46** (1973) 109.
- [27] J. Wess and B. Zumino, *A Lagrangian Model Invariant Under Supergauge Transformations*, *Phys. Lett. B* **49** (1974) 52.
- [28] J. Wess and B. Zumino, *Supergauge Transformations in Four-Dimensions*, *Nucl. Phys. B* **70** (1974) 39.
- [29] R. Barbieri and G. Giudice, *Upper Bounds on Supersymmetric Particle Masses*, *Nucl. Phys. B* **306** (1988) 63.
- [30] P. Fayet, *Supersymmetry and Weak, Electromagnetic and Strong Interactions*, *Phys. Lett. B* **64** (1976) 159.

- [31] P. Fayet, *Spontaneously Broken Supersymmetric Theories of Weak, Electromagnetic and Strong Interactions*, *Phys. Lett. B* **69** (1977) 489.
- [32] G. R. Farrar and P. Fayet, *Phenomenology of the Production, Decay, and Detection of New Hadronic States Associated with Supersymmetry*, *Phys. Lett. B* **76** (1978) 575.
- [33] P. Fayet, *Relations Between the Masses of the Superpartners of Leptons and Quarks, the Goldstino Couplings and the Neutral Currents*, *Phys. Lett. B* **84** (1979) 416.
- [34] S. Dimopoulos and H. Georgi, *Softly Broken Supersymmetry and SU(5)*, *Nucl. Phys. B* **193** (1981) 150.
- [35] N. Arkani-Hamed, S. Dimopoulos and G. Dvali, *The hierarchy problem and new dimensions at a millimeter*, *Phys. Lett. B* **429** (1998) 263, arXiv: [hep-ph/9803315](#).
- [36] ATLAS Collaboration, *The ATLAS Experiment at the CERN Large Hadron Collider*, *JINST* **3** (2008) S08003.
- [37] ATLAS Collaboration, *ATLAS Insertable B-Layer Technical Design Report*, ATLAS-TDR-19, 2010, URL: <https://cds.cern.ch/record/1291633>, *ATLAS Insertable B-Layer Technical Design Report Addendum*, ATLAS-TDR-19-ADD-1, 2012, URL: <https://cds.cern.ch/record/1451888>.
- [38] ATLAS Collaboration, *Performance of the ATLAS Trigger System in 2015*, *Eur. Phys. J. C* **77** (2017) 317, arXiv: [1611.09661 \[hep-ex\]](#).
- [39] ATLAS Collaboration, *The ATLAS Simulation Infrastructure*, *Eur. Phys. J. C* **70** (2010) 823, arXiv: [1005.4568 \[physics.ins-det\]](#).
- [40] S. Agostinelli et al., *GEANT4: a simulation toolkit*, *Nucl. Instrum. Meth. A* **506** (2003) 250.
- [41] T. Sjöstrand, S. Mrenna and P. Z. Skands, *PYTHIA 6.4 physics and manual*, *JHEP* **05** (2006) 026, arXiv: [hep-ph/0603175](#).
- [42] S. Alioli, P. Nason, C. Oleari and E. Re, *A general framework for implementing NLO calculations in shower Monte Carlo programs: the POWHEG BOX*, *JHEP* **06** (2010) 043, arXiv: [1002.2581 \[hep-ph\]](#).
- [43] S. Frixione, P. Nason and C. Oleari, *Matching NLO QCD computations with Parton Shower simulations: the POWHEG method*, *JHEP* **11** (2007) 070, arXiv: [0709.2092 \[hep-ph\]](#).
- [44] P. Nason, *A New method for combining NLO QCD with shower Monte Carlo algorithms*, *JHEP* **11** (2004) 040, arXiv: [hep-ph/0409146](#).
- [45] U. Haisch, F. Kahlhöfer and E. Re, *QCD effects in mono-jet searches for dark matter*, *JHEP* **12** (2013) 007, arXiv: [1310.4491 \[hep-ph\]](#).
- [46] U. Haisch and E. Re, *Simplified dark matter top-quark interactions at the LHC*, *JHEP* **06** (2015) 078, arXiv: [1503.00691 \[hep-ph\]](#).
- [47] R. D. Ball et al., *Parton distributions for the LHC Run II*, *JHEP* **04** (2015) 040, arXiv: [1410.8849 \[hep-ph\]](#).
- [48] ATLAS Collaboration, *ATLAS Run 1 Pythia8 tunes*, ATL-PHYS-PUB-2014-021, 2014, URL: <https://cds.cern.ch/record/1966419>.

- [49] J. Alwall et al., *The automated computation of tree-level and next-to-leading order differential cross sections, and their matching to parton shower simulations*, *JHEP* **07** (2014) 079, arXiv: [1405.0301 \[hep-ph\]](#).
- [50] R. D. Ball et al., *Parton distributions with LHC data*, *Nucl. Phys. B* **867** (2013) 244, arXiv: [1207.1303 \[hep-ph\]](#).
- [51] L. Lönnblad and S. Prestel, *Matching tree-Level matrix elements with interleaved showers*, *JHEP* **03** (2012) 019, arXiv: [1109.4829 \[hep-ph\]](#).
- [52] W. Beenakker, M. Kramer, T. Plehn, M. Spira and P. M. Zerwas, *Stop production at hadron colliders*, *Nucl. Phys. B* **515** (1998) 3, arXiv: [hep-ph/9710451](#).
- [53] W. Beenakker et al., *Supersymmetric top and bottom squark production at hadron colliders*, *JHEP* **08** (2010) 098, arXiv: [1006.4771 \[hep-ph\]](#).
- [54] W. Beenakker et al., *Squark and gluino hadroproduction*, *Int. J. Mod. Phys. A* **26** (2011) 2637, arXiv: [1105.1110 \[hep-ph\]](#).
- [55] C. Borschensky et al., *Squark and gluino production cross sections in pp collisions at $\sqrt{s} = 13, 14, 33$ and 100 TeV*, *Eur. Phys. J. C* **74** (2014) 3174, arXiv: [1407.5066 \[hep-ph\]](#).
- [56] T. Gleisberg et al., *Event generation with SHERPA 1.1*, *JHEP* **02** (2009) 007, arXiv: [0811.4622 \[hep-ph\]](#).
- [57] F. Cascioli, P. Maierhofer and S. Pozzorini, *Scattering Amplitudes with Open Loops*, *Phys. Rev. Lett.* **108** (2012) 111601, arXiv: [1111.5206 \[hep-ph\]](#).
- [58] T. Gleisberg and S. Höche, *Comix, a new matrix element generator*, *JHEP* **12** (2008) 039, arXiv: [0808.3674 \[hep-ph\]](#).
- [59] S. Schumann and F. Krauss, *A Parton shower algorithm based on Catani-Seymour dipole factorisation*, *JHEP* **03** (2008) 038, arXiv: [0709.1027 \[hep-ph\]](#).
- [60] S. Höche, F. Krauss, M. Schönher and F. Siegert, *QCD matrix elements + parton showers: The NLO case*, *JHEP* **04** (2013) 027, arXiv: [1207.5030 \[hep-ph\]](#).
- [61] S. Catani, L. Cieri, G. Ferrera, D. de Florian and M. Grazzini, *Vector boson production at hadron colliders: a fully exclusive QCD calculation at NNLO*, *Phys. Rev. Lett.* **103** (2009) 082001, arXiv: [0903.2120 \[hep-ph\]](#).
- [62] S. Catani and M. Grazzini, *An NNLO subtraction formalism in hadron collisions and its application to Higgs boson production at the LHC*, *Phys. Rev. Lett.* **98** (2007) 222002, arXiv: [hep-ph/0703012](#).
- [63] A. D. Martin, W. J. Stirling, R. S. Thorne and G. Watt, *Parton distributions for the LHC*, *Eur. Phys. J. C* **63** (2009) 189, arXiv: [0901.0002 \[hep-ph\]](#).
- [64] J. M. Lindert et al., *Precise predictions for V+jets dark matter backgrounds*, (2017), arXiv: [1705.04664v1 \[hep-ph\]](#).
- [65] ATLAS Collaboration, *Measurements of the production cross section of a Z boson in association with jets in pp collisions at $\sqrt{s} = 13$ TeV with the ATLAS detector*, *Eur. Phys. J. C* **77** (2017) 361, arXiv: [1702.05725 \[hep-ex\]](#).

- [66] S. Frixione, P. Nason and G. Ridolfi,
A Positive-weight next-to-leading-order Monte Carlo for heavy flavour hadroproduction,
JHEP **09** (2007) 126, arXiv: [0707.3088 \[hep-ph\]](#).
- [67] H.-L. Lai et al., *New parton distributions for collider physics*, **Phys. Rev. D** **82** (2010) 074024, arXiv: [1007.2241 \[hep-ph\]](#).
- [68] D. J. Lange, *The EvtGen particle decay simulation package*, **Nucl. Instrum. Meth. A** **462** (2001) 152.
- [69] M. Bahr et al., *Herwig++ physics and manual*, **Eur. Phys. J. C** **58** (2008) 639, arXiv: [0803.0883 \[hep-ph\]](#).
- [70] J. M. Campbell, R. K. Ellis and C. Williams, *Vector boson pair production at the LHC*, **JHEP** **07** (2011) 018, arXiv: [1105.0020 \[hep-ph\]](#).
- [71] M. Cacciari, G. P. Salam and G. Soyez, *The anti- k_t jet clustering algorithm*, **JHEP** **04** (2008) 063, arXiv: [0802.1189 \[hep-ph\]](#).
- [72] M. Cacciari, G. P. Salam and G. Soyez, *FastJet user manual*, **Eur. Phys. J. C** **72** (2012) 1896, arXiv: [1111.6097 \[hep-ph\]](#).
- [73] ATLAS Collaboration,
Jet energy measurement with the ATLAS detector in proton-proton collisions at $\sqrt{s} = 7$ TeV, **Eur. Phys. J. C** **73** (2013) 2304, arXiv: [1112.6426 \[hep-ex\]](#).
- [74] ATLAS Collaboration, *Tagging and suppression of pileup jets with the ATLAS detector*, ATLAS-CONF-2014-018, 2014, URL: <https://cds.cern.ch/record/1700870>.
- [75] ATLAS Collaboration, *Performance of b-jet identification in the ATLAS experiment*, **JINST** **11** (2016) P04008, arXiv: [1512.01094 \[hep-ex\]](#).
- [76] ATLAS Collaboration, *Optimisation of the ATLAS b-tagging performance for the 2016 LHC Run*, ATL-PHYS-PUB-2016-012, 2016, URL: <https://cds.cern.ch/record/2160731>.
- [77] ATLAS Collaboration, *Electron efficiency measurements with the ATLAS detector using the 2012 LHC proton–proton collision data*, ATLAS-CONF-2014-032, 2014, URL: <https://cds.cern.ch/record/1706245>.
- [78] ATLAS Collaboration, *Muon reconstruction performance of the ATLAS detector in proton–proton collision data at $\sqrt{s} = 13$ TeV*, **Eur. Phys. J. C** **76** (2016) 292, arXiv: [1603.05598 \[hep-ex\]](#).
- [79] ATLAS Collaboration, *Expected performance of missing transverse momentum reconstruction for the ATLAS detector at $\sqrt{s} = 13$ TeV*, ATL-PHYS-PUB-2015-023, 2015, URL: <https://cds.cern.ch/record/2037700>.
- [80] ATLAS Collaboration,
Luminosity determination in pp collisions at $\sqrt{s} = 8$ TeV using the ATLAS detector at the LHC, **Eur. Phys. J. C** **76** (2016) 653, arXiv: [1608.03953 \[hep-ex\]](#).
- [81] ATLAS Collaboration,
Selection of jets produced in 13 TeV proton-proton collisions with the ATLAS detector, ATLAS-CONF-2015-029, 2015, URL: <https://cds.cern.ch/record/2037702>.
- [82] ATLAS Collaboration, *Characterisation and mitigation of beam-induced backgrounds observed in the ATLAS detector during the 2011 proton-proton run*, **JINST** **8** (2013) P07004, arXiv: [1303.0223 \[hep-ex\]](#).

- [83] ATLAS Collaboration, *Search for squarks and gluinos with the ATLAS detector in final states with jets and missing transverse momentum using 4.7 fb^{-1} of $\sqrt{s} = 7 \text{ TeV}$ proton-proton collision data*, *Phys. Rev. D* **87** (2013) 012008, arXiv: [1208.0949 \[hep-ex\]](#).
- [84] G. Cowan, K. Cranmer, E. Gross and O. Vitells, *Asymptotic formulae for likelihood-based tests of new physics*, *Eur. Phys. J. C* **71** (2011) 1554, arXiv: [1007.1727 \[physics.data-an\]](#), Erratum: *Eur. Phys. J. C* **73** (2013) 2501.
- [85] ATLAS Collaboration, *Electron efficiency measurements with the ATLAS detector using the 2015 LHC proton–proton collision data*, ATLAS-CONF-2016-024, 2016, URL: <https://cds.cern.ch/record/2157687>.
- [86] ATLAS Collaboration, *Electron and photon energy calibration with the ATLAS detector using LHC Run 1 data*, *Eur. Phys. J. C* **74** (2014) 3071, arXiv: [1407.5063 \[hep-ex\]](#).
- [87] ATLAS Collaboration, *ATLAS simulation of boson plus jets processes in Run 2*, ATL-PHYS-PUB-2017-006, 2017, URL: <https://cds.cern.ch/record/2261937>.
- [88] ATLAS Collaboration, *Studies on top-quark Monte Carlo modelling with Sherpa and MG5_aMC@NLO*, ATL-PHYS-PUB-2017-007, 2017, URL: <https://cds.cern.ch/record/2261938>.
- [89] ATLAS Collaboration, *Multi-Boson Simulation for 13 TeV ATLAS Analyses*, ATL-PHYS-PUB-2017-005, 2017, URL: <https://cds.cern.ch/record/2261933>.
- [90] L. A. Harland-Lang, A. D. Martin, P. Motylinski and R. S. Thorne, *Parton distributions in the LHC era: MMHT 2014 PDFs*, *Eur. Phys. J. C* **75** (2015) 204, arXiv: [1412.3989 \[hep-ph\]](#).
- [91] A. L. Read, *Presentation of search results: The CL_s technique*, *J. Phys. G* **28** (2002) 2693.
- [92] F. Kahlhöfer, K. Schmidt-Hoberg, T. Schwetz and S. Vogl, *Implications of unitarity and gauge invariance for simplified dark matter models*, *JHEP* **02** (2016) 016, arXiv: [1510.02110 \[hep-ph\]](#).
- [93] A. Boveia et al., *Recommendations on presenting LHC searches for missing transverse energy signals using simplified s-channel models of dark matter*, (2016), arXiv: [1603.04156 \[hep-ex\]](#).
- [94] M. Backović, A. Martini, O. Mattelaer, K. Kong and G. Mohlabeng, *Direct Detection of Dark Matter with MadDM v.2.0*, *Phys. Dark Univ.* **9-10** (2015) 37, arXiv: [1505.04190 \[hep-ph\]](#).
- [95] C. Amole et al., *Dark Matter Search Results from the PICO-60 C_3F_8 Bubble Chamber*, *Phys. Rev. Lett.* **118** (2017) 251301, arXiv: [1702.07666 \[astro-ph.CO\]](#).
- [96] ATLAS Collaboration, *Search for squarks and gluinos in final states with jets and missing transverse momentum at $\sqrt{s} = 13 \text{ TeV}$ with the ATLAS detector*, *Eur. Phys. J. C* **76** (2016) 392, arXiv: [1605.03814 \[hep-ex\]](#).
- [97] ATLAS Collaboration, *Search for dark matter candidates and large extra dimensions in events with a jet and missing transverse momentum with the ATLAS detector*, *JHEP* **04** (2013) 075, arXiv: [1210.4491 \[hep-ex\]](#).
- [98] ATLAS Collaboration, *ATLAS Computing Acknowledgements 2016–2017*, ATL-GEN-PUB-2016-002, URL: <https://cds.cern.ch/record/2202407>.

The ATLAS Collaboration

M. Aaboud^{137d}, G. Aad⁸⁸, B. Abbott¹¹⁵, O. Abdinov^{12,*}, B. Abeloos¹¹⁹, S.H. Abidi¹⁶¹, O.S. AbouZeid¹³⁹, N.L. Abraham¹⁵¹, H. Abramowicz¹⁵⁵, H. Abreu¹⁵⁴, R. Abreu¹¹⁸, Y. Abulaiti^{148a,148b}, B.S. Acharya^{167a,167b,a}, S. Adachi¹⁵⁷, L. Adamczyk^{41a}, J. Adelman¹¹⁰, M. Adersberger¹⁰², T. Adye¹³³, A.A. Affolder¹³⁹, Y. Afik¹⁵⁴, T. Agatonovic-Jovin¹⁴, C. Agheorghiesei^{28c}, J.A. Aguilar-Saavedra^{128a,128f}, S.P. Ahlen²⁴, F. Ahmadov^{68,b}, G. Aielli^{135a,135b}, S. Akatsuka⁷¹, H. Akerstedt^{148a,148b}, T.P.A. Åkesson⁸⁴, E. Akilli⁵², A.V. Akimov⁹⁸, G.L. Alberghi^{22a,22b}, J. Albert¹⁷², P. Albicocco⁵⁰, M.J. Alconada Verzini⁷⁴, S.C. Alderweireldt¹⁰⁸, M. Aleksa³², I.N. Aleksandrov⁶⁸, C. Alexa^{28b}, G. Alexander¹⁵⁵, T. Alexopoulos¹⁰, M. Alhroob¹¹⁵, B. Ali¹³⁰, M. Aliev^{76a,76b}, G. Alimonti^{94a}, J. Alison³³, S.P. Alkire³⁸, B.M.M. Allbrooke¹⁵¹, B.W. Allen¹¹⁸, P.P. Allport¹⁹, A. Aloisio^{106a,106b}, A. Alonso³⁹, F. Alonso⁷⁴, C. Alpigiani¹⁴⁰, A.A. Alshehri⁵⁶, M.I. Alstaty⁸⁸, B. Alvarez Gonzalez³², D. Álvarez Piqueras¹⁷⁰, M.G. Alvaggi^{106a,106b}, B.T. Amadio¹⁶, Y. Amaral Coutinho^{26a}, C. Amelung²⁵, D. Amidei⁹², S.P. Amor Dos Santos^{128a,128c}, S. Amoroso³², G. Amundsen²⁵, C. Anastopoulos¹⁴¹, L.S. Ancu⁵², N. Andari¹⁹, T. Andeen¹¹, C.F. Anders^{60b}, J.K. Anders⁷⁷, K.J. Anderson³³, A. Andreazza^{94a,94b}, V. Andrei^{60a}, S. Angelidakis³⁷, I. Angelozzi¹⁰⁹, A. Angerami³⁸, A.V. Anisenkov^{111,c}, N. Anjos¹³, A. Annovi^{126a}, C. Antel^{60a}, M. Antonelli⁵⁰, A. Antonov^{100,*}, D.J. Antrim¹⁶⁶, F. Anulli^{134a}, M. Aoki⁶⁹, L. Aperio Bella³², G. Arabidze⁹³, Y. Arai⁶⁹, J.P. Araque^{128a}, V. Araujo Ferraz^{26a}, A.T.H. Arce⁴⁸, R.E. Ardell⁸⁰, F.A. Arduh⁷⁴, J.-F. Arguin⁹⁷, S. Argyropoulos⁶⁶, M. Arik^{20a}, A.J. Armbruster³², L.J. Armitage⁷⁹, O. Arnaez¹⁶¹, H. Arnold⁵¹, M. Arratia³⁰, O. Arslan²³, A. Artamonov^{99,*}, G. Artoni¹²², S. Artz⁸⁶, S. Asai¹⁵⁷, N. Asbah⁴⁵, A. Ashkenazi¹⁵⁵, L. Asquith¹⁵¹, K. Assamagan²⁷, R. Astalos^{146a}, M. Atkinson¹⁶⁹, N.B. Atlay¹⁴³, K. Augsten¹³⁰, G. Avolio³², B. Axen¹⁶, M.K. Ayoub^{35a}, G. Azuelos^{97,d}, A.E. Baas^{60a}, M.J. Baca¹⁹, H. Bachacou¹³⁸, K. Bachas^{76a,76b}, M. Backes¹²², P. Bagnaia^{134a,134b}, M. Bahmani⁴², H. Bahrasemani¹⁴⁴, J.T. Baines¹³³, M. Bajic³⁹, O.K. Baker¹⁷⁹, P.J. Bakker¹⁰⁹, E.M. Baldin^{111,c}, P. Balek¹⁷⁵, F. Balli¹³⁸, W.K. Balunas¹²⁴, E. Banas⁴², A. Bandyopadhyay²³, Sw. Banerjee^{176,e}, A.A.E. Bannoura¹⁷⁸, L. Barak¹⁵⁵, E.L. Barberio⁹¹, D. Barberis^{53a,53b}, M. Barbero⁸⁸, T. Barillari¹⁰³, M-S Barisits³², J.T. Barkeloo¹¹⁸, T. Barklow¹⁴⁵, N. Barlow³⁰, S.L. Barnes^{36c}, B.M. Barnett¹³³, R.M. Barnett¹⁶, Z. Barnovska-Blenessy^{36a}, A. Baroncelli^{136a}, G. Barone²⁵, A.J. Barr¹²², L. Barranco Navarro¹⁷⁰, F. Barreiro⁸⁵, J. Barreiro Guimarães da Costa^{35a}, R. Bartoldus¹⁴⁵, A.E. Barton⁷⁵, P. Bartos^{146a}, A. Basalaev¹²⁵, A. Bassalat^{119,f}, R.L. Bates⁵⁶, S.J. Batista¹⁶¹, J.R. Batley³⁰, M. Battaglia¹³⁹, M. Bauce^{134a,134b}, F. Bauer¹³⁸, H.S. Bawa^{145,g}, J.B. Beacham¹¹³, M.D. Beattie⁷⁵, T. Beau⁸³, P.H. Beauchemin¹⁶⁵, P. Bechtle²³, H.P. Beck^{18,h}, H.C. Beck⁵⁷, K. Becker¹²², M. Becker⁸⁶, C. Becot¹¹², A.J. Beddall^{20e}, A. Beddall^{20b}, V.A. Bednyakov⁶⁸, M. Bedognetti¹⁰⁹, C.P. Bee¹⁵⁰, T.A. Beermann³², M. Begalli^{26a}, M. Begel²⁷, J.K. Behr⁴⁵, A.S. Bell⁸¹, G. Bella¹⁵⁵, L. Bellagamba^{22a}, A. Bellerive³¹, M. Bellomo¹⁵⁴, K. Belotskiy¹⁰⁰, O. Beltramello³², N.L. Belyaev¹⁰⁰, O. Benary^{155,*}, D. Benchekroun^{137a}, M. Bender¹⁰², N. Benekos¹⁰, Y. Benhammou¹⁵⁵, E. Benhar Noccioli¹⁷⁹, J. Benitez⁶⁶, D.P. Benjamin⁴⁸, M. Benoit⁵², J.R. Bensinger²⁵, S. Bentvelsen¹⁰⁹, L. Beresford¹²², M. Beretta⁵⁰, D. Berge¹⁰⁹, E. Bergeaas Kuutmann¹⁶⁸, N. Berger⁵, L.J. Bergsten²⁵, J. Beringer¹⁶, S. Berlendis⁵⁸, N.R. Bernard⁸⁹, G. Bernardi⁸³, C. Bernius¹⁴⁵, F.U. Bernlochner²³, T. Berry⁸⁰, P. Berta⁸⁶, C. Bertella^{35a}, G. Bertoli^{148a,148b}, I.A. Bertram⁷⁵, C. Bertsche⁴⁵, G.J. Besjes³⁹, O. Bessidskaia Bylund^{148a,148b}, M. Bessner⁴⁵, N. Besson¹³⁸, A. Bethani⁸⁷, S. Bethke¹⁰³, A. Betti²³, A.J. Bevan⁷⁹, J. Beyer¹⁰³, R.M. Bianchi¹²⁷, O. Biebel¹⁰², D. Biedermann¹⁷, R. Bielski⁸⁷, K. Bierwagen⁸⁶, N.V. Biesuz^{126a,126b}, M. Biglietti^{136a}, T.R.V. Billoud⁹⁷, H. Bilokon⁵⁰, M. Bindi⁵⁷, A. Bingul^{20b}, C. Bini^{134a,134b}, S. Biondi^{22a,22b}, T. Bisanz⁵⁷, C. Bittrich⁴⁷, D.M. Bjergaard⁴⁸, J.E. Black¹⁴⁵, K.M. Black²⁴, R.E. Blair⁶, T. Blazek^{146a}, I. Bloch⁴⁵, C. Blocker²⁵, A. Blue⁵⁶, U. Blumenschein⁷⁹, S. Blunier^{34a}, G.J. Bobbink¹⁰⁹, V.S. Bobrovnikov^{111,c}, S.S. Bocchetta⁸⁴, A. Bocci⁴⁸,

C. Bock¹⁰², M. Boehler⁵¹, D. Boerner¹⁷⁸, D. Bogavac¹⁰², A.G. Bogdanchikov¹¹¹, C. Bohm^{148a},
 V. Boisvert⁸⁰, P. Bokan^{168,i}, T. Bold^{41a}, A.S. Boldyrev¹⁰¹, A.E. Bolz^{60b}, M. Bomben⁸³, M. Bona⁷⁹,
 M. Boonekamp¹³⁸, A. Borisov¹³², G. Borissov⁷⁵, J. Bortfeldt³², D. Bortoletto¹²², V. Bortolotto^{62a},
 D. Boscherini^{22a}, M. Bosman¹³, J.D. Bossio Sola²⁹, J. Boudreau¹²⁷, E.V. Bouhova-Thacker⁷⁵,
 D. Boumediene³⁷, C. Bourdarios¹¹⁹, S.K. Boutle⁵⁶, A. Boveia¹¹³, J. Boyd³², I.R. Boyko⁶⁸,
 A.J. Bozson⁸⁰, J. Bracinik¹⁹, A. Brandt⁸, G. Brandt⁵⁷, O. Brandt^{60a}, F. Braren⁴⁵, U. Bratzler¹⁵⁸,
 B. Brau⁸⁹, J.E. Brau¹¹⁸, W.D. Breaden Madden⁵⁶, K. Brendlinger⁴⁵, A.J. Brennan⁹¹, L. Brenner¹⁰⁹,
 R. Brenner¹⁶⁸, S. Bressler¹⁷⁵, D.L. Briglin¹⁹, T.M. Bristow⁴⁹, D. Britton⁵⁶, D. Britzger⁴⁵,
 F.M. Brochu³⁰, I. Brock²³, R. Brock⁹³, G. Brooijmans³⁸, T. Brooks⁸⁰, W.K. Brooks^{34b}, J. Brosamer¹⁶,
 E. Brost¹¹⁰, J.H. Broughton¹⁹, P.A. Bruckman de Renstrom⁴², D. Bruncko^{146b}, A. Bruni^{22a}, G. Bruni^{22a},
 L.S. Bruni¹⁰⁹, S. Bruno^{135a,135b}, BH Brunt³⁰, M. Bruschi^{22a}, N. Bruscino¹²⁷, P. Bryant³³,
 L. Bryngemark⁴⁵, T. Buanes¹⁵, Q. Buat¹⁴⁴, P. Buchholz¹⁴³, A.G. Buckley⁵⁶, I.A. Budagov⁶⁸,
 F. Buehrer⁵¹, M.K. Bugge¹²¹, O. Bulekov¹⁰⁰, D. Bullock⁸, T.J. Burch¹¹⁰, S. Burdin⁷⁷, C.D. Burgard¹⁰⁹,
 A.M. Burger⁵, B. Burghgrave¹¹⁰, K. Burka⁴², S. Burke¹³³, I. Burmeister⁴⁶, J.T.P. Burr¹²², D. Büscher⁵¹,
 V. Büscher⁸⁶, P. Bussey⁵⁶, J.M. Butler²⁴, C.M. Buttar⁵⁶, J.M. Butterworth⁸¹, P. Butti³², W. Buttinger²⁷,
 A. Buzatu¹⁵³, A.R. Buzykaev^{111,c}, Changqiao C.-Q.^{36a}, S. Cabrera Urbán¹⁷⁰, D. Caforio¹³⁰, H. Cai¹⁶⁹,
 V.M. Cairo^{40a,40b}, O. Cakir^{4a}, N. Calace⁵², P. Calafiura¹⁶, A. Calandri⁸⁸, G. Calderini⁸³, P. Calfayan⁶⁴,
 G. Callea^{40a,40b}, L.P. Caloba^{26a}, S. Calvente Lopez⁸⁵, D. Calvet³⁷, S. Calvet³⁷, T.P. Calvet⁸⁸,
 R. Camacho Toro³³, S. Camarda³², P. Camarri^{135a,135b}, D. Cameron¹²¹, R. Caminal Armadans¹⁶⁹,
 C. Camincher⁵⁸, S. Campana³², M. Campanelli⁸¹, A. Camplani^{94a,94b}, A. Campoverde¹⁴³,
 V. Canale^{106a,106b}, M. Cano Bret^{36c}, J. Cantero¹¹⁶, T. Cao¹⁵⁵, M.D.M. Capeans Garrido³², I. Caprini^{28b},
 M. Caprini^{28b}, M. Capua^{40a,40b}, R.M. Carbone³⁸, R. Cardarelli^{135a}, F. Cardillo⁵¹, I. Carli¹³¹, T. Carli³²,
 G. Carlino^{106a}, B.T. Carlson¹²⁷, L. Carminati^{94a,94b}, R.M.D. Carney^{148a,148b}, S. Caron¹⁰⁸, E. Carquin^{34b},
 S. Carrá^{94a,94b}, G.D. Carrillo-Montoya³², D. Casadei¹⁹, M.P. Casado^{13,j}, A.F. Casha¹⁶¹, M. Casolino¹³,
 D.W. Casper¹⁶⁶, R. Castelijn¹⁰⁹, V. Castillo Gimenez¹⁷⁰, N.F. Castro^{128a,k}, A. Catinaccio³²,
 J.R. Catmore¹²¹, A. Cattai³², J. Caudron²³, V. Cavaliere¹⁶⁹, E. Cavallaro¹³, D. Cavalli^{94a},
 M. Cavalli-Sforza¹³, V. Cavasinni^{126a,126b}, E. Celebi^{20d}, F. Ceradini^{136a,136b}, L. Cerdà Alberich¹⁷⁰,
 A.S. Cerqueira^{26b}, A. Cerri¹⁵¹, L. Cerrito^{135a,135b}, F. Cerutti¹⁶, A. Cervelli^{22a,22b}, S.A. Cetin^{20d},
 A. Chafaq^{137a}, D. Chakraborty¹¹⁰, S.K. Chan⁵⁹, W.S. Chan¹⁰⁹, Y.L. Chan^{62a}, P. Chang¹⁶⁹,
 J.D. Chapman³⁰, D.G. Charlton¹⁹, C.C. Chau³¹, C.A. Chavez Barajas¹⁵¹, S. Che¹¹³,
 S. Cheatham^{167a,167c}, A. Chegwidden⁹³, S. Chekanov⁶, S.V. Chekulaev^{163a}, G.A. Chelkov^{68,l},
 M.A. Chelstowska³², C. Chen^{36a}, C. Chen⁶⁷, H. Chen²⁷, J. Chen^{36a}, S. Chen^{35b}, S. Chen¹⁵⁷,
 X. Chen^{35c,m}, Y. Chen⁷⁰, H.C. Cheng⁹², H.J. Cheng^{35a,35d}, A. Cheplakov⁶⁸, E. Cheremushkina¹³²,
 R. Cherkaoui El Moursli^{137e}, E. Cheu⁷, K. Cheung⁶³, L. Chevalier¹³⁸, V. Chiarella⁵⁰, G. Chiarelli^{126a},
 G. Chiodini^{76a}, A.S. Chisholm³², A. Chitan^{28b}, Y.H. Chiu¹⁷², M.V. Chizhov⁶⁸, K. Choi⁶⁴,
 A.R. Chomont³⁷, S. Chouridou¹⁵⁶, Y.S. Chow^{62a}, V. Christodoulou⁸¹, M.C. Chu^{62a}, J. Chudoba¹²⁹,
 A.J. Chuinard⁹⁰, J.J. Chwastowski⁴², L. Chytka¹¹⁷, A.K. Ciftci^{4a}, D. Cinca⁴⁶, V. Cindro⁷⁸, I.A. Cioara²³,
 A. Ciocio¹⁶, F. Cirotto^{106a,106b}, Z.H. Citron¹⁷⁵, M. Citterio^{94a}, M. Ciubancan^{28b}, A. Clark⁵²,
 B.L. Clark⁵⁹, M.R. Clark³⁸, P.J. Clark⁴⁹, R.N. Clarke¹⁶, C. Clement^{148a,148b}, Y. Coadou⁸⁸,
 M. Cobal^{167a,167c}, A. Coccaro⁵², J. Cochran⁶⁷, L. Colasurdo¹⁰⁸, B. Cole³⁸, A.P. Colijn¹⁰⁹, J. Collot⁵⁸,
 T. Colombo¹⁶⁶, P. Conde Muiño^{128a,128b}, E. Coniavitis⁵¹, S.H. Connell^{147b}, I.A. Connelly⁸⁷,
 S. Constantinescu^{28b}, G. Conti³², F. Conventi^{106a,n}, M. Cooke¹⁶, A.M. Cooper-Sarkar¹²², F. Cormier¹⁷¹,
 K.J.R. Cormier¹⁶¹, M. Corradi^{134a,134b}, F. Corriveau^{90,o}, A. Cortes-Gonzalez³², G. Costa^{94a},
 M.J. Costa¹⁷⁰, D. Costanzo¹⁴¹, G. Cottin³⁰, G. Cowan⁸⁰, B.E. Cox⁸⁷, K. Cranmer¹¹², S.J. Crawley⁵⁶,
 R.A. Creager¹²⁴, G. Cree³¹, S. Crépé-Renaudin⁵⁸, F. Crescioli⁸³, W.A. Cribbs^{148a,148b}, M. Cristinziani²³,
 V. Croft¹¹², G. Crosetti^{40a,40b}, A. Cueto⁸⁵, T. Cuhadar Donszelmann¹⁴¹, A.R. Cukierman¹⁴⁵,
 J. Cummings¹⁷⁹, M. Curatolo⁵⁰, J. Cúth⁸⁶, S. Czekierda⁴², P. Czodrowski³², G. D'amen^{22a,22b},

S. D'Auria⁵⁶, L. D'eramo⁸³, M. D'Onofrio⁷⁷, M.J. Da Cunha Sargedas De Sousa^{128a,128b}, C. Da Via⁸⁷,
 W. Dabrowski^{41a}, T. Dado^{146a}, T. Dai⁹², O. Dale¹⁵, F. Dallaire⁹⁷, C. Dallapiccola⁸⁹, M. Dam³⁹,
 J.R. Dandoy¹²⁴, M.F. Daneri²⁹, N.P. Dang¹⁷⁶, A.C. Daniells¹⁹, N.S. Dann⁸⁷, M. Danninger¹⁷¹,
 M. Dano Hoffmann¹³⁸, V. Dao¹⁵⁰, G. Darbo^{53a}, S. Darmora⁸, J. Dassoulas³, A. Dattagupta¹¹⁸,
 T. Daubney⁴⁵, W. Davey²³, C. David⁴⁵, T. Davidek¹³¹, D.R. Davis⁴⁸, P. Davison⁸¹, E. Dawe⁹¹,
 I. Dawson¹⁴¹, K. De⁸, R. de Asmundis^{106a}, A. De Benedetti¹¹⁵, S. De Castro^{22a,22b}, S. De Cecco⁸³,
 N. De Groot¹⁰⁸, P. de Jong¹⁰⁹, H. De la Torre⁹³, F. De Lorenzi⁶⁷, A. De Maria⁵⁷, D. De Pedis^{134a},
 A. De Salvo^{134a}, U. De Sanctis^{135a,135b}, A. De Santo¹⁵¹, K. De Vasconcelos Corga⁸⁸,
 J.B. De Vivie De Regie¹¹⁹, R. Debbe²⁷, C. Debenedetti¹³⁹, D.V. Dedovich⁶⁸, N. Dehghanian³,
 I. Deigaard¹⁰⁹, M. Del Gaudio^{40a,40b}, J. Del Peso⁸⁵, D. Delgove¹¹⁹, F. Deliot¹³⁸, C.M. Delitzsch⁷,
 A. Dell'Acqua³², L. Dell'Asta²⁴, M. Dell'Orso^{126a,126b}, M. Della Pietra^{106a,106b}, D. della Volpe⁵²,
 M. Delmastro⁵, C. Delporte¹¹⁹, P.A. Delsart⁵⁸, D.A. DeMarco¹⁶¹, S. Demers¹⁷⁹, M. Demichev⁶⁸,
 A. Demilly⁸³, S.P. Denisov¹³², D. Denysiuk¹³⁸, D. Derendarz⁴², J.E. Derkaoui^{137d}, F. Derue⁸³,
 P. Dervan⁷⁷, K. Desch²³, C. Deterre⁴⁵, K. Dette¹⁶¹, M.R. Devesa²⁹, P.O. Deviveiros³², A. Dewhurst¹³³,
 S. Dhaliwal²⁵, F.A. Di Bello⁵², A. Di Ciaccio^{135a,135b}, L. Di Ciaccio⁵, W.K. Di Clemente¹²⁴,
 C. Di Donato^{106a,106b}, A. Di Girolamo³², B. Di Girolamo³², B. Di Micco^{136a,136b}, R. Di Nardo³²,
 K.F. Di Petrillo⁵⁹, A. Di Simone⁵¹, R. Di Sipio¹⁶¹, D. Di Valentino³¹, C. Diaconu⁸⁸, M. Diamond¹⁶¹,
 F.A. Dias³⁹, M.A. Diaz^{34a}, J. Dickinson¹⁶, E.B. Diehl⁹², J. Dietrich¹⁷, S. Díez Cornell⁴⁵,
 A. Dimitrievska¹⁴, J. Dingfelder²³, P. Dita^{28b}, S. Dita^{28b}, F. Dittus³², F. Djama⁸⁸, T. Djobava^{54b},
 J.I. Djuvslund^{60a}, M.A.B. do Vale^{26c}, D. Dobos³², M. Dobre^{28b}, D. Dodsworth²⁵, C. Doglioni⁸⁴,
 J. Dolejsi¹³¹, Z. Dolezal¹³¹, M. Donadelli^{26d}, S. Donati^{126a,126b}, P. Dondero^{123a,123b}, J. Donini³⁷,
 J. Dopke¹³³, A. Doria^{106a}, M.T. Dova⁷⁴, A.T. Doyle⁵⁶, E. Drechsler⁵⁷, M. Dris¹⁰, Y. Du^{36b},
 J. Duarte-Campderros¹⁵⁵, F. Dubinin⁹⁸, A. Dubreuil⁵², E. Duchovni¹⁷⁵, G. Duckeck¹⁰²,
 A. Ducourthial⁸³, O.A. Ducu^{97,p}, D. Duda¹⁰⁹, A. Dudarev³², A.Chr. Dudder⁸⁶, E.M. Duffield¹⁶,
 L. Duflot¹¹⁹, M. Dührssen³², C. Dulsen¹⁷⁸, M. Dumancic¹⁷⁵, A.E. Dumitriu^{28b}, A.K. Duncan⁵⁶,
 M. Dunford^{60a}, A. Duperrin⁸⁸, H. Duran Yildiz^{4a}, M. Düren⁵⁵, A. Durglishvili^{54b}, D. Duschinger⁴⁷,
 B. Dutta⁴⁵, D. Duvnjak¹, M. Dyndal⁴⁵, B.S. Dziedzic⁴², C. Eckardt⁴⁵, K.M. Ecker¹⁰³, R.C. Edgar⁹²,
 T. Eifert³², G. Eigen¹⁵, K. Einsweiler¹⁶, T. Ekelof¹⁶⁸, M. El Kacimi^{137c}, R. El Kosseifi⁸⁸,
 V. Ellajosyula⁸⁸, M. Ellert¹⁶⁸, S. Elles⁵, F. Ellinghaus¹⁷⁸, A.A. Elliot¹⁷², N. Ellis³², J. Elmsheuser²⁷,
 M. Elsing³², D. Emelyanov¹³³, Y. Enari¹⁵⁷, J.S. Ennis¹⁷³, M.B. Epland⁴⁸, J. Erdmann⁴⁶, A. Ereditato¹⁸,
 M. Ernst²⁷, S. Errede¹⁶⁹, M. Escalier¹¹⁹, C. Escobar¹⁷⁰, B. Esposito⁵⁰, O. Estrada Pastor¹⁷⁰,
 A.I. Etienvre¹³⁸, E. Etzion¹⁵⁵, H. Evans⁶⁴, A. Ezhilov¹²⁵, M. Ezzi^{137e}, F. Fabbri^{22a,22b}, L. Fabbri^{22a,22b},
 V. Fabiani¹⁰⁸, G. Facini⁸¹, R.M. Fakhrutdinov¹³², S. Falciano^{134a}, R.J. Falla⁸¹, J. Faltova³², Y. Fang^{35a},
 M. Fanti^{94a,94b}, A. Farbin⁸, A. Farilla^{136a}, C. Farina¹²⁷, E.M. Farina^{123a,123b}, T. Farooque⁹³, S. Farrell¹⁶,
 S.M. Farrington¹⁷³, P. Farthouat³², F. Fassi^{137e}, P. Fassnacht³², D. Fassouliotis⁹, M. Faucci Giannelli⁴⁹,
 A. Favareto^{53a,53b}, W.J. Fawcett¹²², L. Fayard¹¹⁹, O.L. Fedin^{125,q}, W. Fedorko¹⁷¹, S. Feigl¹²¹,
 L. Feligioni⁸⁸, C. Feng^{36b}, E.J. Feng³², M.J. Fenton⁵⁶, A.B. Fenyuk¹³², L. Feremenga⁸,
 P. Fernandez Martinez¹⁷⁰, J. Ferrando⁴⁵, A. Ferrari¹⁶⁸, P. Ferrari¹⁰⁹, R. Ferrari^{123a},
 D.E. Ferreira de Lima^{60b}, A. Ferrer¹⁷⁰, D. Ferrere⁵², C. Ferretti⁹², F. Fiedler⁸⁶, A. Filipčič⁷⁸,
 M. Filippuzzi⁴⁵, F. Filthaut¹⁰⁸, M. Fincke-Keeler¹⁷², K.D. Finelli²⁴, M.C.N. Fiolhais^{128a,128c,r},
 L. Fiorini¹⁷⁰, A. Fischer², C. Fischer¹³, J. Fischer¹⁷⁸, W.C. Fisher⁹³, N. Flaschel⁴⁵, I. Fleck¹⁴³,
 P. Fleischmann⁹², R.R.M. Fletcher¹²⁴, T. Flick¹⁷⁸, B.M. Flierl¹⁰², L.R. Flores Castillo^{62a},
 M.J. Flowerdew¹⁰³, G.T. Forcolin⁸⁷, A. Formica¹³⁸, F.A. Förster¹³, A. Forti⁸⁷, A.G. Foster¹⁹,
 D. Fournier¹¹⁹, H. Fox⁷⁵, S. Fracchia¹⁴¹, P. Francavilla^{126a,126b}, M. Franchini^{22a,22b}, S. Franchino^{60a},
 D. Francis³², L. Franconi¹²¹, M. Franklin⁵⁹, M. Frate¹⁶⁶, M. Fraternali^{123a,123b}, D. Freeborn⁸¹,
 S.M. Fressard-Batraneanu³², B. Freund⁹⁷, D. Froidevaux³², J.A. Frost¹²², C. Fukunaga¹⁵⁸,
 T. Fusayasu¹⁰⁴, J. Fuster¹⁷⁰, O. Gabizon¹⁵⁴, A. Gabrielli^{22a,22b}, A. Gabrielli¹⁶, G.P. Gach^{41a},

S. Gadatsch³², S. Gadowski⁸⁰, G. Gagliardi^{53a,53b}, L.G. Gagnon⁹⁷, C. Galea¹⁰⁸, B. Galhardo^{128a,128c}, E.J. Gallas¹²², B.J. Gallop¹³³, P. Gallus¹³⁰, G. Galster³⁹, K.K. Gan¹¹³, S. Ganguly³⁷, Y. Gao⁷⁷, Y.S. Gao^{145,g}, F.M. Garay Walls^{34a}, C. García¹⁷⁰, J.E. García Navarro¹⁷⁰, J.A. García Pascual^{35a}, M. Garcia-Sciveres¹⁶, R.W. Gardner³³, N. Garelli¹⁴⁵, V. Garonne¹²¹, A. Gascon Bravo⁴⁵, K. Gasnikova⁴⁵, C. Gatti⁵⁰, A. Gaudiello^{53a,53b}, G. Gaudio^{123a}, I.L. Gavrilenko⁹⁸, C. Gay¹⁷¹, G. Gaycken²³, E.N. Gazis¹⁰, C.N.P. Gee¹³³, J. Geisen⁵⁷, M. Geisen⁸⁶, M.P. Geisler^{60a}, K. Gellerstedt^{148a,148b}, C. Gemme^{53a}, M.H. Genest⁵⁸, C. Geng⁹², S. Gentile^{134a,134b}, C. Gentsos¹⁵⁶, S. George⁸⁰, D. Gerbaudo¹³, G. Geßner⁴⁶, S. Ghasemi¹⁴³, M. Ghneimat²³, B. Giacobbe^{22a}, S. Giagu^{134a,134b}, N. Giangiacomi^{22a,22b}, P. Giannetti^{126a}, S.M. Gibson⁸⁰, M. Gignac¹⁷¹, M. Gilchriese¹⁶, D. Gillberg³¹, G. Gilles¹⁷⁸, D.M. Gingrich^{3,d}, M.P. Giordani^{167a,167c}, F.M. Giorgi^{22a}, P.F. Giraud¹³⁸, P. Giromini⁵⁹, G. Giugliarelli^{167a,167c}, D. Giugni^{94a}, F. Giuli¹²², C. Giuliani¹⁰³, M. Giuliani^{60b}, B.K. Gjelsten¹²¹, S. Gkaitatzis¹⁵⁶, I. Gkalias^{9,s}, E.L. Gkougkousis¹³, P. Gkountoumis¹⁰, L.K. Gladilin¹⁰¹, C. Glasman⁸⁵, J. Glatzer¹³, P.C.F. Glaysher⁴⁵, A. Glazov⁴⁵, M. Goblirsch-Kolb²⁵, J. Godlewski⁴², S. Goldfarb⁹¹, T. Golling⁵², D. Golubkov¹³², A. Gomes^{128a,128b,128d}, R. Gonçalo^{128a}, R. Goncalves Gama^{26a}, J. Goncalves Pinto Firmino Da Costa¹³⁸, G. Gonella⁵¹, L. Gonella¹⁹, A. Gongadze⁶⁸, J.L. Gonski⁵⁹, S. González de la Hoz¹⁷⁰, S. Gonzalez-Sevilla⁵², L. Goossens³², P.A. Gorbounov⁹⁹, H.A. Gordon²⁷, I. Gorelov¹⁰⁷, B. Gorini³², E. Gorini^{76a,76b}, A. Gorišek⁷⁸, A.T. Goshaw⁴⁸, C. Gössling⁴⁶, M.I. Gostkin⁶⁸, C.A. Gottardo²³, C.R. Goudet¹¹⁹, D. Goujdami^{137c}, A.G. Goussiou¹⁴⁰, N. Govender^{147b,t}, E. Gozani¹⁵⁴, I. Grabowska-Bold^{41a}, P.O.J. Gradin¹⁶⁸, J. Gramling¹⁶⁶, E. Gramstad¹²¹, S. Grancagnolo¹⁷, V. Gratchev¹²⁵, P.M. Gravila^{28f}, C. Gray⁵⁶, H.M. Gray¹⁶, Z.D. Greenwood^{82,u}, C. Grefe²³, K. Gregersen⁸¹, I.M. Gregor⁴⁵, P. Grenier¹⁴⁵, K. Grevtsov⁵, J. Griffiths⁸, A.A. Grillo¹³⁹, K. Grimm⁷⁵, S. Grinstein^{13,v}, Ph. Gris³⁷, J.-F. Grivaz¹¹⁹, S. Groh⁸⁶, E. Gross¹⁷⁵, J. Grosse-Knetter⁵⁷, G.C. Grossi⁸², Z.J. Grout⁸¹, A. Grummer¹⁰⁷, L. Guan⁹², W. Guan¹⁷⁶, J. Guenther³², F. Guescini^{163a}, D. Guest¹⁶⁶, O. Gueta¹⁵⁵, B. Gui¹¹³, E. Guido^{53a,53b}, T. Guillemin⁵, S. Guindon³², U. Gul⁵⁶, C. Gumpert³², J. Guo^{36c}, W. Guo⁹², Y. Guo^{36a,w}, R. Gupta⁴³, S. Gurbuz^{20a}, G. Gustavino¹¹⁵, B.J. Gutelman¹⁵⁴, P. Gutierrez¹¹⁵, N.G. Gutierrez Ortiz⁸¹, C. Gutschow⁸¹, C. Guyot¹³⁸, M.P. Guzik^{41a}, C. Gwenlan¹²², C.B. Gwilliam⁷⁷, A. Haas¹¹², C. Haber¹⁶, H.K. Hadavand⁸, N. Haddad^{137e}, A. Hadef⁸⁸, S. Hageböck²³, M. Hagihara¹⁶⁴, H. Hakobyan^{180,*}, M. Haleem⁴⁵, J. Haley¹¹⁶, G. Halladjian⁹³, G.D. Hallewell⁸⁸, K. Hamacher¹⁷⁸, P. Hamal¹¹⁷, K. Hamano¹⁷², A. Hamilton^{147a}, G.N. Hamity¹⁴¹, P.G. Hamnett⁴⁵, L. Han^{36a}, S. Han^{35a,35d}, K. Hanagaki^{69,x}, K. Hanawa¹⁵⁷, M. Hance¹³⁹, D.M. Handl¹⁰², B. Haney¹²⁴, P. Hanke^{60a}, J.B. Hansen³⁹, J.D. Hansen³⁹, M.C. Hansen²³, P.H. Hansen³⁹, K. Hara¹⁶⁴, A.S. Hard¹⁷⁶, T. Harenberg¹⁷⁸, F. Hariri¹¹⁹, S. Harkusha⁹⁵, P.F. Harrison¹⁷³, N.M. Hartmann¹⁰², Y. Hasegawa¹⁴², A. Hasib⁴⁹, S. Hassani¹³⁸, S. Haug¹⁸, R. Hauser⁹³, L. Hauswald⁴⁷, L.B. Havener³⁸, M. Havranek¹³⁰, C.M. Hawkes¹⁹, R.J. Hawkings³², D. Hayakawa¹⁵⁹, D. Hayden⁹³, C.P. Hays¹²², J.M. Hays⁷⁹, H.S. Hayward⁷⁷, S.J. Haywood¹³³, S.J. Head¹⁹, T. Heck⁸⁶, V. Hedberg⁸⁴, L. Heelan⁸, S. Heer²³, K.K. Heidegger⁵¹, S. Heim⁴⁵, T. Heim¹⁶, B. Heinemann^{45,y}, J.J. Heinrich¹⁰², L. Heinrich¹¹², C. Heinz⁵⁵, J. Hejbal¹²⁹, L. Helary³², A. Held¹⁷¹, S. Hellman^{148a,148b}, C. Helsens³², R.C.W. Henderson⁷⁵, Y. Heng¹⁷⁶, S. Henkelmann¹⁷¹, A.M. Henriques Correia³², S. Henrot-Versille¹¹⁹, G.H. Herbert¹⁷, H. Herde²⁵, V. Herget¹⁷⁷, Y. Hernández Jiménez^{147c}, H. Herr⁸⁶, G. Herten⁵¹, R. Hertenberger¹⁰², L. Hervas³², T.C. Herwig¹²⁴, G.G. Hesketh⁸¹, N.P. Hessey^{163a}, J.W. Hetherly⁴³, S. Higashino⁶⁹, E. Higón-Rodríguez¹⁷⁰, K. Hildebrand³³, E. Hill¹⁷², J.C. Hill³⁰, K.H. Hiller⁴⁵, S.J. Hillier¹⁹, M. Hils⁴⁷, I. Hinchliffe¹⁶, M. Hirose⁵¹, D. Hirschbuehl¹⁷⁸, B. Hiti⁷⁸, O. Hladík¹²⁹, D.R. Hlálučku^{147c}, X. Hoad⁴⁹, J. Hobbs¹⁵⁰, N. Hod^{163a}, M.C. Hodgkinson¹⁴¹, P. Hodgson¹⁴¹, A. Hoecker³², M.R. Hoeferkamp¹⁰⁷, F. Hoenig¹⁰², D. Hohn²³, T.R. Holmes³³, M. Holzbock¹⁰², M. Homann⁴⁶, S. Honda¹⁶⁴, T. Honda⁶⁹, T.M. Hong¹²⁷, B.H. Hooberman¹⁶⁹, W.H. Hopkins¹¹⁸, Y. Horii¹⁰⁵, A.J. Horton¹⁴⁴, J.-Y. Hostachy⁵⁸, A. Hostiuc¹⁴⁰, S. Hou¹⁵³, A. Hoummada^{137a}, J. Howarth⁸⁷, J. Hoya⁷⁴, M. Hrabovsky¹¹⁷, J. Hrdinka³²,

I. Hristova¹⁷, J. Hrvnac¹¹⁹, T. Hrynn'ova⁵, A. Hrynevich⁹⁶, P.J. Hsu⁶³, S.-C. Hsu¹⁴⁰, Q. Hu²⁷, S. Hu^{36c},
 Y. Huang^{35a}, Z. Hubacek¹³⁰, F. Hubaut⁸⁸, F. Huegging²³, T.B. Huffman¹²², E.W. Hughes³⁸,
 M. Huhtinen³², R.F.H. Hunter³¹, P. Huo¹⁵⁰, N. Huseynov^{68,b}, J. Huston⁹³, J. Huth⁵⁹, R. Hyneman⁹²,
 G. Iacobucci⁵², G. Iakovidis²⁷, I. Ibragimov¹⁴³, L. Iconomou-Fayard¹¹⁹, Z. Idrissi^{137e}, P. Iengo³²,
 O. Igonkina^{109,z}, T. Iizawa¹⁷⁴, Y. Ikegami⁶⁹, M. Ikeno⁶⁹, Y. Ilchenko^{11,aa}, D. Iliadis¹⁵⁶, N. Ilic¹⁴⁵,
 F. Iltzsche⁴⁷, G. Introzzi^{123a,123b}, P. Ioannou^{9,*}, M. Iodice^{136a}, K. Iordanidou³⁸, V. Ippolito⁵⁹,
 M.F. Isaacson¹⁶⁸, N. Ishijima¹²⁰, M. Ishino¹⁵⁷, M. Ishitsuka¹⁵⁹, C. Issever¹²², S. Istin^{20a}, F. Ito¹⁶⁴,
 J.M. Iturbe Ponce^{62a}, R. Iuppa^{162a,162b}, H. Iwasaki⁶⁹, J.M. Izen⁴⁴, V. Izzo^{106a}, S. Jabbar³, P. Jackson¹,
 R.M. Jacobs²³, V. Jain², K.B. Jakobi⁸⁶, K. Jakobs⁵¹, S. Jakobsen⁶⁵, T. Jakoubek¹²⁹, D.O. Jamin¹¹⁶,
 D.K. Jana⁸², R. Jansky⁵², J. Janssen²³, M. Janus⁵⁷, P.A. Janus^{41a}, G. Jarlskog⁸⁴, N. Javadov^{68,b},
 T. Javůrek⁵¹, M. Javurkova⁵¹, F. Jeanneau¹³⁸, L. Jeanty¹⁶, J. Jejelava^{54a,ab}, A. Jelinskas¹⁷³, P. Jenni^{51,ac},
 C. Jeske¹⁷³, S. Jézéquel⁵, H. Ji¹⁷⁶, J. Jia¹⁵⁰, H. Jiang⁶⁷, Y. Jiang^{36a}, Z. Jiang¹⁴⁵, S. Jiggins⁸¹,
 J. Jimenez Pena¹⁷⁰, S. Jin^{35b}, A. Jinaru^{28b}, O. Jinnouchi¹⁵⁹, H. Jivan^{147c}, P. Johansson¹⁴¹, K.A. Johns⁷,
 C.A. Johnson⁶⁴, W.J. Johnson¹⁴⁰, K. Jon-And^{148a,148b}, R.W.L. Jones⁷⁵, S.D. Jones¹⁵¹, S. Jones⁷,
 T.J. Jones⁷⁷, J. Jongmanns^{60a}, P.M. Jorge^{128a,128b}, J. Jovicevic^{163a}, X. Ju¹⁷⁶, A. Juste Rozas^{13,v},
 M.K. Köhler¹⁷⁵, A. Kaczmarska⁴², M. Kado¹¹⁹, H. Kagan¹¹³, M. Kagan¹⁴⁵, S.J. Kahn⁸⁸, T. Kaji¹⁷⁴,
 E. Kajomovitz¹⁵⁴, C.W. Kalderon⁸⁴, A. Kaluza⁸⁶, S. Kama⁴³, A. Kamenshchikov¹³², N. Kanaya¹⁵⁷,
 L. Kanjur⁷⁸, V.A. Kantserov¹⁰⁰, J. Kanzaki⁶⁹, B. Kaplan¹¹², L.S. Kaplan¹⁷⁶, D. Kar^{147c}, K. Karakostas¹⁰,
 N. Karastathis¹⁰, M.J. Kareem^{163b}, E. Karentzos¹⁰, S.N. Karpov⁶⁸, Z.M. Karpova⁶⁸, K. Karthik¹¹²,
 V. Kartvelishvili⁷⁵, A.N. Karyukhin¹³², K. Kasahara¹⁶⁴, L. Kashif¹⁷⁶, R.D. Kass¹¹³, A. Kastanas¹⁴⁹,
 Y. Kataoka¹⁵⁷, C. Kato¹⁵⁷, A. Katre⁵², J. Katzy⁴⁵, K. Kawade⁷⁰, K. Kawagoe⁷³, T. Kawamoto¹⁵⁷,
 G. Kawamura⁵⁷, E.F. Kay⁷⁷, V.F. Kazanin^{111,c}, R. Keeler¹⁷², R. Kehoe⁴³, J.S. Keller³¹, E. Kellermann⁸⁴,
 J.J. Kempster⁸⁰, J Kendrick¹⁹, H. Keoshkerian¹⁶¹, O. Kepka¹²⁹, B.P. Kerševan⁷⁸, S. Kersten¹⁷⁸,
 R.A. Keyes⁹⁰, M. Khader¹⁶⁹, F. Khalil-zada¹², A. Khanov¹¹⁶, A.G. Kharlamov^{111,c}, T. Kharlamova^{111,c},
 A. Khodinov¹⁶⁰, T.J. Khoo⁵², V. Khovanskiy^{99,*}, E. Khramov⁶⁸, J. Khubua^{54b,ad}, S. Kido⁷⁰,
 C.R. Kilby⁸⁰, H.Y. Kim⁸, S.H. Kim¹⁶⁴, Y.K. Kim³³, N. Kimura¹⁵⁶, O.M. Kind¹⁷, B.T. King⁷⁷,
 D. Kirchmeier⁴⁷, J. Kirk¹³³, A.E. Kiryunin¹⁰³, T. Kishimoto¹⁵⁷, D. Kisielewska^{41a}, V. Kitali⁴⁵,
 O. Kiverny⁵, E. Kladiva^{146b}, T. Klapdor-Kleingrothaus⁵¹, M.H. Klein⁹², M. Klein⁷⁷, U. Klein⁷⁷,
 K. Kleinknecht⁸⁶, P. Klimek¹¹⁰, A. Klimentov²⁷, R. Klingenberg^{46,*}, T. Klingl²³, T. Klioutchnikova³²,
 F.F. Klitzner¹⁰², E.-E. Kluge^{60a}, P. Kluit¹⁰⁹, S. Kluth¹⁰³, E. Kneringer⁶⁵, E.B.F.G. Knoops⁸⁸, A. Knue¹⁰³,
 A. Kobayashi¹⁵⁷, D. Kobayashi⁷³, T. Kobayashi¹⁵⁷, M. Kobel⁴⁷, M. Kocian¹⁴⁵, P. Kodys¹³¹, T. Koffas³¹,
 E. Koffeman¹⁰⁹, N.M. Köhler¹⁰³, T. Koi¹⁴⁵, M. Kolb^{60b}, I. Koletsou⁵, T. Kondo⁶⁹, N. Kondrashova^{36c},
 K. Köneke⁵¹, A.C. König¹⁰⁸, T. Kono^{69,ae}, R. Konoplich^{112,af}, N. Konstantinidis⁸¹, B. Konya⁸⁴,
 R. Kopeliansky⁶⁴, S. Koperny^{41a}, A.K. Kopp⁵¹, K. Korcyl⁴², K. Kordas¹⁵⁶, A. Korn⁸¹, A.A. Korol^{111,c},
 I. Korolkov¹³, E.V. Korolkova¹⁴¹, O. Kortner¹⁰³, S. Kortner¹⁰³, T. Kosek¹³¹, V.V. Kostyukhin²³,
 A. Kotwal⁴⁸, A. Koulouris¹⁰, A. Kourkoumeli-Charalampidi^{123a,123b}, C. Kourkoumelis⁹, E. Kourlitis¹⁴¹,
 V. Kouskoura²⁷, A.B. Kowalewska⁴², R. Kowalewski¹⁷², T.Z. Kowalski^{41a}, C. Kozakai¹⁵⁷,
 W. Kozanecki¹³⁸, A.S. Kozhin¹³², V.A. Kramarenko¹⁰¹, G. Kramberger⁷⁸, D. Krasnopevtsev¹⁰⁰,
 M.W. Krasny⁸³, A. Krasznahorkay³², D. Krauss¹⁰³, J.A. Kremer^{41a}, J. Kretzschmar⁷⁷, K. Kreutzfeldt⁵⁵,
 P. Krieger¹⁶¹, K. Krizka¹⁶, K. Kroeninger⁴⁶, H. Kroha¹⁰³, J. Kroll¹²⁹, J. Kroll¹²⁴, J. Kroseberg²³,
 J. Krstic¹⁴, U. Kruchonak⁶⁸, H. Krüger²³, N. Krumnack⁶⁷, M.C. Kruse⁴⁸, T. Kubota⁹¹, H. Kucuk⁸¹,
 S. Kuday^{4b}, J.T. Kuechler¹⁷⁸, S. Kuehn³², A. Kugel^{60a}, F. Kuger¹⁷⁷, T. Kuhl⁴⁵, V. Kukhtin⁶⁸, R. Kukla⁸⁸,
 Y. Kulchitsky⁹⁵, S. Kuleshov^{34b}, Y.P. Kulinich¹⁶⁹, M. Kuna^{134a,134b}, T. Kunigo⁷¹, A. Kupco¹²⁹,
 T. Kupfer⁴⁶, O. Kuprash¹⁵⁵, H. Kurashige⁷⁰, L.L. Kurchaninov^{163a}, Y.A. Kurochkin⁹⁵,
 M.G. Kurth^{35a,35d}, E.S. Kuwertz¹⁷², M. Kuze¹⁵⁹, J. Kvita¹¹⁷, T. Kwan¹⁷², D. Kyriazopoulos¹⁴¹,
 A. La Rosa¹⁰³, J.L. La Rosa Navarro^{26d}, L. La Rotonda^{40a,40b}, F. La Ruffa^{40a,40b}, C. Lacasta¹⁷⁰,
 F. Lacava^{134a,134b}, J. Lacey⁴⁵, D.P.J. Lack⁸⁷, H. Lacker¹⁷, D. Lacour⁸³, E. Ladygin⁶⁸, R. Lafaye⁵,

B. Laforge⁸³, T. Lagouri¹⁷⁹, S. Lai⁵⁷, S. Lammers⁶⁴, W. Lampl⁷, E. Lançon²⁷, U. Landgraf⁵¹,
 M.P.J. Landon⁷⁹, M.C. Lanfermann⁵², V.S. Lang⁴⁵, J.C. Lange¹³, R.J. Langenberg³², A.J. Lankford¹⁶⁶,
 F. Lanni²⁷, K. Lantzsch²³, A. Lanza^{123a}, A. Lapertosa^{53a,53b}, S. Laplace⁸³, J.F. Laporte¹³⁸, T. Lari^{94a},
 F. Lasagni Manghi^{22a,22b}, M. Lassnig³², T.S. Lau^{62a}, P. Laurelli⁵⁰, W. Lavrijsen¹⁶, A.T. Law¹³⁹,
 P. Laycock⁷⁷, T. Lazovich⁵⁹, M. Lazzaroni^{94a,94b}, B. Le⁹¹, O. Le Dortz⁸³, E. Le Guiriec⁸⁸,
 E.P. Le Quilleuc¹³⁸, M. LeBlanc¹⁷², T. LeCompte⁶, F. Ledroit-Guillon⁵⁸, C.A. Lee²⁷, G.R. Lee^{34a},
 S.C. Lee¹⁵³, L. Lee⁵⁹, B. Lefebvre⁹⁰, G. Lefebvre⁸³, M. Lefebvre¹⁷², F. Legger¹⁰², C. Leggett¹⁶,
 G. Lehmann Miotto³², X. Lei⁷, W.A. Leight⁴⁵, M.A.L. Leite^{26d}, R. Leitner¹³¹, D. Lellouch¹⁷⁵,
 B. Lemmer⁵⁷, K.J.C. Leney⁸¹, T. Lenz²³, B. Lenzi³², R. Leone⁷, S. Leone^{126a}, C. Leonidopoulos⁴⁹,
 G. Lerner¹⁵¹, C. Leroy⁹⁷, R. Les¹⁶¹, A.A.J. Lesage¹³⁸, C.G. Lester³⁰, M. Levchenko¹²⁵, J. Levêque⁵,
 D. Levin⁹², L.J. Levinson¹⁷⁵, M. Levy¹⁹, D. Lewis⁷⁹, B. Li^{36a,w}, H. Li¹⁵⁰, L. Li^{36c}, Q. Li^{35a,35d}, Q. Li^{36a},
 S. Li⁴⁸, X. Li^{36c}, Y. Li¹⁴³, Z. Liang^{35a}, B. Liberti^{135a}, A. Liblong¹⁶¹, K. Lie^{62c}, J. Liebal²³, W. Liebig¹⁵,
 A. Limosani¹⁵², C.Y. Lin³⁰, K. Lin⁹³, S.C. Lin¹⁸², T.H. Lin⁸⁶, R.A. Linck⁶⁴, B.E. Lindquist¹⁵⁰,
 A.E. Lioni⁵², E. Lipeles¹²⁴, A. Lipniacka¹⁵, M. Lisovyi^{60b}, T.M. Liss^{169,ag}, A. Lister¹⁷¹, A.M. Litke¹³⁹,
 B. Liu⁶⁷, H. Liu⁹², H. Liu²⁷, J.K.K. Liu¹²², J. Liu^{36b}, J.B. Liu^{36a}, K. Liu⁸⁸, L. Liu¹⁶⁹, M. Liu^{36a},
 Y.L. Liu^{36a}, Y. Liu^{36a}, M. Livan^{123a,123b}, A. Lleres⁵⁸, J. Llorente Merino^{35a}, S.L. Lloyd⁷⁹, C.Y. Lo^{62b},
 F. Lo Sterzo⁴³, E.M. Lobodzinska⁴⁵, P. Loch⁷, F.K. Loebinger⁸⁷, A. Loesle⁵¹, K.M. Loew²⁵, T. Lohse¹⁷,
 K. Lohwasser¹⁴¹, M. Lokajicek¹²⁹, B.A. Long²⁴, J.D. Long¹⁶⁹, R.E. Long⁷⁵, L. Longo^{76a,76b},
 K.A.Looper¹¹³, J.A. Lopez^{34b}, I. Lopez Paz¹³, A. Lopez Solis⁸³, J. Lorenz¹⁰², N. Lorenzo Martinez⁵,
 M. Losada²¹, P.J. Lösel¹⁰², X. Lou^{35a}, A. Lounis¹¹⁹, J. Love⁶, P.A. Love⁷⁵, H. Lu^{62a}, N. Lu⁹², Y.J. Lu⁶³,
 H.J. Lubatti¹⁴⁰, C. Luci^{134a,134b}, A. Lucotte⁵⁸, C. Luedtke⁵¹, F. Luehring⁶⁴, W. Lukas⁶⁵, L. Luminari^{134a},
 O. Lundberg^{148a,148b}, B. Lund-Jensen¹⁴⁹, M.S. Lutz⁸⁹, P.M. Luzi⁸³, D. Lynn²⁷, R. Lysak¹²⁹, E. Lytken⁸⁴,
 F. Lyu^{35a}, V. Lyubushkin⁶⁸, H. Ma²⁷, L.L. Ma^{36b}, Y. Ma^{36b}, G. Maccarrone⁵⁰, A. Macchiolo¹⁰³,
 C.M. Macdonald¹⁴¹, B. Maček⁷⁸, J. Machado Miguens^{124,128b}, D. Madaffari¹⁷⁰, R. Madar³⁷,
 W.F. Mader⁴⁷, A. Madsen⁴⁵, N. Madysa⁴⁷, J. Maeda⁷⁰, S. Maeland¹⁵, T. Maeno²⁷, A.S. Maevskiy¹⁰¹,
 V. Magerl⁵¹, C. Maiani¹¹⁹, C. Maidantchik^{26a}, T. Maier¹⁰², A. Maio^{128a,128b,128d}, O. Majersky^{146a},
 S. Majewski¹¹⁸, Y. Makida⁶⁹, N. Makovec¹¹⁹, B. Malaescu⁸³, Pa. Malecki⁴², V.P. Maleev¹²⁵, F. Malek⁵⁸,
 U. Mallik⁶⁶, D. Malon⁶, C. Malone³⁰, S. Maltezos¹⁰, S. Malyukov³², J. Mamuzic¹⁷⁰, G. Mancini⁵⁰,
 I. Mandić⁷⁸, J. Maneira^{128a,128b}, L. Manhaes de Andrade Filho^{26b}, J. Manjarres Ramos⁴⁷,
 K.H. Mankinen⁸⁴, A. Mann¹⁰², A. Manousos³², B. Mansoulie¹³⁸, J.D. Mansour^{35a}, R. Mantefel⁹⁰,
 M. Mantoani⁵⁷, S. Manzoni^{94a,94b}, L. Mapelli³², G. Marceca²⁹, L. March⁵², L. Marchese¹²²,
 G. Marchiori⁸³, M. Marcisovsky¹²⁹, C.A. Marin Tobon³², M. Marjanovic³⁷, D.E. Marley⁹²,
 F. Marroquim^{26a}, S.P. Marsden⁸⁷, Z. Marshall¹⁶, M.U.F Martensson¹⁶⁸, S. Marti-Garcia¹⁷⁰,
 C.B. Martin¹¹³, T.A. Martin¹⁷³, V.J. Martin⁴⁹, B. Martin dit Latour¹⁵, M. Martinez^{13,v},
 V.I. Martinez Outschoorn¹⁶⁹, S. Martin-Haugh¹³³, V.S. Martoiu^{28b}, A.C. Martyniuk⁸¹, A. Marzin³²,
 L. Masetti⁸⁶, T. Mashimo¹⁵⁷, R. Mashinistov⁹⁸, J. Masik⁸⁷, A.L. Maslennikov^{111,c}, L.H. Mason⁹¹,
 L. Massa^{135a,135b}, P. Mastrandrea⁵, A. Mastroberardino^{40a,40b}, T. Masubuchi¹⁵⁷, P. Mättig¹⁷⁸,
 J. Maurer^{28b}, S.J. Maxfield⁷⁷, D.A. Maximov^{111,c}, R. Mazini¹⁵³, I. Maznas¹⁵⁶, S.M. Mazza^{94a,94b},
 N.C. Mc Fadden¹⁰⁷, G. Mc Goldrick¹⁶¹, S.P. Mc Kee⁹², A. McCarn⁹², R.L. McCarthy¹⁵⁰,
 T.G. McCarthy¹⁰³, L.I. McClymont⁸¹, E.F. McDonald⁹¹, J.A. McFayden³², G. Mchedlidze⁵⁷,
 S.J. McMahon¹³³, P.C. McNamara⁹¹, C.J. McNicol¹⁷³, R.A. McPherson^{172,o}, S. Meehan¹⁴⁰,
 T.J. Megy⁵¹, S. Mehlhase¹⁰², A. Mehta⁷⁷, T. Meideck⁵⁸, K. Meier^{60a}, B. Meirose⁴⁴, D. Melini^{170,ah},
 B.R. Mellado Garcia^{147c}, J.D. Mellenthin⁵⁷, M. Melo^{146a}, F. Meloni¹⁸, A. Melzer²³, S.B. Menary⁸⁷,
 L. Meng⁷⁷, X.T. Meng⁹², A. Mengarelli^{22a,22b}, S. Menke¹⁰³, E. Meoni^{40a,40b}, S. Mergelmeyer¹⁷,
 C. Merlassino¹⁸, P. Mermod⁵², L. Merola^{106a,106b}, C. Meroni^{94a}, F.S. Merritt³³, A. Messina^{134a,134b},
 J. Metcalfe⁶, A.S. Mete¹⁶⁶, C. Meyer¹²⁴, J.-P. Meyer¹³⁸, J. Meyer¹⁰⁹, H. Meyer Zu Theenhausen^{60a},
 F. Miano¹⁵¹, R.P. Middleton¹³³, S. Miglioranzi^{53a,53b}, L. Mijović⁴⁹, G. Mikenberg¹⁷⁵,

M. Mikestikova¹²⁹, M. Mikuž⁷⁸, M. Milesi⁹¹, A. Milic¹⁶¹, D.A. Millar⁷⁹, D.W. Miller³³, C. Mills⁴⁹,
 A. Milov¹⁷⁵, D.A. Milstead^{148a,148b}, A.A. Minaenko¹³², Y. Minami¹⁵⁷, I.A. Minashvili^{54b},
 A.I. Mincer¹¹², B. Mindur^{41a}, M. Mineev⁶⁸, Y. Minegishi¹⁵⁷, Y. Ming¹⁷⁶, L.M. Mir¹³, A. Mirto^{76a,76b},
 K.P. Mistry¹²⁴, T. Mitani¹⁷⁴, J. Mitrevski¹⁰², V.A. Mitsou¹⁷⁰, A. Miucci¹⁸, P.S. Miyagawa¹⁴¹,
 A. Mizukami⁶⁹, J.U. Mjörnmark⁸⁴, T. Mkrtchyan¹⁸⁰, M. Mlynarikova¹³¹, T. Moa^{148a,148b},
 K. Mochizuki⁹⁷, P. Mogg⁵¹, S. Mohapatra³⁸, S. Molander^{148a,148b}, R. Moles-Valls²³, M.C. Mondragon⁹³,
 K. Mönig⁴⁵, J. Monk³⁹, E. Monnier⁸⁸, A. Montalbano¹⁵⁰, J. Montejo Berlingen³², F. Monticelli⁷⁴,
 S. Monzani^{94a}, R.W. Moore³, N. Morange¹¹⁹, D. Moreno²¹, M. Moreno Llácer³², P. Morettini^{53a},
 S. Morgenstern³², D. Mori¹⁴⁴, T. Mori¹⁵⁷, M. Morii⁵⁹, M. Morinaga¹⁷⁴, V. Morisbak¹²¹, A.K. Morley³²,
 G. Mornacchi³², J.D. Morris⁷⁹, L. Morvaj¹⁵⁰, P. Moschovakos¹⁰, M. Mosidze^{54b}, H.J. Moss¹⁴¹,
 J. Moss^{145,ai}, K. Motohashi¹⁵⁹, R. Mount¹⁴⁵, E. Mountricha²⁷, E.J.W. Moyse⁸⁹, S. Muanza⁸⁸,
 F. Mueller¹⁰³, J. Mueller¹²⁷, R.S.P. Mueller¹⁰², D. Muenstermann⁷⁵, P. Mullen⁵⁶, G.A. Mullier¹⁸,
 F.J. Munoz Sanchez⁸⁷, W.J. Murray^{173,133}, H. Musheghyan³², M. Muškinja⁷⁸, A.G. Myagkov^{132,aj},
 M. Myska¹³⁰, B.P. Nachman¹⁶, O. Nackenhorst⁵², K. Nagai¹²², R. Nagai^{69,ae}, K. Nagano⁶⁹,
 Y. Nagasaka⁶¹, K. Nagata¹⁶⁴, M. Nagel⁵¹, E. Nagy⁸⁸, A.M. Nairz³², Y. Nakahama¹⁰⁵, K. Nakamura⁶⁹,
 T. Nakamura¹⁵⁷, I. Nakano¹¹⁴, R.F. Naranjo Garcia⁴⁵, R. Narayan¹¹, D.I. Narrias Villar^{60a},
 I. Naryshkin¹²⁵, T. Naumann⁴⁵, G. Navarro²¹, R. Nayyar⁷, H.A. Neal⁹², P.Yu. Nechaeva⁹⁸, T.J. Neep¹³⁸,
 A. Negri^{123a,123b}, M. Negrini^{22a}, S. Nektarievic¹⁰⁸, C. Nellist⁵⁷, A. Nelson¹⁶⁶, M.E. Nelson¹²²,
 S. Nemecek¹²⁹, P. Nemethy¹¹², M. Nessi^{32,ak}, M.S. Neubauer¹⁶⁹, M. Neumann¹⁷⁸, P.R. Newman¹⁹,
 T.Y. Ng^{62c}, Y.S. Ng¹⁷, T. Nguyen Manh⁹⁷, R.B. Nickerson¹²², R. Nicolaïdou¹³⁸, J. Nielsen¹³⁹,
 N. Nikiforou¹¹, V. Nikolaenko^{132,aj}, I. Nikolic-Audit⁸³, K. Nikolopoulos¹⁹, P. Nilsson²⁷, Y. Ninomiya⁶⁹,
 A. Nisati^{134a}, N. Nishu^{36c}, R. Nisius¹⁰³, I. Nitsche⁴⁶, T. Nitta¹⁷⁴, T. Nobe¹⁵⁷, Y. Noguchi⁷¹,
 M. Nomachi¹²⁰, I. Nomidis³¹, M.A. Nomura²⁷, T. Nooney⁷⁹, M. Nordberg³², N. Norjoharuddeen¹²²,
 O. Novgorodova⁴⁷, M. Nozaki⁶⁹, L. Nozka¹¹⁷, K. Ntekas¹⁶⁶, E. Nurse⁸¹, F. Nuti⁹¹, K. O'connor²⁵,
 D.C. O'Neil¹⁴⁴, A.A. O'Rourke⁴⁵, V. O'Shea⁵⁶, F.G. Oakham^{31,d}, H. Oberlack¹⁰³, T. Obermann²³,
 J. Ocariz⁸³, A. Ochi⁷⁰, I. Ochoa³⁸, J.P. Ochoa-Ricoux^{34a}, S. Oda⁷³, S. Odaka⁶⁹, A. Oh⁸⁷, S.H. Oh⁴⁸,
 C.C. Ohm¹⁴⁹, H. Ohman¹⁶⁸, H. Oide^{53a,53b}, H. Okawa¹⁶⁴, Y. Okumura¹⁵⁷, T. Okuyama⁶⁹, A. Olariu^{28b},
 L.F. Oleiro Seabra^{128a}, S.A. Olivares Pino^{34a}, D. Oliveira Damazio²⁷, M.J.R. Olsson³³, A. Olszewski⁴²,
 J. Olszowska⁴², A. Onofre^{128a,128e}, K. Onogi¹⁰⁵, P.U.E. Onyisi^{11,aa}, H. Oppen¹²¹, M.J. Oreglia³³,
 Y. Oren¹⁵⁵, D. Orestano^{136a,136b}, N. Orlando^{62b}, R.S. Orr¹⁶¹, B. Osculati^{53a,53b,*}, R. Ospanov^{36a},
 G. Otero y Garzon²⁹, H. Otono⁷³, M. Ouchrif^{137d}, F. Ould-Saada¹²¹, A. Ouraou¹³⁸, K.P. Oussoren¹⁰⁹,
 Q. Ouyang^{35a}, M. Owen⁵⁶, R.E. Owen¹⁹, V.E. Ozcan^{20a}, N. Ozturk⁸, K. Pachal¹⁴⁴, A. Pacheco Pages¹³,
 L. Pacheco Rodriguez¹³⁸, C. Padilla Aranda¹³, S. Pagan Griso¹⁶, M. Paganini¹⁷⁹, F. Paige²⁷,
 G. Palacino⁶⁴, S. Palazzo^{40a,40b}, S. Palestini³², M. Palka^{41b}, D. Pallin³⁷, E.St. Panagiotopoulou¹⁰,
 I. Panagoulias¹⁰, C.E. Pandini⁵², J.G. Panduro Vazquez⁸⁰, P. Pani³², S. Panitkin²⁷, D. Pantea^{28b},
 L. Paolozzi⁵², Th.D. Papadopoulou¹⁰, K. Papageorgiou^{9,s}, A. Paramonov⁶, D. Paredes Hernandez¹⁷⁹,
 A.J. Parker⁷⁵, M.A. Parker³⁰, K.A. Parker⁴⁵, F. Parodi^{53a,53b}, J.A. Parsons³⁸, U. Parzefall⁵¹,
 V.R. Pascuzzi¹⁶¹, J.M. Pasner¹³⁹, E. Pasqualucci^{134a}, S. Passaggio^{53a}, Fr. Pastore⁸⁰, S. Pataria⁸⁶,
 J.R. Pater⁸⁷, T. Pauly³², B. Pearson¹⁰³, S. Pedraza Lopez¹⁷⁰, R. Pedro^{128a,128b}, S.V. Peleganchuk^{111,c},
 O. Penc¹²⁹, C. Peng^{35a,35d}, H. Peng^{36a}, J. Penwell⁶⁴, B.S. Peralva^{26b}, M.M. Perego¹³⁸,
 D.V. Perepelitsa²⁷, F. Peri¹⁷, L. Perini^{94a,94b}, H. Pernegger³², S. Perrella^{106a,106b}, R. Peschke⁴⁵,
 V.D. Peshekhanov^{68,*}, K. Peters⁴⁵, R.F.Y. Peters⁸⁷, B.A. Petersen³², T.C. Petersen³⁹, E. Petit⁵⁸,
 A. Petridis¹, C. Petridou¹⁵⁶, P. Petroff¹¹⁹, E. Petrolo^{134a}, M. Petrov¹²², F. Petrucci^{136a,136b},
 N.E. Pettersson⁸⁹, A. Peyaud¹³⁸, R. Pezoa^{34b}, F.H. Phillips⁹³, P.W. Phillips¹³³, G. Piacquadio¹⁵⁰,
 E. Pianori¹⁷³, A. Picazio⁸⁹, M.A. Pickering¹²², R. Piegaia²⁹, J.E. Pilcher³³, A.D. Pilkington⁸⁷,
 M. Pinamonti^{135a,135b}, J.L. Pinfold³, H. Pirumov⁴⁵, M. Pitt¹⁷⁵, L. Plazak^{146a}, M.-A. Pleier²⁷,
 V. Pleskot⁸⁶, E. Plotnikova⁶⁸, D. Pluth⁶⁷, P. Podberezko¹¹¹, R. Poettgen⁸⁴, R. Poggi^{123a,123b},

L. Poggioli¹¹⁹, I. Pogrebnyak⁹³, D. Pohl²³, I. Pokharel⁵⁷, G. Polesello^{123a}, A. Poley⁴⁵,
 A. Policicchio^{40a,40b}, R. Polifka³², A. Polini^{22a}, C.S. Pollard⁵⁶, V. Polychronakos²⁷, K. Pommès³²,
 D. Ponomarenko¹⁰⁰, L. Pontecorvo^{134a}, G.A. Popeneciu^{28d}, D.M. Portillo Quintero⁸³, S. Pospisil¹³⁰,
 K. Potamianos⁴⁵, I.N. Potrap⁶⁸, C.J. Potter³⁰, H. Potti¹¹, T. Poulsen⁸⁴, J. Poveda³²,
 M.E. Pozo Astigarraga³², P. Pralavorio⁸⁸, A. Pranko¹⁶, S. Prell⁶⁷, D. Price⁸⁷, M. Primavera^{76a},
 S. Prince⁹⁰, N. Proklova¹⁰⁰, K. Prokofiev^{62c}, F. Prokoshin^{34b}, S. Protopopescu²⁷, J. Proudfoot⁶,
 M. Przybycien^{41a}, A. Puri¹⁶⁹, P. Puzo¹¹⁹, J. Qian⁹², G. Qin⁵⁶, Y. Qin⁸⁷, A. Quadt⁵⁷,
 M. Queitsch-Maitland⁴⁵, D. Quilty⁵⁶, S. Raddum¹²¹, V. Radeka²⁷, V. Radescu¹²²,
 S.K. Radhakrishnan¹⁵⁰, P. Radloff¹¹⁸, P. Rados⁹¹, F. Ragusa^{94a,94b}, G. Rahal¹⁸¹, J.A. Raine⁸⁷,
 S. Rajagopalan²⁷, C. Rangel-Smith¹⁶⁸, T. Rashid¹¹⁹, S. Raspopov⁵, M.G. Ratti^{94a,94b}, D.M. Rauch⁴⁵,
 F. Rauscher¹⁰², S. Rave⁸⁶, I. Ravinovich¹⁷⁵, J.H. Rawling⁸⁷, M. Raymond³², A.L. Read¹²¹,
 N.P. Readioff⁵⁸, M. Reale^{76a,76b}, D.M. Rebuzzi^{123a,123b}, A. Redelbach¹⁷⁷, G. Redlinger²⁷, R. Reece¹³⁹,
 R.G. Reed^{147c}, K. Reeves⁴⁴, L. Rehnisch¹⁷, J. Reichert¹²⁴, A. Reiss⁸⁶, C. Rembser³², H. Ren^{35a,35d},
 M. Rescigno^{134a}, S. Resconi^{94a}, E.D. Ressegue¹²⁴, S. Rettie¹⁷¹, E. Reynolds¹⁹, O.L. Rezanova^{111,c},
 P. Reznicek¹³¹, R. Rezvani⁹⁷, R. Richter¹⁰³, S. Richter⁸¹, E. Richter-Was^{41b}, O. Ricken²³, M. Ridel⁸³,
 P. Rieck¹⁰³, C.J. Riegel¹⁷⁸, J. Rieger⁵⁷, O. Rifki¹¹⁵, M. Rijssenbeek¹⁵⁰, A. Rimoldi^{123a,123b},
 M. Rimoldi¹⁸, L. Rinaldi^{22a}, G. Ripellino¹⁴⁹, B. Ristic³², E. Ritsch³², I. Riu¹³, F. Rizatdinova¹¹⁶,
 E. Rizvi⁷⁹, C. Rizzi¹³, R.T. Roberts⁸⁷, S.H. Robertson^{90,o}, A. Robichaud-Veronneau⁹⁰, D. Robinson³⁰,
 J.E.M. Robinson⁴⁵, A. Robson⁵⁶, E. Rocco⁸⁶, C. Roda^{126a,126b}, Y. Rodina^{88,al}, S. Rodriguez Bosca¹⁷⁰,
 A. Rodriguez Perez¹³, D. Rodriguez Rodriguez¹⁷⁰, S. Roe³², C.S. Rogan⁵⁹, O. Røhne¹²¹, J. Roloff⁵⁹,
 A. Romaniouk¹⁰⁰, M. Romano^{22a,22b}, S.M. Romano Saez³⁷, E. Romero Adam¹⁷⁰, N. Rompotis⁷⁷,
 M. Ronzani⁵¹, L. Roos⁸³, S. Rosati^{134a}, K. Rosbach⁵¹, P. Rose¹³⁹, N.-A. Rosien⁵⁷, E. Rossi^{106a,106b},
 L.P. Rossi^{53a}, J.H.N. Rosten³⁰, R. Rosten¹⁴⁰, M. Rotaru^{28b}, J. Rothberg¹⁴⁰, D. Rousseau¹¹⁹, D. Roy^{147c},
 A. Rozanov⁸⁸, Y. Rozen¹⁵⁴, X. Ruan^{147c}, F. Rubbo¹⁴⁵, F. Rühr⁵¹, A. Ruiz-Martinez³¹, Z. Rurikova⁵¹,
 N.A. Rusakovich⁶⁸, H.L. Russell⁹⁰, J.P. Rutherford⁷, N. Ruthmann³², E.M. Rüttinger⁴⁵,
 Y.F. Ryabov¹²⁵, M. Rybar¹⁶⁹, G. Rybkin¹¹⁹, S. Ryu⁶, A. Ryzhov¹³², G.F. Rzehorz⁵⁷, A.F. Saavedra¹⁵²,
 G. Sabato¹⁰⁹, S. Sacerdoti²⁹, H.F-W. Sadrozinski¹³⁹, R. Sadykov⁶⁸, F. Safai Tehrani^{134a}, P. Saha¹¹⁰,
 M. Sahinsoy^{60a}, M. Saimpert⁴⁵, M. Saito¹⁵⁷, T. Saito¹⁵⁷, H. Sakamoto¹⁵⁷, Y. Sakurai¹⁷⁴,
 G. Salamanna^{136a,136b}, J.E. Salazar Loyola^{34b}, D. Salek¹⁰⁹, P.H. Sales De Bruin¹⁶⁸, D. Salihagic¹⁰³,
 A. Salnikov¹⁴⁵, J. Salt¹⁷⁰, D. Salvatore^{40a,40b}, F. Salvatore¹⁵¹, A. Salvucci^{62a,62b,62c}, A. Salzburger³²,
 D. Sammel⁵¹, D. Sampsonidis¹⁵⁶, D. Sampsonidou¹⁵⁶, J. Sánchez¹⁷⁰, V. Sanchez Martinez¹⁷⁰,
 A. Sanchez Pineda^{167a,167c}, H. Sandaker¹²¹, R.L. Sandbach⁷⁹, C.O. Sander⁴⁵, M. Sandhoff¹⁷⁸,
 C. Sandoval²¹, D.P.C. Sankey¹³³, M. Sannino^{53a,53b}, Y. Sano¹⁰⁵, A. Sansoni⁵⁰, C. Santoni³⁷,
 H. Santos^{128a}, I. Santoyo Castillo¹⁵¹, A. Sapronov⁶⁸, J.G. Saraiva^{128a,128d}, B. Sarrazin²³, O. Sasaki⁶⁹,
 K. Sato¹⁶⁴, E. Sauvan⁵, G. Savage⁸⁰, P. Savard^{161,d}, N. Savic¹⁰³, C. Sawyer¹³³, L. Sawyer^{82,u},
 J. Saxon³³, C. Sbarra^{22a}, A. Sbrizzi^{22a,22b}, T. Scanlon⁸¹, D.A. Scannicchio¹⁶⁶, J. Schaarschmidt¹⁴⁰,
 P. Schacht¹⁰³, B.M. Schachtner¹⁰², D. Schaefer³³, L. Schaefer¹²⁴, R. Schaefer⁴⁵, J. Schaeffer⁸⁶,
 S. Schaepe³², S. Schaetzle^{60b}, U. Schäfer⁸⁶, A.C. Schaffer¹¹⁹, D. Schaile¹⁰², R.D. Schamberger¹⁵⁰,
 V.A. Schegelsky¹²⁵, D. Scheirich¹³¹, F. Schenck¹⁷, M. Schernau¹⁶⁶, C. Schiavi^{53a,53b}, S. Schier¹³⁹,
 L.K. Schildgen²³, C. Schillo⁵¹, M. Schioppa^{40a,40b}, S. Schlenker³², K.R. Schmidt-Sommerfeld¹⁰³,
 K. Schmieden³², C. Schmitt⁸⁶, S. Schmitz⁸⁶, U. Schnoor⁵¹, L. Schoeffel¹³⁸,
 A. Schoening^{60b}, B.D. Schoenrock⁹³, E. Schopf²³, M. Schott⁸⁶, J.F.P. Schouwenberg¹⁰⁸,
 J. Schovancova³², S. Schramm⁵², N. Schuh⁸⁶, A. Schulte⁸⁶, M.J. Schultens²³, H.-C. Schultz-Coulon^{60a},
 H. Schulz¹⁷, M. Schumacher⁵¹, B.A. Schumm¹³⁹, Ph. Schune¹³⁸, A. Schwartzman¹⁴⁵, T.A. Schwarz⁹²,
 H. Schweiger⁸⁷, Ph. Schwemling¹³⁸, R. Schwienhorst⁹³, J. Schwindling¹³⁸, A. Sciandra²³, G. Sciolla²⁵,
 M. Scornajenghi^{40a,40b}, F. Scuri^{126a}, F. Scutti⁹¹, J. Searcy⁹², P. Seema²³, S.C. Seidel¹⁰⁷, A. Seiden¹³⁹,
 J.M. Seixas^{26a}, G. Sekhniaidze^{106a}, K. Sekhon⁹², S.J. Sekula⁴³, N. Semprini-Cesari^{22a,22b}, S. Senkin³⁷,

C. Serfon¹²¹, L. Serin¹¹⁹, L. Serkin^{167a,167b}, M. Sessa^{136a,136b}, R. Seuster¹⁷², H. Severini¹¹⁵, T. Šfiligoj⁷⁸, F. Sforza¹⁶⁵, A. Sfyrla⁵², E. Shabalina⁵⁷, N.W. Shaikh^{148a,148b}, L.Y. Shan^{35a}, R. Shang¹⁶⁹, J.T. Shank²⁴, M. Shapiro¹⁶, P.B. Shatalov⁹⁹, K. Shaw^{167a,167b}, S.M. Shaw⁸⁷, A. Shcherbakova^{148a,148b}, C.Y. Shehu¹⁵¹, Y. Shen¹¹⁵, N. Sherafati³¹, A.D. Sherman²⁴, P. Sherwood⁸¹, L. Shi^{153,am}, S. Shimizu⁷⁰, C.O. Shimmin¹⁷⁹, M. Shimojima¹⁰⁴, I.P.J. Shipsey¹²², S. Shirabe⁷³, M. Shiyakova^{68,an}, J. Shlomi¹⁷⁵, A. Shmeleva⁹⁸, D. Shoaleh Saadi⁹⁷, M.J. Shochet³³, S. Shojaii^{94a,94b}, D.R. Shope¹¹⁵, S. Shrestha¹¹³, E. Shulga¹⁰⁰, M.A. Shupe⁷, P. Sicho¹²⁹, A.M. Sickles¹⁶⁹, P.E. Sidebo¹⁴⁹, E. Sideras Haddad^{147c}, O. Sidiropoulou¹⁷⁷, A. Sidoti^{22a,22b}, F. Siegert⁴⁷, Dj. Sijacki¹⁴, J. Silva^{128a,128d}, S.B. Silverstein^{148a}, V. Simak¹³⁰, L. Simic⁶⁸, S. Simion¹¹⁹, E. Simioni⁸⁶, B. Simmons⁸¹, M. Simon⁸⁶, P. Sinervo¹⁶¹, N.B. Sinev¹¹⁸, M. Sioli^{22a,22b}, G. Siragusa¹⁷⁷, I. Siral⁹², S.Yu. Sivoklokov¹⁰¹, J. Sjölin^{148a,148b}, M.B. Skinner⁷⁵, P. Skubic¹¹⁵, M. Slater¹⁹, T. Slavicek¹³⁰, M. Slawinska⁴², K. Sliwa¹⁶⁵, R. Slovak¹³¹, V. Smakhtin¹⁷⁵, B.H. Smart⁵, J. Smiesko^{146a}, N. Smirnov¹⁰⁰, S.Yu. Smirnov¹⁰⁰, Y. Smirnov¹⁰⁰, L.N. Smirnova^{101,ao}, O. Smirnova⁸⁴, J.W. Smith⁵⁷, M.N.K. Smith³⁸, R.W. Smith³⁸, M. Smizanska⁷⁵, K. Smolek¹³⁰, A.A. Snesarev⁹⁸, I.M. Snyder¹¹⁸, S. Snyder²⁷, R. Sobie^{172,o}, F. Socher⁴⁷, A. Soffer¹⁵⁵, A. Søgaard⁴⁹, D.A. Soh¹⁵³, G. Sokhrannyi⁷⁸, C.A. Solans Sanchez³², M. Solar¹³⁰, E.Yu. Soldatov¹⁰⁰, U. Soldevila¹⁷⁰, A.A. Solodkov¹³², A. Soloshenko⁶⁸, O.V. Solovyanov¹³², V. Solovyev¹²⁵, P. Sommer¹⁴¹, H. Son¹⁶⁵, A. Sopczak¹³⁰, D. Sosa^{60b}, C.L. Sotiropoulou^{126a,126b}, S. Sottocornola^{123a,123b}, R. Soualah^{167a,167c}, A.M. Soukharev^{111,c}, D. South⁴⁵, B.C. Sowden⁸⁰, S. Spagnolo^{76a,76b}, M. Spalla^{126a,126b}, M. Spangenberg¹⁷³, F. Spanò⁸⁰, D. Sperlich¹⁷, F. Spettel¹⁰³, T.M. Speker^{60a}, R. Spighi^{22a}, G. Spigo³², L.A. Spiller⁹¹, M. Spousta¹³¹, R.D. St. Denis^{56,*}, A. Stabile^{94a,94b}, R. Stamen^{60a}, S. Stamm¹⁷, E. Stanecka⁴², R.W. Stanek⁶, C. Stanescu^{136a}, M.M. Stanitzki⁴⁵, B.S. Stapf¹⁰⁹, S. Stapnes¹²¹, E.A. Starchenko¹³², G.H. Stark³³, J. Stark⁵⁸, S.H Stark³⁹, P. Staroba¹²⁹, P. Starovoitov^{60a}, S. Stärz³², R. Staszewski⁴², M. Stegler⁴⁵, P. Steinberg²⁷, B. Stelzer¹⁴⁴, H.J. Stelzer³², O. Stelzer-Chilton^{163a}, H. Stenzel⁵⁵, T.J. Stevenson⁷⁹, G.A. Stewart⁵⁶, M.C. Stockton¹¹⁸, M. Stoebe⁹⁰, G. Stoica^{28b}, P. Stolte⁵⁷, S. Stonjek¹⁰³, A.R. Stradling⁸, A. Straessner⁴⁷, M.E. Stramaglia¹⁸, J. Strandberg¹⁴⁹, S. Strandberg^{148a,148b}, M. Strauss¹¹⁵, P. Strizenec^{146b}, R. Ströhmer¹⁷⁷, D.M. Strom¹¹⁸, R. Stroynowski⁴³, A. Strubig⁴⁹, S.A. Stucci²⁷, B. Stugu¹⁵, N.A. Styles⁴⁵, D. Su¹⁴⁵, J. Su¹²⁷, S. Suchek^{60a}, Y. Sugaya¹²⁰, M. Suk¹³⁰, V.V. Sulin⁹⁸, DMS Sultan^{162a,162b}, S. Sultansoy^{4c}, T. Sumida⁷¹, S. Sun⁵⁹, X. Sun³, K. Suruliz¹⁵¹, C.J.E. Suster¹⁵², M.R. Sutton¹⁵¹, S. Suzuki⁶⁹, M. Svatos¹²⁹, M. Swiatlowski³³, S.P. Swift², I. Sykora^{146a}, T. Sykora¹³¹, D. Ta⁵¹, K. Tackmann⁴⁵, J. Taenzer¹⁵⁵, A. Taffard¹⁶⁶, R. Tafirout^{163a}, E. Tahirovic⁷⁹, N. Taiblum¹⁵⁵, H. Takai²⁷, R. Takashima⁷², E.H. Takasugi¹⁰³, K. Takeda⁷⁰, T. Takeshita¹⁴², Y. Takubo⁶⁹, M. Talby⁸⁸, A.A. Talyshев^{111,c}, J. Tanaka¹⁵⁷, M. Tanaka¹⁵⁹, R. Tanaka¹¹⁹, S. Tanaka⁶⁹, R. Tanioka⁷⁰, B.B. Tannenwald¹¹³, S. Tapia Araya^{34b}, S. Tapprogge⁸⁶, S. Tarem¹⁵⁴, G.F. Tartarelli^{94a}, P. Tas¹³¹, M. Tasevsky¹²⁹, T. Tashiro⁷¹, E. Tassi^{40a,40b}, A. Tavares Delgado^{128a,128b}, Y. Tayalati^{137e}, A.C. Taylor¹⁰⁷, A.J. Taylor⁴⁹, G.N. Taylor⁹¹, P.T.E. Taylor⁹¹, W. Taylor^{163b}, P. Teixeira-Dias⁸⁰, D. Temple¹⁴⁴, H. Ten Kate³², P.K. Teng¹⁵³, J.J. Teoh¹²⁰, F. Tepel¹⁷⁸, S. Terada⁶⁹, K. Terashi¹⁵⁷, J. Terron⁸⁵, S. Terzo¹³, M. Testa⁵⁰, R.J. Teuscher^{161,o}, S.J. Thais¹⁷⁹, T. Theveneaux-Pelzer⁸⁸, F. Thiele³⁹, J.P. Thomas¹⁹, J. Thomas-Wilske⁸⁰, P.D. Thompson¹⁹, A.S. Thompson⁵⁶, L.A. Thomsen¹⁷⁹, E. Thomson¹²⁴, Y. Tian³⁸, M.J. Tibbetts¹⁶, R.E. Ticse Torres⁵⁷, V.O. Tikhomirov^{98,ap}, Yu.A. Tikhonov^{111,c}, S. Timoshenko¹⁰⁰, P. Tipton¹⁷⁹, S. Tisserant⁸⁸, K. Todome¹⁵⁹, S. Todorova-Nova⁵, S. Todt⁴⁷, J. Tojo⁷³, S. Tokár^{146a}, K. Tokushuku⁶⁹, E. Tolley¹¹³, L. Tomlinson⁸⁷, M. Tomoto¹⁰⁵, L. Tompkins^{145,aq}, K. Toms¹⁰⁷, B. Tong⁵⁹, P. Tornambe⁵¹, E. Torrence¹¹⁸, H. Torres⁴⁷, E. Torró Pastor¹⁴⁰, J. Toth^{88,ar}, F. Touchard⁸⁸, D.R. Tovey¹⁴¹, C.J. Treado¹¹², T. Trefzger¹⁷⁷, F. Tresoldi¹⁵¹, A. Tricoli²⁷, I.M. Trigger^{163a}, S. Trincaz-Duvold⁸³, M.F. Tripiana¹³, W. Trischuk¹⁶¹, B. Trocmé⁵⁸, A. Trofymov⁴⁵, C. Troncon^{94a}, M. Trottier-McDonald¹⁶, M. Trovatelli¹⁷², L. Truong^{147b}, M. Trzebinski⁴², A. Trzupek⁴², K.W. Tsang^{62a}, J.C-L. Tseng¹²², P.V. Tsiareshka⁹⁵, N. Tsirintanis⁹, S. Tsiskaridze¹³, V. Tsiskaridze⁵¹,

E.G. Tskhadadze^{54a}, I.I. Tsukerman⁹⁹, V. Tsulaia¹⁶, S. Tsuno⁶⁹, D. Tsybychev¹⁵⁰, Y. Tu^{62b},
 A. Tudorache^{28b}, V. Tudorache^{28b}, T.T. Tulbure^{28a}, A.N. Tuna⁵⁹, S. Turchikhin⁶⁸, D. Turgeman¹⁷⁵,
 I. Turk Cakir^{4b,as}, R. Turra^{94a}, P.M. Tuts³⁸, G. Ucchielli^{22a,22b}, I. Ueda⁶⁹, M. Ughetto^{148a,148b},
 F. Ukegawa¹⁶⁴, G. Unař³², A. Undrus²⁷, G. Unel¹⁶⁶, F.C. Ungaro⁹¹, Y. Unno⁶⁹, K. Uno¹⁵⁷,
 C. Unverdorben¹⁰², J. Urban^{146b}, P. Urquijo⁹¹, P. Urrejola⁸⁶, G. Usai⁸, J. Usui⁶⁹, L. Vacavant⁸⁸,
 V. Vacek¹³⁰, B. Vachon⁹⁰, K.O.H. Vadla¹²¹, A. Vaidya⁸¹, C. Valderanis¹⁰², E. Valdes Santurio^{148a,148b},
 M. Valente⁵², S. Valentini^{22a,22b}, A. Valero¹⁷⁰, L. Valéry¹³, S. Valkar¹³¹, A. Vallier⁵,
 J.A. Valls Ferrer¹⁷⁰, W. Van Den Wollenberg¹⁰⁹, H. van der Graaf¹⁰⁹, P. van Gemmeren⁶,
 J. Van Nieuwkoop¹⁴⁴, I. van Vulpen¹⁰⁹, M.C. van Woerden¹⁰⁹, M. Vanadia^{135a,135b}, W. Vandelli³²,
 A. Vaniachine¹⁶⁰, P. Vankov¹⁰⁹, G. Vardanyan¹⁸⁰, R. Vari^{134a}, E.W. Varnes⁷, C. Varni^{53a,53b}, T. Varol⁴³,
 D. Varouchas¹¹⁹, A. Vartapetian⁸, K.E. Varvell¹⁵², J.G. Vasquez¹⁷⁹, G.A. Vasquez^{34b}, F. Vazeille³⁷,
 D. Vazquez Furelos¹³, T. Vazquez Schroeder⁹⁰, J. Veatch⁵⁷, V. Veeraraghavan⁷, L.M. Veloce¹⁶¹,
 F. Veloso^{128a,128c}, S. Veneziano^{134a}, A. Ventura^{76a,76b}, M. Venturi¹⁷², N. Venturi³², A. Venturini²⁵,
 V. Vercesi^{123a}, M. Verducci^{136a,136b}, W. Verkerke¹⁰⁹, A.T. Vermeulen¹⁰⁹, J.C. Vermeulen¹⁰⁹,
 M.C. Vetterli^{144,d}, N. Viaux Maira^{34b}, O. Viazlo⁸⁴, I. Vichou^{169,*}, T. Vickey¹⁴¹, O.E. Vickey Boeriu¹⁴¹,
 G.H.A. Viehhauser¹²², S. Viel¹⁶, L. Vigani¹²², M. Villa^{22a,22b}, M. Villaplana Perez^{94a,94b}, E. Vilucchi⁵⁰,
 M.G. Vincter³¹, V.B. Vinogradov⁶⁸, A. Vishwakarma⁴⁵, C. Vittori^{22a,22b}, I. Vivarelli¹⁵¹, S. Vlachos¹⁰,
 M. Vogel¹⁷⁸, P. Vokac¹³⁰, G. Volpi¹³, H. von der Schmitt¹⁰³, E. von Toerne²³, V. Vorobel¹³¹,
 K. Vorobev¹⁰⁰, M. Vos¹⁷⁰, R. Voss³², J.H. Vossebeld⁷⁷, N. Vranjes¹⁴, M. Vranjes Milosavljevic¹⁴,
 V. Vrba¹³⁰, M. Vreeswijk¹⁰⁹, R. Vuillermet³², I. Vukotic³³, P. Wagner²³, W. Wagner¹⁷⁸,
 J. Wagner-Kuhr¹⁰², H. Wahlberg⁷⁴, S. Wahrmund⁴⁷, K. Wakamiya⁷⁰, J. Walder⁷⁵, R. Walker¹⁰²,
 W. Walkowiak¹⁴³, V. Wallangen^{148a,148b}, C. Wang^{35b}, C. Wang^{36b,at}, F. Wang¹⁷⁶, H. Wang¹⁶, H. Wang³,
 J. Wang⁴⁵, J. Wang¹⁵², Q. Wang¹¹⁵, R.-J. Wang⁸³, R. Wang⁶, S.M. Wang¹⁵³, T. Wang³⁸, W. Wang^{153,au},
 W. Wang^{36a,av}, Z. Wang^{36c}, C. Wanotayaroj⁴⁵, A. Warburton⁹⁰, C.P. Ward³⁰, D.R. Wardrope⁸¹,
 A. Washbrook⁴⁹, P.M. Watkins¹⁹, A.T. Watson¹⁹, M.F. Watson¹⁹, G. Watts¹⁴⁰, S. Watts⁸⁷,
 B.M. Waugh⁸¹, A.F. Webb¹¹, S. Webb⁸⁶, M.S. Weber¹⁸, S.M. Weber^{60a}, S.W. Weber¹⁷⁷, S.A. Weber³¹,
 J.S. Webster⁶, A.R. Weidberg¹²², B. Weinert⁶⁴, J. Weingarten⁵⁷, M. Weirich⁸⁶, C. Weiser⁵¹, H. Weits¹⁰⁹,
 P.S. Wells³², T. Wenaus²⁷, T. Wengler³², S. Wenig³², N. Wermes²³, M.D. Werner⁶⁷, P. Werner³²,
 M. Wessels^{60a}, T.D. Weston¹⁸, K. Whalen¹¹⁸, N.L. Whallon¹⁴⁰, A.M. Wharton⁷⁵, A.S. White⁹²,
 A. White⁸, M.J. White¹, R. White^{34b}, D. Whiteson¹⁶⁶, B.W. Whitmore⁷⁵, F.J. Wickens¹³³,
 W. Wiedenmann¹⁷⁶, M. Wielers¹³³, C. Wiglesworth³⁹, L.A.M. Wiik-Fuchs⁵¹, A. Wildauer¹⁰³, F. Wilk⁸⁷,
 H.G. Wilkens³², H.H. Williams¹²⁴, S. Williams¹⁰⁹, C. Willis⁹³, S. Willocq⁸⁹, J.A. Wilson¹⁹,
 I. Wingerter-Seez⁵, E. Winkels¹⁵¹, F. Winklmeier¹¹⁸, O.J. Winston¹⁵¹, B.T. Winter²³, M. Wittgen¹⁴⁵,
 M. Wobisch^{82,uu}, A. Wolf⁸⁶, T.M.H. Wolf¹⁰⁹, R. Wolff⁸⁸, M.W. Wolter⁴², H. Wolters^{128a,128c},
 V.W.S. Wong¹⁷¹, N.L. Woods¹³⁹, S.D. Worm¹⁹, B.K. Wosiek⁴², J. Wotschack³², K.W. Wozniak⁴²,
 M. Wu³³, S.L. Wu¹⁷⁶, X. Wu⁵², Y. Wu⁹², T.R. Wyatt⁸⁷, B.M. Wynne⁴⁹, S. Xella³⁹, Z. Xi⁹², L. Xia^{35c},
 D. Xu^{35a}, L. Xu²⁷, T. Xu¹³⁸, W. Xu⁹², B. Yabsley¹⁵², S. Yacoob^{147a}, D. Yamaguchi¹⁵⁹, Y. Yamaguchi¹⁵⁹,
 A. Yamamoto⁶⁹, S. Yamamoto¹⁵⁷, T. Yamanaka¹⁵⁷, F. Yamane⁷⁰, M. Yamatani¹⁵⁷, T. Yamazaki¹⁵⁷,
 Y. Yamazaki⁷⁰, Z. Yan²⁴, H. Yang^{36c}, H. Yang¹⁶, Y. Yang¹⁵³, Z. Yang¹⁵, W.-M. Yao¹⁶, Y.C. Yap⁴⁵,
 Y. Yasu⁶⁹, E. Yatsenko⁵, K.H. Yau Wong²³, J. Ye⁴³, S. Ye²⁷, I. Yeletskikh⁶⁸, E. Yigitbasi²⁴,
 E. Yildirim⁸⁶, K. Yorita¹⁷⁴, K. Yoshihara¹²⁴, C. Young¹⁴⁵, C.J.S. Young³², J. Yu⁸, J. Yu⁶⁷, S.P.Y. Yuen²³,
 I. Yusuff^{30,aw}, B. Zabinski⁴², G. Zacharis¹⁰, R. Zaidan¹³, A.M. Zaitsev^{132,aj}, N. Zakharchuk⁴⁵,
 J. Zalieckas¹⁵, A. Zaman¹⁵⁰, S. Zambito⁵⁹, D. Zanzi⁹¹, C. Zeitnitz¹⁷⁸, G. Zemaitytė¹²², A. Zemla^{41a},
 J.C. Zeng¹⁶⁹, Q. Zeng¹⁴⁵, O. Zenin¹³², T. Ženiš^{146a}, D. Zerwas¹¹⁹, D. Zhang^{36b}, D. Zhang⁹², F. Zhang¹⁷⁶,
 G. Zhang^{36a,av}, H. Zhang¹¹⁹, J. Zhang⁶, L. Zhang⁵¹, L. Zhang^{36a}, M. Zhang¹⁶⁹, P. Zhang^{35b}, R. Zhang²³,
 R. Zhang^{36a,at}, X. Zhang^{36b}, Y. Zhang^{35a,35d}, Z. Zhang¹¹⁹, X. Zhao⁴³, Y. Zhao^{36b,ax}, Z. Zhao^{36a},
 A. Zhemchugov⁶⁸, B. Zhou⁹², C. Zhou¹⁷⁶, L. Zhou⁴³, M. Zhou^{35a,35d}, M. Zhou¹⁵⁰, N. Zhou^{36c}, Y. Zhou⁷,

C.G. Zhu^{36b}, H. Zhu^{35a}, J. Zhu⁹², Y. Zhu^{36a}, X. Zhuang^{35a}, K. Zhukov⁹⁸, A. Zibell¹⁷⁷, D. Ziemska⁶⁴, N.I. Zimine⁶⁸, C. Zimmermann⁸⁶, S. Zimmermann⁵¹, Z. Zinonos¹⁰³, M. Zinser⁸⁶, M. Ziolkowski¹⁴³, L. Živković¹⁴, G. Zobernig¹⁷⁶, A. Zoccoli^{22a,22b}, R. Zou³³, M. zur Nedden¹⁷, L. Zwalski³².

¹ Department of Physics, University of Adelaide, Adelaide, Australia

² Physics Department, SUNY Albany, Albany NY, United States of America

³ Department of Physics, University of Alberta, Edmonton AB, Canada

⁴ ^(a) Department of Physics, Ankara University, Ankara; ^(b) Istanbul Aydin University, Istanbul; ^(c) Division of Physics, TOBB University of Economics and Technology, Ankara, Turkey

⁵ LAPP, CNRS/IN2P3 and Université Savoie Mont Blanc, Annecy-le-Vieux, France

⁶ High Energy Physics Division, Argonne National Laboratory, Argonne IL, United States of America

⁷ Department of Physics, University of Arizona, Tucson AZ, United States of America

⁸ Department of Physics, The University of Texas at Arlington, Arlington TX, United States of America

⁹ Physics Department, National and Kapodistrian University of Athens, Athens, Greece

¹⁰ Physics Department, National Technical University of Athens, Zografou, Greece

¹¹ Department of Physics, The University of Texas at Austin, Austin TX, United States of America

¹² Institute of Physics, Azerbaijan Academy of Sciences, Baku, Azerbaijan

¹³ Institut de Física d'Altes Energies (IFAE), The Barcelona Institute of Science and Technology, Barcelona, Spain

¹⁴ Institute of Physics, University of Belgrade, Belgrade, Serbia

¹⁵ Department for Physics and Technology, University of Bergen, Bergen, Norway

¹⁶ Physics Division, Lawrence Berkeley National Laboratory and University of California, Berkeley CA, United States of America

¹⁷ Department of Physics, Humboldt University, Berlin, Germany

¹⁸ Albert Einstein Center for Fundamental Physics and Laboratory for High Energy Physics, University of Bern, Bern, Switzerland

¹⁹ School of Physics and Astronomy, University of Birmingham, Birmingham, United Kingdom

²⁰ ^(a) Department of Physics, Bogazici University, Istanbul; ^(b) Department of Physics Engineering, Gaziantep University, Gaziantep; ^(d) Istanbul Bilgi University, Faculty of Engineering and Natural Sciences, Istanbul; ^(e) Bahcesehir University, Faculty of Engineering and Natural Sciences, Istanbul, Turkey

²¹ Centro de Investigaciones, Universidad Antonio Narino, Bogota, Colombia

²² ^(a) INFN Sezione di Bologna; ^(b) Dipartimento di Fisica e Astronomia, Università di Bologna, Bologna, Italy

²³ Physikalisches Institut, University of Bonn, Bonn, Germany

²⁴ Department of Physics, Boston University, Boston MA, United States of America

²⁵ Department of Physics, Brandeis University, Waltham MA, United States of America

²⁶ ^(a) Universidade Federal do Rio De Janeiro COPPE/EE/IF, Rio de Janeiro; ^(b) Electrical Circuits Department, Federal University of Juiz de Fora (UFJF), Juiz de Fora; ^(c) Federal University of Sao Joao del Rei (UFSJ), Sao Joao del Rei; ^(d) Instituto de Fisica, Universidade de Sao Paulo, Sao Paulo, Brazil

²⁷ Physics Department, Brookhaven National Laboratory, Upton NY, United States of America

²⁸ ^(a) Transilvania University of Brasov, Brasov; ^(b) Horia Hulubei National Institute of Physics and Nuclear Engineering, Bucharest; ^(c) Department of Physics, Alexandru Ioan Cuza University of Iasi, Iasi; ^(d) National Institute for Research and Development of Isotopic and Molecular Technologies, Physics Department, Cluj Napoca; ^(e) University Politehnica Bucharest, Bucharest; ^(f) West University in Timisoara, Timisoara, Romania

²⁹ Departamento de Física, Universidad de Buenos Aires, Buenos Aires, Argentina

- ³⁰ Cavendish Laboratory, University of Cambridge, Cambridge, United Kingdom
³¹ Department of Physics, Carleton University, Ottawa ON, Canada
³² CERN, Geneva, Switzerland
³³ Enrico Fermi Institute, University of Chicago, Chicago IL, United States of America
³⁴ ^(a) Departamento de Física, Pontificia Universidad Católica de Chile, Santiago; ^(b) Departamento de Física, Universidad Técnica Federico Santa María, Valparaíso, Chile
³⁵ ^(a) Institute of High Energy Physics, Chinese Academy of Sciences, Beijing; ^(b) Department of Physics, Nanjing University, Jiangsu; ^(c) Physics Department, Tsinghua University, Beijing 100084; ^(d) University of Chinese Academy of Science (UCAS), Beijing, China
³⁶ ^(a) Department of Modern Physics and State Key Laboratory of Particle Detection and Electronics, University of Science and Technology of China, Anhui; ^(b) School of Physics, Shandong University, Shandong; ^(c) Department of Physics and Astronomy, Key Laboratory for Particle Physics, Astrophysics and Cosmology, Ministry of Education; Shanghai Key Laboratory for Particle Physics and Cosmology, Shanghai Jiao Tong University, Tsung-Dao Lee Institute, China
³⁷ Université Clermont Auvergne, CNRS/IN2P3, LPC, Clermont-Ferrand, France
³⁸ Nevis Laboratory, Columbia University, Irvington NY, United States of America
³⁹ Niels Bohr Institute, University of Copenhagen, Kobenhavn, Denmark
⁴⁰ ^(a) INFN Gruppo Collegato di Cosenza, Laboratori Nazionali di Frascati; ^(b) Dipartimento di Fisica, Università della Calabria, Rende, Italy
⁴¹ ^(a) AGH University of Science and Technology, Faculty of Physics and Applied Computer Science, Krakow; ^(b) Marian Smoluchowski Institute of Physics, Jagiellonian University, Krakow, Poland
⁴² Institute of Nuclear Physics Polish Academy of Sciences, Krakow, Poland
⁴³ Physics Department, Southern Methodist University, Dallas TX, United States of America
⁴⁴ Physics Department, University of Texas at Dallas, Richardson TX, United States of America
⁴⁵ DESY, Hamburg and Zeuthen, Germany
⁴⁶ Lehrstuhl für Experimentelle Physik IV, Technische Universität Dortmund, Dortmund, Germany
⁴⁷ Institut für Kern- und Teilchenphysik, Technische Universität Dresden, Dresden, Germany
⁴⁸ Department of Physics, Duke University, Durham NC, United States of America
⁴⁹ SUPA - School of Physics and Astronomy, University of Edinburgh, Edinburgh, United Kingdom
⁵⁰ INFN e Laboratori Nazionali di Frascati, Frascati, Italy
⁵¹ Fakultät für Mathematik und Physik, Albert-Ludwigs-Universität, Freiburg, Germany
⁵² Departement de Physique Nucleaire et Corpusculaire, Université de Genève, Geneva, Switzerland
⁵³ ^(a) INFN Sezione di Genova; ^(b) Dipartimento di Fisica, Università di Genova, Genova, Italy
⁵⁴ ^(a) E. Andronikashvili Institute of Physics, Iv. Javakhishvili Tbilisi State University, Tbilisi; ^(b) High Energy Physics Institute, Tbilisi State University, Tbilisi, Georgia
⁵⁵ II Physikalisches Institut, Justus-Liebig-Universität Giessen, Giessen, Germany
⁵⁶ SUPA - School of Physics and Astronomy, University of Glasgow, Glasgow, United Kingdom
⁵⁷ II Physikalisches Institut, Georg-August-Universität, Göttingen, Germany
⁵⁸ Laboratoire de Physique Subatomique et de Cosmologie, Université Grenoble-Alpes, CNRS/IN2P3, Grenoble, France
⁵⁹ Laboratory for Particle Physics and Cosmology, Harvard University, Cambridge MA, United States of America
⁶⁰ ^(a) Kirchhoff-Institut für Physik, Ruprecht-Karls-Universität Heidelberg, Heidelberg; ^(b) Physikalisches Institut, Ruprecht-Karls-Universität Heidelberg, Heidelberg, Germany
⁶¹ Faculty of Applied Information Science, Hiroshima Institute of Technology, Hiroshima, Japan
⁶² ^(a) Department of Physics, The Chinese University of Hong Kong, Shatin, N.T., Hong Kong; ^(b) Department of Physics, The University of Hong Kong, Hong Kong; ^(c) Department of Physics and

- Institute for Advanced Study, The Hong Kong University of Science and Technology, Clear Water Bay, Kowloon, Hong Kong, China
- ⁶³ Department of Physics, National Tsing Hua University, Taiwan, Taiwan
- ⁶⁴ Department of Physics, Indiana University, Bloomington IN, United States of America
- ⁶⁵ Institut für Astro- und Teilchenphysik, Leopold-Franzens-Universität, Innsbruck, Austria
- ⁶⁶ University of Iowa, Iowa City IA, United States of America
- ⁶⁷ Department of Physics and Astronomy, Iowa State University, Ames IA, United States of America
- ⁶⁸ Joint Institute for Nuclear Research, JINR Dubna, Dubna, Russia
- ⁶⁹ KEK, High Energy Accelerator Research Organization, Tsukuba, Japan
- ⁷⁰ Graduate School of Science, Kobe University, Kobe, Japan
- ⁷¹ Faculty of Science, Kyoto University, Kyoto, Japan
- ⁷² Kyoto University of Education, Kyoto, Japan
- ⁷³ Research Center for Advanced Particle Physics and Department of Physics, Kyushu University, Fukuoka, Japan
- ⁷⁴ Instituto de Física La Plata, Universidad Nacional de La Plata and CONICET, La Plata, Argentina
- ⁷⁵ Physics Department, Lancaster University, Lancaster, United Kingdom
- ⁷⁶ ^(a) INFN Sezione di Lecce; ^(b) Dipartimento di Matematica e Fisica, Università del Salento, Lecce, Italy
- ⁷⁷ Oliver Lodge Laboratory, University of Liverpool, Liverpool, United Kingdom
- ⁷⁸ Department of Experimental Particle Physics, Jožef Stefan Institute and Department of Physics, University of Ljubljana, Ljubljana, Slovenia
- ⁷⁹ School of Physics and Astronomy, Queen Mary University of London, London, United Kingdom
- ⁸⁰ Department of Physics, Royal Holloway University of London, Surrey, United Kingdom
- ⁸¹ Department of Physics and Astronomy, University College London, London, United Kingdom
- ⁸² Louisiana Tech University, Ruston LA, United States of America
- ⁸³ Laboratoire de Physique Nucléaire et de Hautes Energies, UPMC and Université Paris-Diderot and CNRS/IN2P3, Paris, France
- ⁸⁴ Fysiska institutionen, Lunds universitet, Lund, Sweden
- ⁸⁵ Departamento de Fisica Teorica C-15, Universidad Autonoma de Madrid, Madrid, Spain
- ⁸⁶ Institut für Physik, Universität Mainz, Mainz, Germany
- ⁸⁷ School of Physics and Astronomy, University of Manchester, Manchester, United Kingdom
- ⁸⁸ CPPM, Aix-Marseille Université and CNRS/IN2P3, Marseille, France
- ⁸⁹ Department of Physics, University of Massachusetts, Amherst MA, United States of America
- ⁹⁰ Department of Physics, McGill University, Montreal QC, Canada
- ⁹¹ School of Physics, University of Melbourne, Victoria, Australia
- ⁹² Department of Physics, The University of Michigan, Ann Arbor MI, United States of America
- ⁹³ Department of Physics and Astronomy, Michigan State University, East Lansing MI, United States of America
- ⁹⁴ ^(a) INFN Sezione di Milano; ^(b) Dipartimento di Fisica, Università di Milano, Milano, Italy
- ⁹⁵ B.I. Stepanov Institute of Physics, National Academy of Sciences of Belarus, Minsk, Republic of Belarus
- ⁹⁶ Research Institute for Nuclear Problems of Byelorussian State University, Minsk, Republic of Belarus
- ⁹⁷ Group of Particle Physics, University of Montreal, Montreal QC, Canada
- ⁹⁸ P.N. Lebedev Physical Institute of the Russian Academy of Sciences, Moscow, Russia
- ⁹⁹ Institute for Theoretical and Experimental Physics (ITEP), Moscow, Russia
- ¹⁰⁰ National Research Nuclear University MEPhI, Moscow, Russia
- ¹⁰¹ D.V. Skobeltsyn Institute of Nuclear Physics, M.V. Lomonosov Moscow State University, Moscow,

Russia

- ¹⁰² Fakultät für Physik, Ludwig-Maximilians-Universität München, München, Germany
¹⁰³ Max-Planck-Institut für Physik (Werner-Heisenberg-Institut), München, Germany
¹⁰⁴ Nagasaki Institute of Applied Science, Nagasaki, Japan
¹⁰⁵ Graduate School of Science and Kobayashi-Maskawa Institute, Nagoya University, Nagoya, Japan
¹⁰⁶ ^(a) INFN Sezione di Napoli; ^(b) Dipartimento di Fisica, Università di Napoli, Napoli, Italy
¹⁰⁷ Department of Physics and Astronomy, University of New Mexico, Albuquerque NM, United States of America
¹⁰⁸ Institute for Mathematics, Astrophysics and Particle Physics, Radboud University Nijmegen/Nikhef, Nijmegen, Netherlands
¹⁰⁹ Nikhef National Institute for Subatomic Physics and University of Amsterdam, Amsterdam, Netherlands
¹¹⁰ Department of Physics, Northern Illinois University, DeKalb IL, United States of America
¹¹¹ Budker Institute of Nuclear Physics, SB RAS, Novosibirsk, Russia
¹¹² Department of Physics, New York University, New York NY, United States of America
¹¹³ Ohio State University, Columbus OH, United States of America
¹¹⁴ Faculty of Science, Okayama University, Okayama, Japan
¹¹⁵ Homer L. Dodge Department of Physics and Astronomy, University of Oklahoma, Norman OK, United States of America
¹¹⁶ Department of Physics, Oklahoma State University, Stillwater OK, United States of America
¹¹⁷ Palacký University, RCPTM, Olomouc, Czech Republic
¹¹⁸ Center for High Energy Physics, University of Oregon, Eugene OR, United States of America
¹¹⁹ LAL, Univ. Paris-Sud, CNRS/IN2P3, Université Paris-Saclay, Orsay, France
¹²⁰ Graduate School of Science, Osaka University, Osaka, Japan
¹²¹ Department of Physics, University of Oslo, Oslo, Norway
¹²² Department of Physics, Oxford University, Oxford, United Kingdom
¹²³ ^(a) INFN Sezione di Pavia; ^(b) Dipartimento di Fisica, Università di Pavia, Pavia, Italy
¹²⁴ Department of Physics, University of Pennsylvania, Philadelphia PA, United States of America
¹²⁵ National Research Centre "Kurchatov Institute" B.P.Konstantinov Petersburg Nuclear Physics Institute, St. Petersburg, Russia
¹²⁶ ^(a) INFN Sezione di Pisa; ^(b) Dipartimento di Fisica E. Fermi, Università di Pisa, Pisa, Italy
¹²⁷ Department of Physics and Astronomy, University of Pittsburgh, Pittsburgh PA, United States of America
¹²⁸ ^(a) Laboratório de Instrumentação e Física Experimental de Partículas - LIP, Lisboa; ^(b) Faculdade de Ciências, Universidade de Lisboa, Lisboa; ^(c) Department of Physics, University of Coimbra, Coimbra; ^(d) Centro de Física Nuclear da Universidade de Lisboa, Lisboa; ^(e) Departamento de Física, Universidade do Minho, Braga; ^(f) Departamento de Física Teórica y del Cosmos, Universidad de Granada, Granada; ^(g) Dep Física and CEFITEC of Faculdade de Ciencias e Tecnologia, Universidade Nova de Lisboa, Caparica, Portugal
¹²⁹ Institute of Physics, Academy of Sciences of the Czech Republic, Praha, Czech Republic
¹³⁰ Czech Technical University in Prague, Praha, Czech Republic
¹³¹ Charles University, Faculty of Mathematics and Physics, Prague, Czech Republic
¹³² State Research Center Institute for High Energy Physics (Protvino), NRC KI, Russia
¹³³ Particle Physics Department, Rutherford Appleton Laboratory, Didcot, United Kingdom
¹³⁴ ^(a) INFN Sezione di Roma; ^(b) Dipartimento di Fisica, Sapienza Università di Roma, Roma, Italy
¹³⁵ ^(a) INFN Sezione di Roma Tor Vergata; ^(b) Dipartimento di Fisica, Università di Roma Tor Vergata, Roma, Italy

- ¹³⁶ ^(a) INFN Sezione di Roma Tre; ^(b) Dipartimento di Matematica e Fisica, Università Roma Tre, Roma, Italy
- ¹³⁷ ^(a) Faculté des Sciences Ain Chock, Réseau Universitaire de Physique des Hautes Energies - Université Hassan II, Casablanca; ^(b) Centre National de l'Energie des Sciences Techniques Nucléaires, Rabat; ^(c) Faculté des Sciences Semlalia, Université Cadi Ayyad, LPHEA-Marrakech; ^(d) Faculté des Sciences, Université Mohamed Premier and LPTPM, Oujda; ^(e) Faculté des sciences, Université Mohammed V, Rabat, Morocco
- ¹³⁸ DSM/IRFU (Institut de Recherches sur les Lois Fondamentales de l'Univers), CEA Saclay (Commissariat à l'Energie Atomique et aux Energies Alternatives), Gif-sur-Yvette, France
- ¹³⁹ Santa Cruz Institute for Particle Physics, University of California Santa Cruz, Santa Cruz CA, United States of America
- ¹⁴⁰ Department of Physics, University of Washington, Seattle WA, United States of America
- ¹⁴¹ Department of Physics and Astronomy, University of Sheffield, Sheffield, United Kingdom
- ¹⁴² Department of Physics, Shinshu University, Nagano, Japan
- ¹⁴³ Department Physik, Universität Siegen, Siegen, Germany
- ¹⁴⁴ Department of Physics, Simon Fraser University, Burnaby BC, Canada
- ¹⁴⁵ SLAC National Accelerator Laboratory, Stanford CA, United States of America
- ¹⁴⁶ ^(a) Faculty of Mathematics, Physics & Informatics, Comenius University, Bratislava; ^(b) Department of Subnuclear Physics, Institute of Experimental Physics of the Slovak Academy of Sciences, Kosice, Slovak Republic
- ¹⁴⁷ ^(a) Department of Physics, University of Cape Town, Cape Town; ^(b) Department of Physics, University of Johannesburg, Johannesburg; ^(c) School of Physics, University of the Witwatersrand, Johannesburg, South Africa
- ¹⁴⁸ ^(a) Department of Physics, Stockholm University; ^(b) The Oskar Klein Centre, Stockholm, Sweden
- ¹⁴⁹ Physics Department, Royal Institute of Technology, Stockholm, Sweden
- ¹⁵⁰ Departments of Physics & Astronomy and Chemistry, Stony Brook University, Stony Brook NY, United States of America
- ¹⁵¹ Department of Physics and Astronomy, University of Sussex, Brighton, United Kingdom
- ¹⁵² School of Physics, University of Sydney, Sydney, Australia
- ¹⁵³ Institute of Physics, Academia Sinica, Taipei, Taiwan
- ¹⁵⁴ Department of Physics, Technion: Israel Institute of Technology, Haifa, Israel
- ¹⁵⁵ Raymond and Beverly Sackler School of Physics and Astronomy, Tel Aviv University, Tel Aviv, Israel
- ¹⁵⁶ Department of Physics, Aristotle University of Thessaloniki, Thessaloniki, Greece
- ¹⁵⁷ International Center for Elementary Particle Physics and Department of Physics, The University of Tokyo, Tokyo, Japan
- ¹⁵⁸ Graduate School of Science and Technology, Tokyo Metropolitan University, Tokyo, Japan
- ¹⁵⁹ Department of Physics, Tokyo Institute of Technology, Tokyo, Japan
- ¹⁶⁰ Tomsk State University, Tomsk, Russia
- ¹⁶¹ Department of Physics, University of Toronto, Toronto ON, Canada
- ¹⁶² ^(a) INFN-TIFPA; ^(b) University of Trento, Trento, Italy
- ¹⁶³ ^(a) TRIUMF, Vancouver BC; ^(b) Department of Physics and Astronomy, York University, Toronto ON, Canada
- ¹⁶⁴ Faculty of Pure and Applied Sciences, and Center for Integrated Research in Fundamental Science and Engineering, University of Tsukuba, Tsukuba, Japan
- ¹⁶⁵ Department of Physics and Astronomy, Tufts University, Medford MA, United States of America
- ¹⁶⁶ Department of Physics and Astronomy, University of California Irvine, Irvine CA, United States of

America

- ¹⁶⁷ ^(a) INFN Gruppo Collegato di Udine, Sezione di Trieste, Udine; ^(b) ICTP, Trieste; ^(c) Dipartimento di Chimica, Fisica e Ambiente, Università di Udine, Udine, Italy
- ¹⁶⁸ Department of Physics and Astronomy, University of Uppsala, Uppsala, Sweden
- ¹⁶⁹ Department of Physics, University of Illinois, Urbana IL, United States of America
- ¹⁷⁰ Instituto de Fisica Corpuscular (IFIC), Centro Mixto Universidad de Valencia - CSIC, Spain
- ¹⁷¹ Department of Physics, University of British Columbia, Vancouver BC, Canada
- ¹⁷² Department of Physics and Astronomy, University of Victoria, Victoria BC, Canada
- ¹⁷³ Department of Physics, University of Warwick, Coventry, United Kingdom
- ¹⁷⁴ Waseda University, Tokyo, Japan
- ¹⁷⁵ Department of Particle Physics, The Weizmann Institute of Science, Rehovot, Israel
- ¹⁷⁶ Department of Physics, University of Wisconsin, Madison WI, United States of America
- ¹⁷⁷ Fakultät für Physik und Astronomie, Julius-Maximilians-Universität, Würzburg, Germany
- ¹⁷⁸ Fakultät für Mathematik und Naturwissenschaften, Fachgruppe Physik, Bergische Universität Wuppertal, Wuppertal, Germany
- ¹⁷⁹ Department of Physics, Yale University, New Haven CT, United States of America
- ¹⁸⁰ Yerevan Physics Institute, Yerevan, Armenia
- ¹⁸¹ Centre de Calcul de l’Institut National de Physique Nucléaire et de Physique des Particules (IN2P3), Villeurbanne, France
- ¹⁸² Academia Sinica Grid Computing, Institute of Physics, Academia Sinica, Taipei, Taiwan
- ^a Also at Department of Physics, King’s College London, London, United Kingdom
- ^b Also at Institute of Physics, Azerbaijan Academy of Sciences, Baku, Azerbaijan
- ^c Also at Novosibirsk State University, Novosibirsk, Russia
- ^d Also at TRIUMF, Vancouver BC, Canada
- ^e Also at Department of Physics & Astronomy, University of Louisville, Louisville, KY, United States of America
- ^f Also at Physics Department, An-Najah National University, Nablus, Palestine
- ^g Also at Department of Physics, California State University, Fresno CA, United States of America
- ^h Also at Department of Physics, University of Fribourg, Fribourg, Switzerland
- ⁱ Also at II Physikalisches Institut, Georg-August-Universität, Göttingen, Germany
- ^j Also at Departament de Fisica de la Universitat Autònoma de Barcelona, Barcelona, Spain
- ^k Also at Departamento de Fisica e Astronomia, Faculdade de Ciencias, Universidade do Porto, Portugal
- ^l Also at Tomsk State University, Tomsk, and Moscow Institute of Physics and Technology State University, Dolgoprudny, Russia
- ^m Also at The Collaborative Innovation Center of Quantum Matter (CICQM), Beijing, China
- ⁿ Also at Universita di Napoli Parthenope, Napoli, Italy
- ^o Also at Institute of Particle Physics (IPP), Canada
- ^p Also at Horia Hulubei National Institute of Physics and Nuclear Engineering, Bucharest, Romania
- ^q Also at Department of Physics, St. Petersburg State Polytechnical University, St. Petersburg, Russia
- ^r Also at Borough of Manhattan Community College, City University of New York, New York City, United States of America
- ^s Also at Department of Financial and Management Engineering, University of the Aegean, Chios, Greece
- ^t Also at Centre for High Performance Computing, CSIR Campus, Rosebank, Cape Town, South Africa
- ^u Also at Louisiana Tech University, Ruston LA, United States of America
- ^v Also at Institucio Catalana de Recerca i Estudis Avancats, ICREA, Barcelona, Spain
- ^w Also at Department of Physics, The University of Michigan, Ann Arbor MI, United States of America

- ^x Also at Graduate School of Science, Osaka University, Osaka, Japan
- ^y Also at Fakultät für Mathematik und Physik, Albert-Ludwigs-Universität, Freiburg, Germany
- ^z Also at Institute for Mathematics, Astrophysics and Particle Physics, Radboud University Nijmegen/Nikhef, Nijmegen, Netherlands
- ^{aa} Also at Department of Physics, The University of Texas at Austin, Austin TX, United States of America
- ^{ab} Also at Institute of Theoretical Physics, Ilia State University, Tbilisi, Georgia
- ^{ac} Also at CERN, Geneva, Switzerland
- ^{ad} Also at Georgian Technical University (GTU), Tbilisi, Georgia
- ^{ae} Also at Ochadai Academic Production, Ochanomizu University, Tokyo, Japan
- ^{af} Also at Manhattan College, New York NY, United States of America
- ^{ag} Also at The City College of New York, New York NY, United States of America
- ^{ah} Also at Departamento de Física Teórica y del Cosmos, Universidad de Granada, Granada, Portugal
- ^{ai} Also at Department of Physics, California State University, Sacramento CA, United States of America
- ^{aj} Also at Moscow Institute of Physics and Technology State University, Dolgoprudny, Russia
- ^{ak} Also at Departement de Physique Nucléaire et Corpusculaire, Université de Genève, Geneva, Switzerland
- ^{al} Also at Institut de Física d'Altes Energies (IFAE), The Barcelona Institute of Science and Technology, Barcelona, Spain
- ^{am} Also at School of Physics, Sun Yat-sen University, Guangzhou, China
- ^{an} Also at Institute for Nuclear Research and Nuclear Energy (INRNE) of the Bulgarian Academy of Sciences, Sofia, Bulgaria
- ^{ao} Also at Faculty of Physics, M.V.Lomonosov Moscow State University, Moscow, Russia
- ^{ap} Also at National Research Nuclear University MEPhI, Moscow, Russia
- ^{aq} Also at Department of Physics, Stanford University, Stanford CA, United States of America
- ^{ar} Also at Institute for Particle and Nuclear Physics, Wigner Research Centre for Physics, Budapest, Hungary
- ^{as} Also at Giresun University, Faculty of Engineering, Turkey
- ^{at} Also at CPPM, Aix-Marseille Université and CNRS/IN2P3, Marseille, France
- ^{au} Also at Department of Physics, Nanjing University, Jiangsu, China
- ^{av} Also at Institute of Physics, Academia Sinica, Taipei, Taiwan
- ^{aw} Also at University of Malaya, Department of Physics, Kuala Lumpur, Malaysia
- ^{ax} Also at LAL, Univ. Paris-Sud, CNRS/IN2P3, Université Paris-Saclay, Orsay, France
- * Deceased